Vibration Monitoring on electrical machine using Vold-Kalman Filter Order Tracking

KeSheng Wang

A dissertation submitted in partial fulfilment of

the requirements for the degree

Master of Science

in the Department of Mechanical and Aeronautical

Engineering

of the Faculty of Engineering, Built Environment and Information Technology

at the

University of Pretoria

2008

Vibration Monitoring on electrical machine using Vold-Kalman Filter Order Tracking

by

KeSheng Wang

Supervisor : Prof. P. S. Heyns

Department : Mechanical and Aeronautical Engineering

Degree : Master of Science

Summary

Conventional rotating machine vibration monitoring techniques are based on the assumption that changes in the measured structural response are caused by deterioration in the condition of the rotating machine. However, due to changing rotational speed, the measured signal may be non-stationary and difficult to interpret. For this reason, the order tracking technique was introduced. One of main advantages of order tracking over traditional vibration monitoring techniques, lies in its ability to clearly identify non-stationary vibration data, and to a large extent exclude the influences from varying rotational speed.

Several order tracking techniques have been developed and researched during the past 20 years. Among these techniques, Fourier Transform Based Order Tracking (FT-OT), Angle Domain Sampling Based Order Tracking (AD-OT) and Vold-Kalman Filter Order Tracking (VKF-OT) are the three most popular techniques and have been commercialised in software. While the VKF-OT is comparatively new, and both its theory and application are different from the other two techniques, the unique advantages of this technique has led to increased research attention in this field. This growing interest in research on the application of the VKF-OT technique on real machines, and its comparative advantages with respect to other order tracking techniques, inspired the present research.

With this work, a comprehensive literature of electrical machine condition monitoring was surveyed, which gives a broad perspective of electrical machine monitoring methods ranging through electrical techniques, vibration techniques, temperature techniques and chemical techniques.

To simply the process of applying VKF-OT in initial investigations, simulated single-degree-of freedom and two-degree-of freedom rotor models were established, and the

application of the VKF-OT technique on these simulated models was explored. Because most of the current research draws significantly on an understanding of the VKF-OT theory, it was also necessary to review and summarize the current status of VKF-OT theory from previous work, as well as explore the procedures for selection of its filter bandwidth when dealing with real data.

An experimental set-up for monitoring an electrical alternator was constructed. Real experimental data were subsequently used to compare the advantages and disadvantages of the three popular order tracking techniques. The unique time domain advantage of VKF-OT was implemented, using crest factor and kurtosis values as indictors of the fault condition of the machine. This gave encouraging results.

Keywords: Crest factor, Kurtosis value, Order tracking, Rotating machinery, Simulation rotor model, Vold-Kalman filter order tracking.

Acknowledgements

A word of gratitude to the following people who enabled me to conduct and complete the research:

● Jesus Christ for his invariable support and love at every moment of my life.

● Professor Stephan Heyns my supervisor for his long term encouragements and guidance throughout the whole process of research.

● Mr. Frans Windell for his help in designing and constructing the experimental set-up, as well as personal encouragement.

● Mr. Jacob Madileng for his manufacturing of the experimental set-up.

● Mr. Jimmy Mokhafela for his help in preparing the experiments.

● Mr. Willem Ras for his help in manufacturing parts for the experimental set-up.

● Ms. Calder for her assisting in administrative tasks

● My parents (YaZhi Sun and BaoZhen Wang) and my brother (JingSheng Sun) for their endless love and encouragement during my studies.

Table of contents

Chapter 1 Introduction

1.1 Problem statement

Condition monitoring of engineering plant has increased in importance as more and more engineering processes are automated and manpower needed to operate and supervise plant is reduced. Electrical machinery has traditionally been thought of as reliable and requiring very little attention, except at infrequent intervals when the plant is shut down for inspection. This might however lead to unpredictable machinery shut down or even serious consequential losses. For example, the unexpected shut down of a generator in a power station, may cause blackouts in large areas. Rotating electrical machines, however, are at the core of most engineering processes and as machines are designed to tighter margins there is a growing need, for the sake of reliability, to monitor their behaviour and performance.

By way of example, the generator is a key component of the electricity generation line. With annually increasing electricity consumption, large-scale generators are now replacing the old small-scale generators. However, most of these large rating generators are only scaled up from their original small size ancestors. This lack of careful consideration of larger scale design issues, has led to an increase of generator problems and unexpected economic losses. Examples of this phenomenon include the very rapid increases in generator ratings in the early 1960s. In the United Kingdom (UK), generator ratings were increased from 350 MW to 500 MW, without any experience of intermediate ratings. The rated currents were then increased in proportion, about 1.4 times what they had been. The forces between conductors were increased to $1.4 \times 1.4 \approx 2$ times of what they had been previously (from ESKOM, electrical training manual). This resulted in end winding problems like the loosening of winding overhang structures, and fatigue failures of winding components, as well as shorts between the stator windings. To limit the newly introduced problems, UK generator manufacturers provided massive support for the stator windings overhang as shown in Figures 1.1 (a) and 1.1 (b).

a. Generator stator

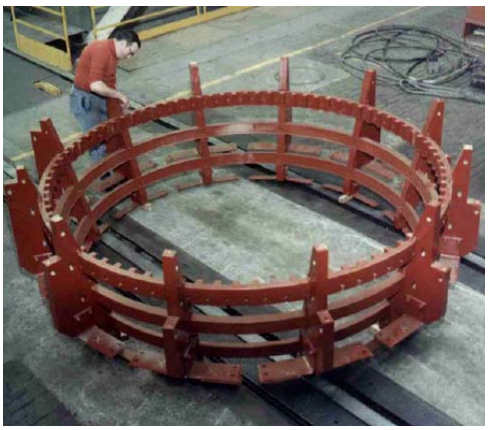

b. Generator stator strength frame

Figure 1.1 Generator and stator strength frame (from ESKOM, electrical training manual)

Thus, reduced productivity, equipment damages, safety issues and life extension have driven continuing research in the area of on-line rotating machinery diagnostics, to recognize incipient failures and avoid the catastrophic results. Various kinds of methods have been applied to monitor the rotating machines. These include electrical techniques, chemical techniques, vibration techniques, and temperature techniques. Most of these are effective for one or more types of faults. No one method is the best for all the fault situations.

Based upon a 1983 study by the Electric Power Research Institute in Palo Alto, CA, 37% of electrical motor failures can be attributed to stator problems. The other 63% are associated with rotating assemblies (including bearings) and caused by imbalance, misalignment, and other mechanical problems that can be diagnosed and mitigated through the proper application of vibration monitoring, tribology, and other well-known practices. Among these monitoring methods, vibration monitoring plays an important role in condition monitoring of rotating electrical machines. Order tracking which relates the vibration to the machine speed is commonly used, because of its ability to provide more information on the rotating system than tradition vibration monitoring techniques.

In this research, the use of order tracking for monitoring rotating electrical machines will be explored. Specific attention will be given to the Vold-Kalman Filter Order Tracking technique, a new technique that offers many advantages over other order tracking methods. Before discussing this order tracking technique in detail, a broad review of the literature on rotating electrical machinery condition monitoring is essential, to obtain an overall picture of monitoring on electrical machines.

This literature survey, therefore, firstly summarizes the available techniques of on-line monitoring for electrical rotating machines. These include electrical techniques, vibration techniques, chemical techniques and temperature techniques. Secondly, order tracking techniques are discussed in detail.

1.2 Literature survey

Within rotating electrical machines, there is a magnetic flux and electric field that varies, circumferentially in the air-gap. Under ideal conditions these magnetic flux and electrical fields will be symmetrical, but electrical defects in the machine will distort them. Defects on either rotor or stator disrupt the radial and circumferential patterns of flux in the machine, causing changes that can be detected outside the machine. Further, any mechanical faults, such as bearing faults, mechanical losses and stator looseness can also be monitored either by vibration techniques or electrical techniques. In order to obtain a bigger picture of the applicable monitoring methods, the following paragraphs will give a broad survey of electrical and vibratory monitoring techniques. This will include some of the seminal work that was done in the 1970s and 1980s.

1.2.1 Electrical methods for monitor electrical rotating machine

a. Partial discharge monitoring

An early indicator of many electrical faults in machine stators is an increase in electrical discharge activities. This activity can also be related to remaining life of the insulation system. The accurate detection of discharge activity would therefore give a valuable early warning of failure and could provide information about the remaining life of the insulation. The earliest work summarized by Emery et al. (1981) describes a technique developed by Westinghouse in the USA to detect the presence of sub-conductor arcing in the stator windings of large steam turbine generators, by measuring perturbations in the winding current. Arcing activity produces very wide-band electromagnetic energy, some of which propagates into the neutral connection of the star connected winding. Emery et al. uses a ferrite-core current transformer (CT) wrapped around the neutral cable to couple to this activity, which they detect using a quasi-peak, Radio Interference Field Intensity (RIFI) meter. The neutral cable was chosen as a good measurement location because it has a low potential with respect to ground and because arcing at any location in the generator causes radio frequency (RF) current to flow into the neutral lead. Wilson et al. (1982) in the UK devised a technique similar to that of Emery et al. as a cheap method of detecting discharge activity on-line in a wide range of high voltage plant. It uses a Rogowski coil, wrapped around the neutral cable of the machine winding, and the detector is a narrow band instrument that measures the average peak energy received by the instrument. An alternative technique, where perturbation in voltage waveforms are detected at the machine terminals, was described by Kurtz et al. (1979) and applied primarily to hydroelectric alternators in Canada. In this method, connection to the winding is made through coupling capacitors connected to the line terminals of the machine. Discharge pulses are coupled through these capacitors to a specialized pulse height analyser, which characterises, in the time domain, the waveforms of the pulses. Kurtz et al. (1980) describe how capacitive couplers can be permanently built into the phase rings of the machine so that the measurements can be made without service interruptions.

All the techniques described above operate at relatively low frequencies (1-80 MHz) and detect the electromagnetic energy propagated along the winding to the neutral or line end connections. In any healthy machine there will be a background of corona and partial discharge activity that vary from machine to machine and also varies over time. Malik et al. (1985) show that damaging discharge pulses, such as serious partial discharges, sparking or arcing, have faster rise-times than the background corona and partial discharge activity and they therefore produce a much higher frequency of electromagnetic energy (350 MHz). Pulses of electromagnetic energy (at frequencies higher than 4 MHz) propagate from the discharge site by radiation from the winding, not by propagation along the winding as in the case with the lower frequency techniques. This radiation can be detected by a RF antenna located either inside the enclosure of the machine or outside, close to an aperture in it.

The lower frequencies (1 MHz – 80 MHz) involving propagation along a homogeneous conductor, suggest that a discharge site can be located by timing the arrival of discharge pulses received at a number of different sensors. However, this has not yet been demonstrated and the existence of reflections at each discontinuity in the winding will make the identification of pulses at the terminals extremely difficult.

At higher frequencies (100 MHz – 1 GHz), a discharge site could be located using a directional antenna. But at the frequencies involved the dimensions of such an antenna (diameter from 0.6 m to 6 m) would be impracticably large and in any case the complex gas space structure will cause reflections and local resonance that will disrupt location.

It has been described how at high frequencies the ratio of damaging activity to background will be much higher than at low frequencies. So the higher frequency technique has the potential for providing a clearer indication when damaging discharge activity occurs. But the problem still remains to determine what level of activity constitutes damage serious enough to be locatable.

Many researchers have worked on partial discharge monitoring in the recent 10 years.

Greg (1995) presents a new type of partial discharge test that can be performed by plant personnel during normal operation of the machine, thus enabling all users of large machines to plan maintenance. The key requirement of the new test is to remove all the interference caused by other sparking and discharging sources in a plant. Such noise has lead to false indications of stator winding deterioration in the past. The new test uses either high-voltage capacitive sensors, high- frequency current transformers, or 1000 MHz electromagnetic couplers to detect the discharge signals. These signals are processed on a pulse-by-pulse basis by a specialized electronic instrument to remove noise and the remaining partial discharges are then categorized according to number, magnitude, and phase position. The test has been implemented on over 100 machines, and results appear promising. Stone and Kapler (1998) described that by combining on-line partial discharge tests, as well as other monitoring techniques such as flux probing or current harmonic analysis and improved temperature sensing, companies could often confidently extend the interval between major machine maintenance and save a considerable capital expenditure.

Li (2004) devised a measuring system for detecting partial discharge of a generator stator bar, based on an ultra-high frequency method. The laboratory test results show that partial discharge in the generator stator bar can be detected by this method. Furthermore, the results of on-line detection on a power generator indicate that the ultra-high frequency method has the ability of detecting partial discharge without external interference coming from the exciter or transformer. Some researchers also studied the factors influencing partial discharge tests. Wu (2005) studied the influence of mechanical vibration on partial discharge monitoring signals. It was found that the partial discharge behaviour at low voltage just above the partial discharge inception voltage, was different from that at high voltage. This was explained in terms of the effects of the field variation in the gap due to the vibration and charges left on the insulation surface due to partial discharge. Besides, Green (2005) reported that IEEE and EPRI in North America and CIGRE in Europe have recently published a number of documents related to the use of on-line partial discharge detection systems on rotating electrical machines, as a diagnostic tool for monitoring the condition of stator winding insulation during operation. This paper presents the most recent developments related to IEEE1434, CIGRE Report 226 and results of EPRI studies and one case study on partial discharge monitoring of two 13.2 kV, 10 MW, motors in a petrochemical plant are presented.

b. Brush-gear monitoring

Brush-gear, in those machines which use it, require a steady maintenance commitment if good performance with the minimum of sparking is to be maintained. Poor performance can be detected by measuring the temperature of a brush or brush-holder. Alternatively a more direct method would be to detect the radio frequency energy generated by sparking, as described by Mchiguchi et al. (1983). They use a wide bandwidth dipole antenna connected to a radio frequency amplifier with a bandwidth from 10 – 100 MHz. The monitoring thereby provides a chart record showing the average area of sparking pulse and

Michguchi relates this to a spark number indicating the intensity of sparking. Maintenance staff may use this indication to decide when brushes should be changed. Makel (1986) described actively cooled current transfer brushes for compact homo-polar generators (HPGs). The brushes have been designed to provide data on the effects of rotor speed, current level, coolant flow rate, and coolant injection pattern. All these data can be used as monitoring parameters.

c. Generator rotor and stator monitoring

The rotors and stators of large turbo-generators are particularly highly rated because of the large mechanical and electrical stresses induced in them, in particular because of the high centrifugal forces on the winding and the relatively high temperatures attained in the winding insulation, thus large electrical machinery stator and rotor works under the severe working condition. High rating generators or motors, experience the problem of winding looseness or shorts due to excessive vibration. Consequently these parts of the machine are prone to faults, and faults tend to develop over a long period of time. The rotor is also relatively inaccessible both for obtaining signals during running and for removal for repair if a fault is detected. These facts, taken together with the high value of turbo-generator plant, have led to monitoring techniques for generator rotors and stators having been developed to a high degree of sophistication.

Earth leakage faults

A single earth leakage fault on a generator rotor winding is not serious in itself, because it can not cause any damage since the earth leakage current is limited due to the leakage resistance of the excitation supply. However, if two well-separated earth faults occur then large currents can flow, leading to significant damage to the winding, its insulation and rotor forging. The normal procedure for detecting earth faults in a large generator rotor is to supply a DC bias voltage to the rotor winding and to monitor the current flowing to the rotor body via an alarm relay (Warrington et al., 1982). If such an alarm occurs many utilities would consider that the machine should be shutdown so that the rotor can be investigated. However, operational pressures are often such that this is not possible, and it is necessary to continue running the unit. The next step then is to monitor the earth leakage current and manually trip the unit if there is any further increase, indicative of a second earth fault. An alternative method is to use a potentiometer feeding to earth via a sensitive galvanometer making a bridge circuit. As the earth fault location alters or a second fault occurs, the bridge becomes unbalanced and an indication occurs on the meter. The problem is that the second earth fault may arise close to the location of the first fault and the resultant change in earth leakage current may not be particularly large. A more sensitive indicator of the onset of a second earth fault is the resistance of the winding to earth, measured from either terminal. Hargis et al. (1985) have described such a technique using two voltmeters.

Turn-to-turn faults

Turn-to-turn faults in a generator rotor winding may lead to local over heating and eventually to rotor earth faults. In addition, the shorting of turns causes unequal heating of the rotor leading to bending and an unbalanced pull, which together cause increased vibration as described by Rosenberg (1978) and Khudabashev (1961). A way of detecting these faults on-line was first described by Albright (1971) using a stationary search coil fitted in the air gap of the machine. The search coil, of diameter less than the tooth width

of the rotor, is fixed to the stator usually in the air gap and detect either radial or circumferential components of magnetic flux. When a shorted turn occurs two things happen. First it disturbs the mechanical and magnetic force (MMF) distribution, causing low-order even harmonics or asymmetry in the search coil voltage waveforms. Secondly, it disrupts the n-th order slot ripple harmonics. Albright used the changes in the heights of the peaks and troughs to determine the number and location of any shorted turns. He identified faults by measuring the peak heights of ripple from Polaroid photographs of the oscilloscope waveform, recorded under open and short circuit test conditions. Since that time a considerable number of large steam turbine-driven generators have been fitted with air-gap search coils and a great deal more experience has been obtained of detecting shorted turns. The detection techniques have therefore been refined to deal not only with the different types and locations of search coils but also to detect shorted turns under both off-load and on-load conditions.

Conolly et al. (1985) described the first on-line monitor, which is continuously connected to the search coil and gives an initial indication of the development of an inter-turn fault. More detailed analysis techniques can then be used on the search coil waveforms, off-line, to positively identify and locate the faults. An alternative way of monitoring for shorted turns uses the stator winding itself as the search coil. The principle of this technique, first suggested by Kryukhin (1972), has been developed and fitted to a number of generators in the UK (Munhlhaus et al., 1985). This technique makes use of the fact that in large two-pole generators, each phase of the stator winding consists of two half-phase windings in parallel, any asymmetry in the rotor MMF will induce counter-MMF currents in the stator winding with a twice-fundamental frequency, which will circulate between the half-phases. The presence of shorted turns is detected by measuring those even harmonic currents. The approach has also been suggested by Buckley (1982).

An advantage of the circulating technique, when compared to an air gap search coil, is that the current transducers can be installed without the need to remove the rotor from the generator. For many generators the half phase windings are joined within the cooling pressure casing in a fairly restricted space that requires special arrangements to gain access. A disadvantage of the circulating current method, however, is that it does not readily give information on the location of a shorted turn, whereas the air gap search coil method does.

d. Other faults monitoring

Some other researchers also use electrical methods or related methods to detect the winding faults. McDonald et al. (1991) discussed a monitoring and diagnosis expert system (MODEES), which forms part of a more general condition monitoring and fault diagnosis system (COMFAD). This is a rule-based system with the ability to categorize power plant performance and recognize impending failure or dangerous trending, and the need for preventative maintenance or remedial action. COMFAD/MODEES is targeted at operator personnel who must decide within a short period if the power plant is fit for continued or prolonged service, and if not, make a thoroughly reasoned ‘guess’ at what faults have occurred and how they can be remedied.

Rankin et al. (1995) stated in his study that electrical machine manufacturers deem that if an induced shaft voltage is measured higher than 250 mV RMS on a ball and roller bearing, or 400 mV RMS on a sleeve type bearing, the non-drive end bearing shall be insulated from the frame to avoid bearing damage due to circulating currents. This paper described the rationale adopted and non-invasive tests conducted to detect malfunctions within

alternator rotors while the machine is in service. Results are presented showing that shaft voltage can be used as a predictive maintenance technique and condition monitoring tool on this type of alternator rotor.

Kliman (1996) analysed the negative sequential currents flowing in the leads on the basis that symmetrical (unfaulted) motors powered by symmetrical multiphase voltage sources will have no negative sequential currents flowing in the leads. A turn-to-turn fault will break that symmetry and give rise to a negative sequential current, which may then be used as a measure of fault severity or to initiate protective action such as a circuit breaker trip. The method was implemented on a PC and tests were conducted in real time on a specially prepared small motor.

Trutt (2002) states that much of the current effort that has been expended on the monitoring of electrical winding health in induction machines, has involved the measurement of voltages and currents at the motor terminals. While these procedures have been shown to provide useful early warning information, they do not provide a direct measure of the internal current in a coil-to-coil or phase-to-phase stator winding fault. One method that might be used to advantage as a measure of internal deterioration currents is to monitor the air gap magnetic fields that these currents produce. Unfortunately, the insertion of search coils for such measurements is a difficult and expensive process. However it has been known for some time that there are links between electrical behaviour and mechanical vibration. As an application of this concept, electrically excited vibration measurements as discussed in this paper appears to provide an alternative approach to the monitoring of internal deterioration currents. This type of information may then be used to supplement other monitoring data with the goal of making more informed electrical and mechanical maintenance decisions.

Fischer (2002) shows how a Bayesian classifier can be implemented for a failure detection system where statistical failure data is not available for one of the classes. Results of field data obtained from a large electric power generator are shown. The proposed system is an improvement over a classical Bayesian implementation and a large improvement over a fixed, arbitrary value threshold classifier.

Arshad (2004) presents a detailed case study of generator stator winding failure leading to core damage, which is meaningful for the industrial maintenance engineer, and also a very good example of condition-based maintenance (CBM).

Subhasis (2005) investigates the induction machine faults and concludes that almost 30 – 40% of all reported induction machine faults are stator related. In fact, going by the number of occurrences, the position of stator faults is only second to bearing related faults. Third harmonic line currents have been reported to increase under stator fault conditions. It has been shown in this paper that they are primarily due to the interaction of saturation caused by permeance waves and reverse rotating fields caused by stator faults or voltage unbalance and machine structural imbalance (usually small). Thus, voltage unbalance cannot be distinguished from stator faults. The third and other triple related harmonics are however found to be a very decisive indicator of the fault, if measured in the machine terminal voltages just after switch-off. The fault detection technique is independent of machine parameters and supply unbalances. Simulation as well as experimental results are presented with very few shorted turns.

Shaft flux, or more generally axial leakage flux, occurs in all electrical machines. It is produced because no machine can be constructed perfectly symmetrically. There will

always be, for example, slight differences in core plate anisotropy, and plate thickness variation. This asymmetry is reflected in the impedances presented by the various phase groups, or coils in the machine stator, and will cause slight variations in the currents flowing in the coils. This, together with small differences in the electrical properties of the conductor, and variations in the physical disposition of the conduction in both the active length and end regions of the machines, will give rise to a net difference between the currents flowing in one section of the end winding, when compared with the corresponding section diametrically opposite. The imbalance leads naturally to a net axial flux component. A similar argument can be applied to the rotor circuits, hence one expects axial flux even in machines that are in 'perfect health'. It is a simple extension to consider what happens when certain fault conditions arise in a machine. Faults, such as winding short circuits, voltage imbalance, and broken rotor bars, represent severe disruptions to the internal symmetry of the machine. Any gross change of magnetic circuit conditions, such as the formation of an eccentric air gap due to bearing wear, will, by the same token, be reflected with a corresponding change in axial leakage flux. The purpose of axial flux monitoring is therefore to translate observed difference in the nature of the axial leakage flux into an indication of fault condition. Erlicki et al. (1971) have shown that it is possible to detect the loss of a supply phase through axial flux monitoring and Rickson (1983) developed a monitoring device. More discrimination between various fault conditions can be achieved by carefully processing the axial flux signal as described by Penman et al. (1980, 1985). The technique relies upon examining the changes in the spectral components of the axial flux. Since the flux is produced by winding currents, the frequency of these flux components must be related to the frequencies of currents. Therefore, the axial flux spectrum will be rich in harmonics, even in a well-constructed, healthy machine. The attraction of the method is that it is completely non-invasive and a single sensor can be used for a variety of fault types.

1.2.2 Vibration techniques

a. Overall level monitoring

This is the simplest form of monitoring and is still the most commonly used technique, despite its limitations for the diagnosis of faults in electrical rotating machines. The measurement taken is simply the RMS value of the vibration level over a pre-selected bandwidth. And in practice the measurement parameter is vibration velocity taken at the bearing cap of the machine under surveillance. The technique has found favour because over the years a considerable statistical base regarding machinery failures has been built up. This has resulted in the publication of recommended running vibration severity level standards, as an indication of overall health. Many operators use a strategy based on such information to aid maintenance scheduling. Several vibration severity guides are available for assessing the severity of machinery vibrations. The major standards currently in use include the ISO standards (International Standards Organisation), the VDI standards (German National Standards), and the BS standards (British Standards Institution). The most widely used vibration severity criteria, which are common to ISO and BS (ISO 10816 and BS 7854) are based on broadband vibration velocity levels between 10 Hz and 1000 Hz. Another useful criterion is given in the Canadian government specification CDA/MS/NVSH107. Further, a comprehensive list of vibration standards is given in section 9 of the Handbook of Noise and Vibration Control (Barber, 1992).

The strength of the overall level technique is its simplicity. It requires only the simplest of instrumentation, and because of this it is a common feature in many installations. But this

technique makes heavy demand upon technical personnel. The sensitivity of the technique is also low, particularly when a defect is at an early stage. Besides, a major limitation of all absolute vibration severity guides is that the vibration measurements on the surface of a bearing also contain the frequency response characteristics of the bearing housing. The further away one is from the "true" vibration signal to be monitored, the larger is the probability that the measured signal is " contaminated". In practice the limitation is overcome by trending the data at specific measurement points over lengthy periods of time, in order to observe relative increases from predefined baseline values. Quite often, these guidelines provide a very reliable and useful indication of a machine's general condition.

b. Frequency spectrum monitoring

Frequency spectrum monitoring is undoubtedly the key to diagnosis, using vibration monitoring, and there are a great deal of sophisticated of techniques and instrumentation available for spectrum analysis. There are various levels of spectrum analysis commonly used, and these may be regarded as a continuous extension of the overall level reading to the narrow band with constant frequency bandwidth presentation. The narrow band spectrum allows the operator to trend the condition of the machine most effectively. This requires that an initial base-line spectrum is taken and subsequent spectra are compared with it. In this way criteria such as ISO 10816 can be applied for each frequency.

The technique described thus far is relatively general, and may be used to identify not just unsatisfactory overall performance, but also to pinpoint specific problems by examining discrete frequencies, or groups of frequencies. Returning to the condition monitoring of electrical machines, during the 1970s and 1980s, several useful papers were published about the application of vibration monitoring electrical machines via the vibration method. Mayes et al. (1981) presented a paper about fault diagnosis in a large turbo-generator by using vibration techniques. Herbert (1984) described computer analysis techniques, which can be applied off-line to vibration data collected on-line. A number of authors have reported the identification of various vibration frequencies associated with defects in induction machines, including Rai (1974), Erskine (1978), Leonard et al. (1984) and Cameron et al. (1985), Maxwell (1983) and Hargis et al. (1982). It has been suggested by Rai that vibration at (or near) 50 Hz, 100 Hz and 200 Hz is indicative of eccentricity. Leonard et al. also show that 100 Hz, 200 Hz and 300 Hz components can be expected when the stator frame vibration is monitored during the occurrence of an inter-turn winding fault or supply voltage unbalance (including single phasing). They also show that higher order harmonics occur in the stator frame vibration, due to eccentricity. Recently Trutt et al. (2002) investigated the effects of stator winding deterioration on the frequency spectrum of mechanical vibration in induction machines. Results of this study show that specific vibration frequencies may be monitored in order to provide an assessment of stator winding integrity.

Obviously, vibration can occur in electrical machinery as a result of either electrical or mechanical action. In order to summarize the dominant frequencies for a given defect, the following table has been compiled (Hewlett Packard, 1983; Neale and Associates, 1979; Brüel and Kjær, 1980).

Table 1.1 Vibration frequencies for specific electrical machine faults

Fault type	Important frequencies	Comments
Unbalanced rotor	f_r	Very common also causes unbalanced magnetic pull that gives 2 f_r vibration.
Misalignment of rotor shaft	f_r, 2 f_r, 3 f_r, 4 f_r	Also manifests as static eccentricity; therefore see components generated from this source, below.
General looseness of shaft in bearing housing	f_r, 2 f_r	Generates a clipped time waveform; therefore produces a high number of harmonics.
Oil whirl and whip in sleeve bearings	(0.43 to 0.48) f_r	Pressure fed bearings only.
General electrical problems	n f_r, n f_s	A problem can usually be identified as having electrical origins by simply removing the supply. If the fault disappears then the problem is associated with the electrical aspect of the machine
Broken rotor bars in induction machines	f_r +2s f_s	May be difficult to detect due to the low level. Speed, leakage field or current changes maybe perferred as a monitoring parameter.
Stator winding fault	f_s, 2 f_s, 4 f_s	Difficult to differentiate between fault types using vibration monitoring alone.
D.C. machine commutator faults	n f_r	Unbalanced rotor components can also be generated.
f_r = rotational frequency, n = an integer, s=slip		

c. Torsional oscillation monitoring

There may be a specific need to monitor the torsional behaviour of long thin machine shafts such as on a turbine generator. The direct approach to this problem would be to mount suitable strain gauges on the shaft, together with suitable telemetry, to transmit the gauge output from the rotating reference frame. This has only been done for experimental purposes and is not appropriate for long term use due to the harsh operational conditions the transducers would need to withstand. Two indirect methods of monitoring the torsional response of shafts have been outlined by Rusche (1985). The results obtained in this paper can be used to plan maintenance intervals on the basis of need, rather than risk catastrophic failure when there has been a high level of system disturbances between fixed outages.

The monitoring of torsional oscillations can also be used to detect defects in induction motors. Gaydon (1979) as well as Gaydon and Hopgood (1979) measure speed and current fluctuation and use a signal averaging technique to monitor the motor. A once-per-revolution pulse is required from the motor shaft, using either an optical or magnetic sensor. This enables the rotational period of the shaft to be measured to a precision of 1 μs.

De Mello (1994) states that generator rotor angle measurement is useful as an indictor of stability of the operating condition. Rotor angle measurements with the appropriate bandwidth are also very useful in the observation of rotor torsional oscillation, both for monitoring and protection against undamped torsional modes, as well as for use in control schemes designed to damp torsional oscillations. A method of measurement of synchronous machine rotor angle from an analysis of the phase angle of zero sequence harmonic components of terminal voltage is presented.

d. Shock pulse monitoring

The shock pulse method is used exclusively for detecting defects in rolling element bearings. This is relevant since a large number of electrical machine failures occur due to bearing problems. As a rolling element bearing deteriorates, the moving surfaces develop small pits. The interaction between such surfaces generates stress waves, known as shock pulses. These shock pulses are at ultrasonic frequencies and can be detected by piezoelectric transducers with a strongly resonant frequency characteristic. It is claimed that this reading is a good measure of the condition of the bearing. The condition of the bearing is assessed through a quantity know as the shock pulse value (SPV), defined as

$$SPV = \frac{R}{n^2 F^2}$$

where R is the meter reading, n is the shaft speed and F is a factor relating to bearing geometry. Low values indicate bearings in good condition. In conjunction with overall level monitoring, the table below can be used to give qualitative guidance on the bearing condition.

Table 1.2 Shock pulse interpretation (Tavner et al., 1987)

Overall vibration level trend	Shock pulse value trend	Comments
Low and rising	Remain low	No bearing damage
Low and rising	Low but rising at same rate as overall level	Bearing damage likely
Low and rising	High value but remaining constant	Damaged bearing but other problem causing rises in level.

Shoel et al. (1984) also suggests that it is possible to determine the relative thickness of the lubricant film in roller element bearings, using the shock pulse method, and indeed he proposes a monitoring system to do this. However, quantitative evaluation using the shock pulse method remains difficult.

e. Special vibration monitoring techniques

There are a number of specialized techniques, and they are beginning to establish themselves as powerful diagnostic tools, Heyns (2003). Cepstrum is described as the inverse Fourier transform of the logarithm of the power spectrum of the function. And it is defined as:

$$C(\tau) = F^{-}\{\log p_{gg}(f)\}$$

where F^{-} represent the backward Fourier transforms. The use of the cepstrum has found favour in examining the behaviour of gearboxes, because such items of equipment tend to produce many families of sidebands in their vibration spectra, due to the variety of meshing frequencies and shaft speeds that may be present. The cepstrum essentially highlights periodicity in complicated signals. The indication of various sidebands in a rich signal may be practically impossible using spectrum analysis, but using cepstrum, they can easily be picked out. Randall (1980) provides an excellent review of the use of cepstrum analysis applied to gearboxes. The cepstrum technique is also promising for discovering the faults of electrical machines. Steqemann (1998) states that knowledge of the vibration machine signatures and their time dependent behaviour is the basis of efficient condition monitoring. By only using vibration thresholds given by norms and standards, alarms often occur without giving hints to the source of excitation. Therefore, modern measurement techniques, in combination with advanced computerized data processing and acquisition, exploit new ways in the field of machine surveillance. These include the use of spectrum and correlation analysis of acceleration, displacement and the operational process parameters (e.g. temperature, pressure, steam flow, etc.). In addition time domain analysis using characteristic values to determine changes through trending, spectrum analysis to identify trends of frequencies, amplitude and phase relations, correlation analysis to evaluate common sources of excitation by comparing different sensor signals, as well as cepstrum analysis to detect periodical components of spectrum, are all used as evaluation tools. Poyhonen et al. (2004) state that vibration monitoring is a key technique of fault detection in induction motors. Several features of vibration signals are compared as indicators of a broken rotor bar of a 35 kW induction motor. Regular fast Fourier

transform (FFT) based power spectral densities (PSDs) estimation is compared to signal processing with higher order spectra (HOS), cepstrum analysis and signal description with autoregressive (AR) modelling. The fault detection routine and feature comparison is carried out with support vector machine (SVM) based classification. The best method for feature extraction seems to be the application of AR coefficients. The result is determined with real measurement data from several motor conditions and load situations.

There still are some other papers reporting the use of the vibration method to detect rotating machine faults: Caryn (1998) proposes a method for sensorless on-line vibration monitoring of induction machines based on the relationship between the current harmonics in the machine and their related vibration harmonics. Initially, the vibration monitoring system records two baseline measurements of current and vibration with the machine operating under normal condition. The baseline data is then evaluated to determine the critical frequencies to monitor on-line. Once these frequencies are determined, the baseline vibration is simply used to scale the current harmonic signal to an estimated vibration level. Based on theoretical analysis, simulation results and the experimental results shown, a linear relationship between the current harmonics and vibration level can be assumed. The results of two experiments on a three phase 230 V 10 hp induction motor operating under no load are discussed and show the feasibility of this method for sensorless on-line vibration monitoring. Watson (1999) describes how commercial FEM packages may be used to simulate rotor faults and hence enhance the capability of practical condition monitoring schemes. Some known causes of inaccuracy between models and experimental data are accounted for and the results compared with experimental data. An accurate model of a machine under faulted conditions is developed which is be used to determine the monitoring strategy for less common faults. Leger et al. (1997) states that stators of large power-station generators are sensitive features in the mechanical design of these machines. These include in particular the parts at the ends of the windings, outside the core, known as the “end winding cages”. These structures are complex, mainly because of their geometry and variety of materials used. They are also subjected to large electromagnetic forces in both steady and transient operation. Their durability is essentially both for safety and uninterrupted service by the alternators. The article presents the approach taken, which includes the use of various experimental and numerical methods. Modelling is also described.

f. Order tracking techniques

The order tracking technique is one of the important vibration analysis techniques for rotating machinery. Because this research is mainly focused on the order tracking technique, this technique is here considered separately and discussed in detail. The advantages of order tracking over other vibration techniques mainly lie in analysing non-stationary noise and vibration, which will vary in frequency and amplitude with the rotation of a reference shaft or shafts. The analysis of non-stationary conditions requires additional information, as compared to steady state conditions, for an accurate result to be obtained. Normally the additional information is presented in the form of a tachometer signal measured on a reference shaft of the machine. Order domain analysis relates the vibration signal to the rotating speed of the shaft, instead of an absolute frequency base. In this way, vibration components that are proportional to multiples of the running speed can easily be identified. Frequency analysis of the instantaneous root-mean-square (RMS) values of the periodic components of rotating machine vibrations as a function of rotational speed is referred to as order tracking.

For many years, order tracking was performed using analog tracking filters and elaborate instrumentation with analog to digital converters controlled by some RPM sensing unit (phase-locked loop or PLL) and performed far from ideal. With the development of computer technology and reduction in digital storage cost, it is now generally preferred to store raw data on a hard disk and perform all subsequent analysis as post-processing. In recent years, many researchers have investigated different kinds of order tracking methods (Fyfe & Munck, 1997; Vold, Mains & Blough, 1997; Vold, Herlufson, Mains & Corwin-Renner, 1997; Gade, Herlufsen, Hansen and Vold, 1999; Blough, 2003a & 2003; Tuma, 2005; Pan & Lin, 2006). Order tracking (OT) can be performed in many different ways, each of them having its advantages and disadvantages. One of the popular classifications is to divide it into three different categories:

Based upon a classification suggested by Blough (2003), the first is Fourier Transform Based Order Tracking (FT-OT). This approach does not perform well with non-stationary data and is usually used for overall observation of the system and obtaining a first impression. The second is Angle Domain Sampling Based Order Tracking (AD-OT). This kind of order tracking was first published by Potter and his colleagues from Hewlett Packard in 1989, although Hewlett Packard considers the exact implementation of the technique to be proprietary, and as such has not published many of the details. It has been 18 years since this method was first introduced, and some papers discussing the theory and implementation of these specific techniques have become available (Fyfe & Munck, 1997). The significance of AD-OT is that this re-sampled data has the same properties as stationary frequency data, but it still needs to be processed further by FFT or DFT, in terms of uniform angular intervals, instead of uniform time intervals. As a result, the disadvantages of FFT or DFT with regard to non-stationary amplitude data remain present with the angle domain Fourier Transform. The third technique is Vold-Kalman Filter Based Order Tracking (VKF-OT). This kind of OT method can overcome many of the limitations of order resolution, but the big difference of this method compared to the above two approaches, is that the time history of a certain order can be extracted from the original data, with its amplitude and phase. Another wave-form reconstruction order tracking technique, Gabor order tracking, which was first proposed by Albright and Qian (2001). Very recently, Pan et al. (2006) public a paper to objectively compare the features of the improved Gabor order tracking scheme and the VKF-OT technique.

In addition to the above-mentioned three OT methods, there still are a few other techniques too. These are Time Variant Discrete Fourier Transform Order Tracking (TVDFT) (Blough, 2003a) which offers many of the advantages of the re-sampling based order tracking methods, while reducing the computational loads of the calculations considerably. The Prony Residue Estimation process, the Maximum Likelihood process, as well as other methods based on conventional digital filtering methods are all OT methods, but they are not available in current software, and most of them having several disadvantages compared to the methods discussed above (Blough, 2003).

To provide a clear overall vision of the different OT methods, the following discuss the pros and cons of the three main order tracking methods.

FT-OT is both the simplest to implement and the most commonly used method. This method is available in most of the commercial order tracking software, but it suffers from two main problems because of the Fast Fourier Transform. One is due to the frequency changing as a function of time, and the other is the amplitude varying with respect to time. Blough (2003) presents a detailed analysis of these two problems and compare the errors both qualitatively and graphically. It can be said that FT-OT is a good tool to get a brief

overall idea of the system at the initial stage, while it is not a good tool to analyse the detail of a system.

AD-OT is commonly referred to as digitally re-sampling based order tracking. The raw measured data is usually sampled with a uniform time interval Δt. As was stated above, two kinds of errors are caused by using the standard FFT method. Blough (2003) summarizes the essence of re-sampling based order tracking, as that the uniformly sampled time data is digitally re-sampled to the angle domain by a re-sampling algorithm. This re-sampling procedure from the time domain to the angle domain transforms non-stationary time domain data into stationary angle domain data, in the sense of a frequency that can be analysed with standard digital signal processing methods. This overcomes the shortcoming of frequency changing as function of time. The kernels of the Fourier transform are also reformulated in terms of the uniform angular intervals:

$$a_m = \frac{1}{N}\sum_{n}^{N} x(n\Delta\theta)\cos(2\pi o_m n\Delta\theta), b_m = \frac{1}{N}\sum_{n}^{N} x(n\Delta\theta)\sin(2\pi o_m n\Delta\theta)$$

where o_m is the order that is being analysed, a_m is the Fourier coefficient of the cosine term for o_m and b_m is the Fourier coefficient of the sine term for o_m. The result from this angle domain Fourier Transform is that the orders fall on spectral lines, regardless of the speed variations. But an obvious limitation with FFT type analysis is the finite order resolution. It will give rise to problems when orders do not fall on spectral lines. This means the minimum sampling rate needed to avoid aliasing is two samples per cycle of the highest order of interest. Another limitation of AD-OT is that its re-sampling procedure does nothing with the non-stationary amplitude of the data, therefore errors will remain present because of varying amplitude, as it happened in time domain. Besides, re-sampling based order tracking only allows to tracking relative to one rotating shaft at a time. Orders that cross one another cannot be analysed accurately. In application of this method, one of the most important things is to know is which factors influence this technique. Fyfe and Munck (1997) present an investigation of factors that have significant effects on AD-OT accuracy. They mention that this method is extremely sensitive to the timing accuracy of the key phasor pulses. They also summarize the equipment used for computed order tracking, see Figure 1.2. The contribution of this paper is its investigation of influence factors of computed order tracking.

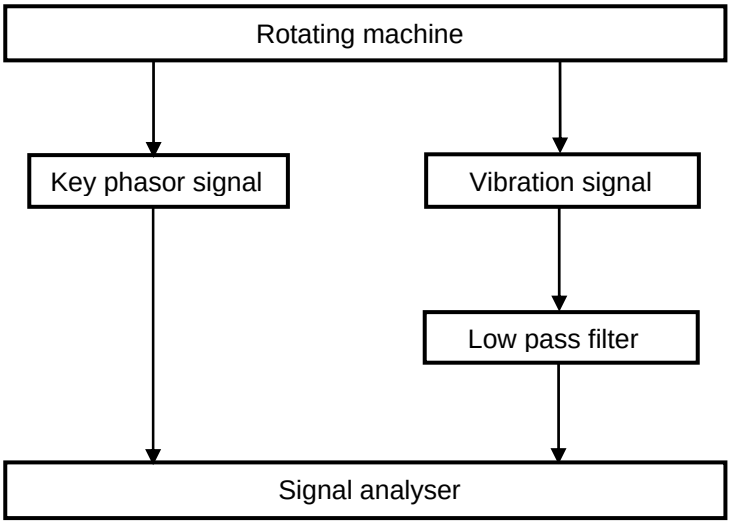

Figure 1.2 Equipment used for computed order tracking

The VKF-OT method is a comparatively new technique. It was first adapted to order tracking by Vold and Leuridan in 1993, but its underlying theory is not as straightforward as the previous order tracking method. It is a fundamentally different method from FT-OT and AD-OT. During the past ten years, many researchers (Vold, Mains & Blough, 1997; Vold, Herlufson, Mains & Corwin-Renner, 1997; Gade, Herlufsen, Hansen & Vold, 1999; Tuma, 2005) have reported on the theory of VKF-OT. Its fundamental theory has therefore become much clearer to the public. Brüel & Kjær developed the Vold-Kalman order tracking filter into a commercial product and states that VKF-OT allows high-performance tracking of harmonic responses, or orders, of periodic loads in mechanical and acoustical systems. This method allows beat free extraction of close and crossing orders in systems with multiple shafts, and features a finer frequency and order resolution than conventional techniques. The tracking capabilities are independent of the rate of change of the rotational speed (slew rate). The product material also documents the advantages of this kind of order tracking method compared with the computed order tracking method, as that of much shorter transients, no phase bias, no slew rate limitations, order wave forms in time domain. It can be seen that the research in the field of VKF-OT hold significant advantages compared to other OT techniques because of these advantages. However, it should also be borne in mind that since the original VKF-OT requires longer calculation time, it is not suitable for real time processing. Quite recently however, Pan and Wu (2007) proposed an adaptive Vold-Kalman filtering order tracking approach to overcome the drawbacks of the original VKF-OT scheme for condition monitoring on this point. This makes VKF-OT a more practical and powerful tool and makes real time condition monitoring by using VKF-OT possible and feasible. Another wave-form reconstruction order tracking technique, Gabor order tracking was first proposed by Albright and Qian (2001), in their paper the notion of the Gabor expansion and the Gabor transform for time/frequency analysis are introduced and the relationship between them is described. Shao et al. (2003) applied Gabor expansion to the order analysis, and compared this technique to the currently used techniques, such as the adaptive filter based approach. They mentioned that the Gabor order tracking is not only more robust and easier to implement, but also offer more insights into the physical process. Very recently, Pan et al. (2006) published a paper to objectively compare the features of the improved Gabor order tracking scheme and the VKF-OT technique, they referred that the improved Gabor order tracking performs less accurately than the VKF_OT scheme at the crossing occurrences, but without end effect in the reconstructed waveform. As OT is not exact science, it may well be that the decrease in computation time can justify the reduced accuracy. Thus, the current wave-form reconstruction order tracking techniques were surveyed, it is clear that more research need to be attached to this area.

Tuma (undated study notes) summarizes the Vold-Kalman filter in his study guide. Both the first and second generation Vold-Kalman filters are explained, and their differences are expressed clearly in terms of the mathematics. Blough (2003) points out that the key advantages of the second generation is its absolutely no frequency or slew rate limitations. Nowadays, VKF-OT is attracting more and more attention of researchers. The basic principle of the VKF-OT was published several times (Feldbauer, 2000; Tuma, 2005; Pan and Lin, 2006). The characteristics of Vold-Kalman order tracking have been presented by Herlufsen et al. (1999). Tuma (2005) further presents a paper to deal with the often-neglected issue of setting the filter pass band, which is fundamental to the theory of his MATLAB scripts. Very recently, the main principles and limitations of current order tracking methods have been summarized by Brandt et al. (2005) where the VKF-OT was also discussed as a main theme.

On the other hand, the application of VKF-OT on real equipment is still in the initial period. Few papers deal with the application of this technique. Pan and Lin (2006) present a comprehensive paper about VKF-OT. They explain the detail of the theory of VKF-OT in two different settings, namely, angular-velocity VKF-OT and angular-displacement VKF-OT. Further they examine the effectiveness of applying the theory in experimental work. It can be seen that the research in the field of VKF-OT hold significant advantages compared to other OT techniques because of these advantages. However, it should also be borne in mind that since the original VKF-OT requires longer calculation time, it is not suitable for real time processing. Quite recently however, Pan and Wu (2007) proposed an adaptive Vold-Kalman filtering order tracking approach to overcome the drawbacks of the original VKF-OT scheme for condition monitoring on this point. This makes VKF-OT a more practical and powerful tool and makes real time condition monitoring by using VKF-OT possible and feasible.

Based upon the preceding literature survey, it is not difficult to conclude that OT is a very effective tool to deal with the non-stationary vibration and noise, which vary in frequency and amplitude and is linked to a reference shaft or shafts. VKF-OT is clearly one of the best available techniques for performing OT, but needs more research on its applications and simplification for new users.

1.2.3 Thermal and chemical monitoring

a. Thermal monitoring

Generally, the limits of the maximum permissible temperature, which the insulation can withstand, are set according to the ratings of electrical machines. Indeed, the performance tests of these machines, before they leave the manufacturer's works, are dominated by the measurement of winding or embedded temperatures and the need to achieve temperature rises within the appropriate standards. The measurement of temperature therefore has an important role in the monitoring of electrical machines.

There are three basic approaches to temperature monitoring (Tavner et al., 1987):

- Measure local temperature at points in the machine using embedded temperature detectors;
- Use a thermal image, fed with suitable variables, to monitor the temperature of what is perceived to be the hottest spot in the machine;
- Measure distributed temperatures in the machine or the bulk temperatures of coolant fluids.

These approaches demonstrate the fundamental difficulty of thermal monitoring, which is resolving the conflict between the fact that temperature measurements are easy to make, but give only local information, whereas bulk temperature measurements are more difficult and run the risk that local hot spots can be overlooked.

Local temperature measurement can be done using thermocouples or resistance temperature detectors (RTD). To monitor the active part of a machine they are usually embedded in the stator windings, and in the stator core. They can also be located in the bearings, to detect hot running. Say (1976) gives some guidance to where embedded

temperature detectors (ETDs) should be fitted. The weakness of these methods is that thermocouples and RTDs are metallic devices and cannot be located on the hottest component, the winding copper, because they require electrical isolation. Alternative methods of measuring temperature on high voltage components where isolation is achieved using fibre-optic techniques. A particular design using the dependence of the polarization of light on the temperature of a material is described by Rogers (1982). The temperature measurements described so far have all been on stationary parts of the machine and on many machines the design is thermal stator critical, which means the stator is prone to reach higher temperatures than the rotor, so the hottest spot will be located there. But many machines are rotor-critical, particularly larger induction motors. In the past, there have been various crude methods of measuring rotor temperatures for experimental purposes, using heat sensitive papers or paints, or thermocouples connected through slip rings. However there has not been a method sufficiently reliable to use for monitoring purposes. Geszti (1986) described a technique using optical coupling between the rotor and a decoding unit on the stator. Siyambalapitiya et al. (1986) described a similar device for monitoring using eight thermocouples, multiplexing the signal on the rotor, and then optically coupling to the stator and decoding in a microcomputer.

Showalter (1999) states that installing a new or replacement generator requires careful consideration during installation, offline acceptance testing and increased diligence during initial start-up and operation. After replacing the first of four 132 MVA, 15 kV, 85.7 RPM Allis-Chalmers hydro-generator stators, Chelan County PUD personnel were confronted with an unexpected distribution of generator stator RTD temperatures during the initial unit start-up. A correlation was established between the location of the higher stator winding RTD readings and the region of overheating, shown on a continuous infrared thermal imaging display provided by data from a permanently installed array of fast-response, infrared sensors mounted on the rotor. The thermal map pattern provided a classic indication of circulating currents in a phase circuit. This condition is often seen in windings that have cut out coils. The generating unit operated in this condition for fewer than three weeks before a coil-to-coil jumper failed, causing a severe arc that finally went to ground, tripping the unit on a ground fault.

The thermal image technique has not received wide application on rotating electrical machines, although it deserves to. The availability of a thermal image hot-spot temperature of a machine could be used for motor protection purposes and a guide to these problems is given by Ramsden and Dring (1966) and Mellor et al. (1985). In the electrically active part of the machine, even when hot spot locations are known or hot spot temperatures can be surmised from a thermal image, there is still a desire to obtain a bulk indication of the thermal state of the machines.

b. Chemical monitoring

Both insulating materials and lubricating oils are complex organic materials which produce a very large number of chemical products in the gas, liquid and solid states when they are degraded by heat or electrical action.

Insulation degradation can be monitored chemically by detecting the presence of particulate matter in the coolant gas or detecting simple gases like carbon monoxide and ozone, or more complex hydrocarbon gases like ethylene and acetylene. Ksala (1966) describes an ion chamber specifically designed to detect the products of heated insulation and this was applied to a large turbo-generator by Carson et al. (1971; 1973). The primary

impetus for this work was the need to provide early warning of core faults, which large size turbo-generators experienced in the mid-1960s. However, the device did have some practical difficulties:

- The monitoring output fluctuates with cooling gas pressure and temperature;
- The monitor responds to oil mist which may be present in the circuit of a hydrogen-cooled machine due to faulty hydrogen seals;
- The monitor is non-specific, That is, it cannot distinguish between the materials being overheated.

A more advanced monitor, described by Wood et al. (1982), was devised to overcome the first two problems by using a differential technique. The monitor consists of two identical ion chambers in series in the gas flow line, with an inter-mediate particulate filter between them. The monitor displays the difference between the ion currents in the two chambers and thereby eliminates fluctuations due to pressure and temperature. The sensitivity of a core monitor to oil-mist can be reduced if the ion chamber is kept at an elevated temperature. Lodge (1982) suggested that an oil mist is only produced by overheating, so that its detection may be useful. For this reason he advises against the use of heated chambers. However, the amount of oil in a turbo-generator casing varies widely and can be particularly high. In this case, Carson et al. (1978) have found that there can be frequent false core monitor alarms, so the use of a heated ion chamber gives a significant advantage. In order to completely vaporize an oil mist it is necessary to raise the ion chamber temperature above $120° C$.

Many authors have advocated taking a sample of particulate material when a core monitor indicates an alarm. Wood et al. (1982) describe a method whereby the pyrolysis products are collected upon a small charge of silica gel and are then released into a gas chromatograph upon the application of strong heat. This technique is applicable only when sampling is carried out immediately upon detection of local overheating.

An alternative to detecting and analysing the particulate matter is to detect the gaseous products, such as the hydrocarbon gases or carbon monoxide and carbon dioxide in the cooling gas. Most of these chemical techniques are a very good indictor of insulation condition of windings.

This chapter outlined the motivation for on-line monitoring, discussed the transition to present technology, and described the variety of methods now in use for rotor winding and stator winding monitoring.

Chapter 2 Vold-Kalman Filter Order Tracking theory and filter bandwidth choice

2.1 Introduction

The first concept of the Vold-Kalman filter was introduced by Vold and Leuridan in 1993. Since then this new approach to order tracking has attracted increasing attention of researchers and engineers, due to its advantages over other order tracking techniques. Various researchers subsequently also developed the Vold-Kalman filter from its first generation into the second generation, which now makes it more capable of solving signal analysis problems previously intractable with other analysis techniques. The successful implementation of the present generation Vold-Kalman filter in commercial software such as MATLAB, makes it even more accessible and useful to analysts. But as far as the application of this technique, there is no one standard procedure to implement it. Analysts will also encounter the problem of understanding the theory and applying this technique.

Tuma (2005) presented a paper dealing with the problem of the filter pass band setting and a mathematical relationship between weighting factor and filter pass band. MATLAB scripts for its application are also available now. This makes the application of VKF-OT practical. But, for the application of this technique, a proper filter bandwidth still needs to be determined to suit the different monitored signals. Researchers from Brüel&Kjær (Herlufsen, Gade and Hansen, 1999) also presented a method to determine the Vold-Kalman filter bandwidth based upon experimental data. However, few papers provide a whole package of how to choose the filter bandwidth for real data with basic theory of the Vold-Kalman filter. Anyone who wants to apply this technique needs to search for the theory of Vold-Kalman filter to understand it first and then search for other relevant papers about its implementation. For this research, a complete package was established, which include Tuma's mathematical relationship between weighting factor and filter pass band that explains the background to the MATLAB software, as well as the choice of Vold-Kalman filter bandwidth from real data that suggests how to choose the filter bandwidth, based upon the monitored signal. Thus the combination of these two steps provides a clearer big picture of implementing the Vold-Kalman filter order tracking technique.

In the chapter 3, this whole application package will be tested on the simulation model, and in chapter 5, real experimental data obtained from the set-up described in chapter 4, will also be discussed in terms of its application of Vold-Kalman Filter Order Tracking.

2.2 Second generation Vold–Kalman Filter Order Tracking

2.2.1 Data equation and structural equation

Several researchers have explained the basic theory of Vold-Kalman filter. In this research, MATLAB scripts developed by Tuma will be used, hence, the basic theory proposed by Tuma (2005) will be stated in the following Vold-Kalman filter theory development. Tuma (2005) shows that the Vold-Kalman filter is based on so-called data and structural equations, with both of these equations that are excited by unknown functions on the right

hand side. In essence, Herlufsen et al.(1999) stated that the Vold-Kalman filter defines local constraints, which state that the unknown phase assigned orders are smooth and that the sum of the orders should approximate the total measured signal. The smoothness condition is called the structural equation and the relationship with the measured data is called the data equation.

The algorithm of the second generation Vold-Kalman filter directly evaluates the order by using a harmonic component envelope, which is different from the first generation Vold-Kalman filter where the order is a harmonic function which is usually expressed as:

$$x(n) = A\cos(\varpi n\Delta t + \phi) \tag{2.1}$$

where Δt is the sampling time increment ($1/f_s$), ϖ is the angular frequency and $n\Delta t$ is the discrete time, $n = 1,2,\cdots,N$.

Assuming the filter is focused at only one harmonic component, these two equations for the second generation Vold-Kalman filter can be written as,

a) The data equation

$$y(n) = x(n)e^{j\Theta(n)} + \eta(n) \tag{2.2}$$

where $y(n)$ is the measured data, $x(n)$ is a complex envelope or filtered signal, $e^{j\Theta(n)}$ is a complex carrier wave, and

$$\Theta(n) = \sum_{i=0}^{n} \varpi(i)\Delta t\,;$$

where $\varpi(i)$ is the discrete angular frequency, $\eta(n)$ is the random noise and other order components, or error term.

In matrix form the equation may be expressed as

$$\{\eta\} = \{y\} - [C]\{x\} \tag{2.3}$$

where

$$[C] = \begin{bmatrix} e^{j\Theta(1)} & 0 & 0 & 0 \\ 0 & e^{j\Theta(2)} & 0 & 0 \\ 0 & 0 & \ddots & 0 \\ 0 & 0 & 0 & e^{j\Theta(n)} \end{bmatrix}$$

The square of the error vector norm is given by

$$\{\eta^H\}\{\eta\} = \left(\{y^T\} - \{x^H\}[C^H]\right)\left(\{y\} - [C]\{x\}\right) \tag{2.4}$$

where the superscript H designates the complex conjugate.

b) The structural equation

The complex envelope $x(n)$ is the low frequency modulation of the complex wave $e^{j\Theta(n)}$. Low frequency modulation causes envelope smoothness. Locally, the envelope is approximated by a low order polynomial. This condition can be expressed by a structural equation with the non-homogeneity term $\varepsilon(n)$. The polynomial order designates the number of the filter poles. The equations for 1-, 2- and 3-pole filters are given by

$$\nabla\, x(n) = x(n) - x(n+1) = \varepsilon(n) \tag{2.5}$$
$$\nabla^2 x(n) = x(n) - 2x(n+1) + x(n+2) = \varepsilon(n) \tag{2.6}$$
$$\nabla^3 x(n) = x(n) - 3x(n+1) + 3x(n+2) - x(n+3) = \varepsilon(n) \tag{2.7}$$

For the examples $x(1) \ldots x(N)$, the structural equations (2.5), (2.6) and (2.7) take the same matrix form as

$$[A]\{x\} = \{\varepsilon\} \tag{2.8}$$

By way of example, equation (2.8) may be expanded in matrix form for the two-pole filter, $n = 1,2,\cdots,N-2 : x(n) - 2x(n+1) + x(n+2) = \varepsilon(n)$

$$\begin{bmatrix} 1 & -2 & 1 & 0 & \ldots & 0 & 0 & 0 \\ 0 & 1 & -2 & 1 & \ldots & 0 & 0 & 0 \\ \ldots & \ldots & \ldots & \ldots & \ldots & \ldots & \ldots & \ldots \\ 0 & 0 & 0 & 0 & \ldots & 1 & -2 & 1 \end{bmatrix} \begin{bmatrix} x(1) \\ x(2) \\ \ldots \\ x(N) \end{bmatrix} = \begin{bmatrix} \varepsilon(1) \\ \varepsilon(2) \\ \ldots \\ \varepsilon(N-2) \end{bmatrix}$$

The square of the error vector norm

$$\{\varepsilon^T\}\{\varepsilon\} = \{x^T\}[A^T][A]\{x\} \tag{2.9}$$

2.2.2 The global solution

Based upon the above analysis, data equation (2.3) and structural equation (2.8) are two underdetermined equations for the unknown waveform $x(n)$. There are two error terms, or additional conditions for each equation. One is the variance of the non-homogeneity terms, $\{\varepsilon\}$, and the other is the background noise and other sinusoidal components $\{\eta\}$. The global solution can be found by using the standard least squares technique to minimize the two error terms, while maintaining the given relationship between them. The weighted sum of the particular sums (2.4) and (2.9) gives the loss function

$\{J\} = r^2\{\varepsilon^T\}\{\varepsilon\} + \{\eta^T\}\{\eta\}$, or

$$\{J\} = r^2 \{x^T\}[A]^T[A]\{x\} + (\{y^T\} - \{x\}^H[C]^H)(\{y\} - [C]\{x\}) \tag{2.10}$$

where r is the weighting factor.

The first derivative of the loss function (2.10) with respect to the vector $\{x\}$ gives a condition for the minimum of this function, which is called a normal equation. Thus $\{x\}$ can be solved for by using

$$\frac{\partial J}{\partial x^H} = \left(r^2[A^T][A] + [E]\right)\{x\} - [C^H]\{y\} = 0 \tag{2.11}$$

which leads to a solution

$$\{x\} = \left(r^2[A]^T[A] + [E]\right)^{-1}[C^H]\{y\} \tag{2.12}$$

2.2.3 Relationship between weighting factor r and filter bandwidth

The following part is to find the relationship between weighting factor r and filter bandwidth, the approximate mathematical equations between them were made and thereafter MATLAB scripts were compiled accordingly, as a result, the Vold-Kalman filter application is practical in MATLAB. This part was abbreviated from Tuma (2005) and Tuma (undated study notes). In order to simplify the discussion, equation (2.12) can be written as

$$\{x\} = [B]^{-1}[C^H]\{y\} \tag{2.13}$$

where $[B] = r^2[A]^T[A] + [E]$ and noticing that $[A]$ is a known matrix for a given number of filter poles.

From equation (2.13), it is easy to find that matrix $[B]$ is a symmetric positive definite matrix. The matrix $[B]$ consists of the limit number of the non-zero diagonals. Employing the Cholesky factorisation of the matrix [B] into the matrix product $[B] = [L] \times [U]$, where $[L]$ is a lower triangular matrix and $[U] = [L]^T$ is an upper-triangular matrix, is the easiest way to solve equation (2.11). The only condition for the Cholesky factorisation is that all the main minor determinants are equal to a positive value what can be easily proved.

Based on the Cholesky factorisation method, equation (2.13) can be rewritten as

$$[B]\{x\} = \{Y\}, \text{ or } [L][U]\{x\} = \{Y\} \tag{2.14}$$

where $\{Y\} = [C^H]\{y\}$, $[B] = [L] \times [U]$, $[\mathrm{L}] = [\mathrm{U}]^{\mathrm{T}}$.
Substitution of $[U]\{x\} = \{z\}$ gives $[L]\{z\} = \{Y\}$ (2.15)
from which the solution
$\{z\} = [L]^{-1}\{Y\} \Rightarrow \{x\} = [U]^{-1}\{z\}$ (2.16)
follows.

To simplify the calculation process, it should be noted that except for the first and last p (number of filter poles) rows of the matrix $[B]$, all the other diagonal elements are identical. To make Tuma's explanation here more clearer to understand, let's make an example, assuming a simple measurement of 6 points, that is $x(1)\ldots x(6)$, a two pole filter was used, weighting factor r = 1000000, matrix $[B]$ can be written as

$$[B]=r^2[A]^T[A]+E=10^{12}\times\begin{bmatrix}1&-2&1&0&0&0\\-2&5&4&1&0&0\\1&-4&6&-4&1&0\\0&1&-4&6&-4&1\\0&0&1&-4&5&-2\\0&0&0&1&-2&1\end{bmatrix}$$

where $[A]=\begin{bmatrix}1&-2&1&0&0&0\\0&1&-2&1&0&0\\0&0&1&-2&1&0\\0&0&0&1&-2&1\end{bmatrix}$.

Therefore, it is possible to simplify the index of these matrix elements
Forward reduction $\{z\}=[L]^{-1}\{Y\}=[U]^{-T}\{Y\}$ under condition

$$u_0=\lim_{j\to\infty}u_{j,j},u_1=\lim_{j\to\infty}u_{j,j+1}\cdots u_p=\lim_{j\to\infty}u_{j,j+p} \qquad (2.17)$$

where $u_{j,j}$ is the diagonal element of matrix $[U]$, u_0 and u_1 are the values of matrix $[U]$.

so that the transfer function in the z-domain now becomes

$$H(z)=\frac{Z(z)}{Y(z)}=\frac{1}{u_0+u_1z^{-1}+\cdots+u_pz^{-p}} \qquad (2.18)$$

Again, to make Tuma's explanation of this z-domain transformation process more clear, Abbreviated Z -transform table was listed in Table 2.1:

Table 2.1 Z-transform table

$x(t)$	$x(z)$
$\delta(t-kT)=1$	z^{-k}

(2.19)

Taking into account the reverse order of the samples $x(N)\ldots x(1)$ in the backward substitution, the filtering process is based on the same transfer function as for the forward reduction. The Vold-Kalman filter transfer function is equal to the square of the transfer function (2.18). Substituting the complex quantity z by the term $e^{j\Omega}$, where $\Omega=\varpi\Delta t$ for $\Omega\in(-\pi,\pi)$, the equation for the –3dB cut off frequencies Ω_L (low pass) and Ω_H (high pass) is obtained. Thus

$$\left|H\left(e^{j\Omega}\right)\right|^2 = \left|\frac{1}{u_0 + u_1 e^{-j\Omega} + u_2 e^{-j2\Omega} + \ldots + u_p e^{-jp\Omega}}\right|^2 = \frac{1}{\sqrt{2}} \qquad (2.20)$$

For the case of a one-pole filter, the values of the elements of the matrix $[B]$ are given by

$$b_0 = b_{j,j} = 2r^2 + 1$$
$$b_1 = b_{j,j+1} = b_{j,j-1} = -r^2 \qquad (2.21)$$

where $b_{j,j}$ is the diagonal element of matrix $[B]$, b_0 and b_1 are the values of matrix $[B]$. Cholesky factorisation of $[B]$ results in

$$u_{j-1,j} = b_{j-1,j} / u_{j-1,j-1}$$

$$u_{j,j} = \sqrt{b_{j,j} - u_{j-1,j}^2} \qquad (2.22)$$

if $j \to \infty$ then the previous formulae turn to

$$u_1 = \frac{b_1}{u_0}$$
$$u_0 = \sqrt{b_0 - u_1^2},$$

it follows that

$$u_0 u_1 = b_1$$
$$u_0^2 + u_1^2 = b_0 \quad . \qquad (2.23)$$

so that substituting (2.21) into (2.23), u_0 and u_1 can be expressed by using coefficient r, from equation (2.20)

$$\left|G\left(e^{j\Omega}\right)_{LP}\right|^2 = \left|\frac{1}{u_0 + u_1 e^{-j\Omega}}\right|^2 = \frac{1}{\sqrt{2}} \Rightarrow r = \sqrt{\frac{\sqrt{2}-1}{2(1-\cos(\pi\Delta f))}} \qquad (2.24)$$

where the relative bandwidth Δf with respect to the Nyquist frequency is given by the formula

$$\Delta f = \frac{f_H}{f_s/2} \qquad (2.25)$$

with f_H the filter bandwidth (low pass filter) and f_s the sampling frequency. Two or three pole filters are similarly derived to the above, and the final result is that a relationship between the relative bandwidth Δf and the weighting factor r can be found. Then using equation (2.16) the final filtered data result can be obtained.

So far the basic theory of the Vold-Kalman filtering method as well as relationship between filter bandwidth and weighting factor were explained. It can be seen from this example that if Δf can be set, the proper weighting factor r can be determined by equation (2.24) or other equations for other kinds of filter. They are listed in Table 2.2

Table 2.2 Weighting factor as a function of the bandwidth (Tuma, 2005)

Number of poles	Solution of the equation	Approximation
1	$r = \sqrt{\frac{\sqrt{2}-1}{2(1-\cos(\pi\Delta f))}}$	$r \approx \frac{0.2048624}{\Delta f}$
2	$r = \sqrt{\frac{\sqrt{2}-1}{6-8\cos(\pi\Delta f)+2\cos(2\pi\Delta f)}}$	$r \approx \frac{0.00652097315}{\Delta f^2}$
3	$r = \sqrt{\frac{\sqrt{2}-1}{20-30\cos(\pi\Delta f)+12\cos(2\pi\Delta f)-2\cos(3\pi\Delta f)}}$	$r \approx \frac{0.020756902}{\Delta f^3}$

Therefore the choice of the weighting factor is determined by the choice of filter's bandwidth. In order to make the relationship between filter bandwidth Δf and weighting factor r clearer, Figure 2.1 was developed:

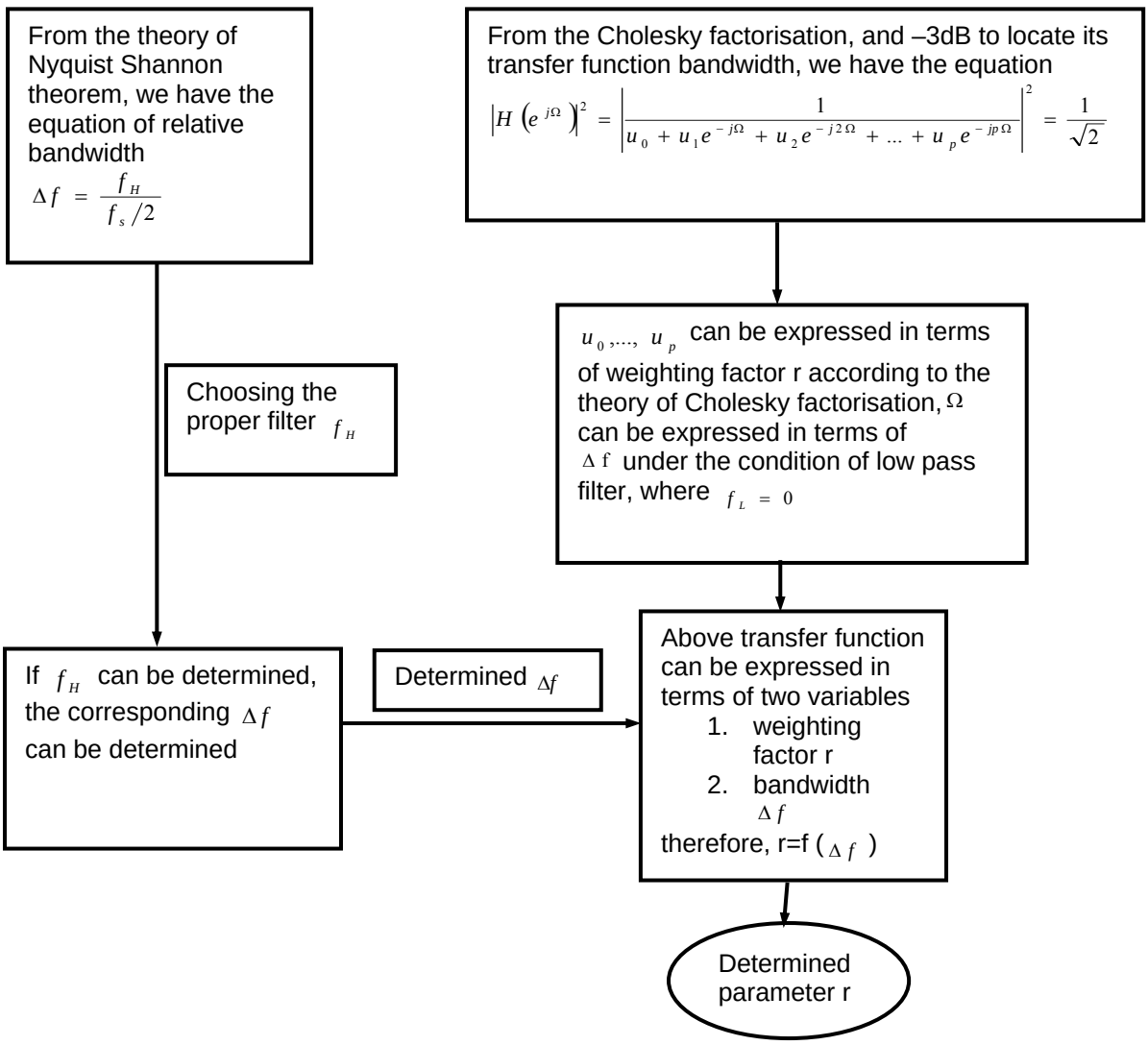

Figure 2.1 Relationship between weighting factor r and filter bandwidth Δf

2.3 Choosing the Vold-Kalman filter bandwidth

From the above analysis, it is clear that a proper Vold-Kalman filter bandwidth must be chosen before performing the Vold-Kalman filter order tracking. In order to choose the proper bandwidth of the Vold-Kalman filter, firstly, the time response of Vold-Kalman filters will be examined, so that a method of choosing the filter bandwidth can be derived. Herlufsen et al. (1999) did research to investigate the different filters' ability to follow amplitude changes. They applied a tone burst with a certain duration to a Vold-Kalman filter with a fixed centre frequency (Figure 2.2). The result shows that for one, two and three pole Vold-Kalman filters, nearly the same characteristic applies in the upper 25dB, which means their behaviour in terms of how fast the different filters can follow amplitude changes of orders is nearly identical. To make this idea clear, 25dB line was drawn in Figure 2.2, it is clear that above this 25 dB line, three filters exhibit nearly the same characteristics.

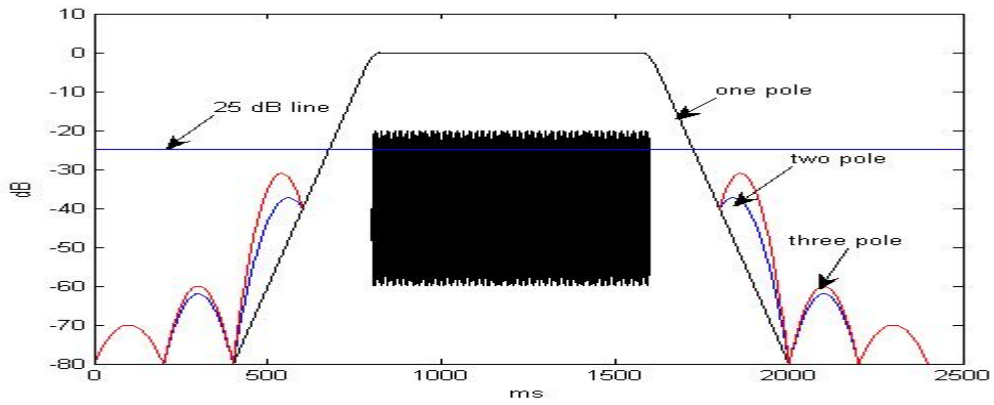

Figure 2.2 Tone burst for one, two and three pole filter (adapted from Herlufsen, 1999)

Further, they use one pole filter for 3 different choices of filter bandwidth (2 Hz, 4 Hz, 8 Hz), see Figure 2.3

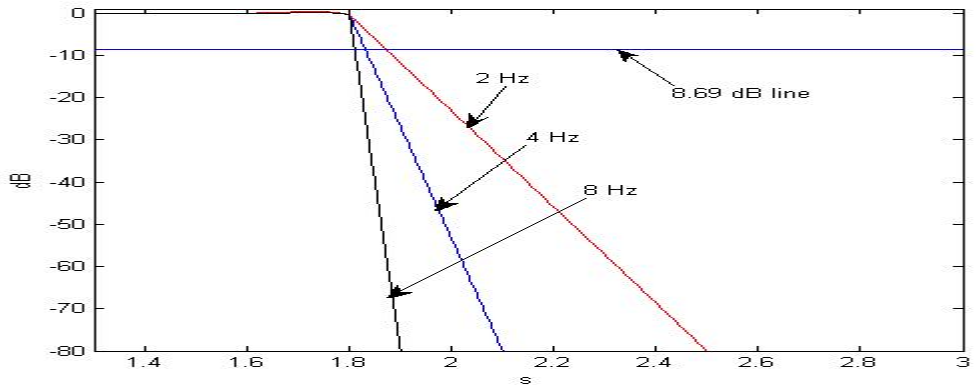

Figure 2.3 One pole filter for different choices of filter bandwidth (adapted from Herlufsen, 1999)

They conclude that the decay time is inversely proportional to the bandwidth as can be seen in Figure 2.3, besides, the slope of the early decay for one, two and three pole filters are similar as can be seen in Figure 2.2, therefore an important time-frequency relationship can be extracted for all three types of Vold-Kalman filters:

$$B_{3dB} \times \tau = 0.2 \tag{2.26}$$

where B_{3dB} is the 3dB bandwidth of the Vold-Kalman filter and τ is the time it takes for the time response to decay 8.69dB, this line was also drawn in the Figure 2.3.

Selection of the filter bandwidth is basically a compromise between having a bandwidth which is sufficiently narrow to separate the various components in the signal and a bandwidth, which is sufficiently wide, giving a short filter response time in order to follow the changes in the signal amplitude. Herlufsen et al. (1999) further state that various research tests have shown that when orders are going through a resonance, the time constant of the filter τ should be shorter than 1/10 of the time T_{3dB} it takes for the particular order to sweep through the 3dB bandwidth of the resonance Δf_{3dB} This ensures an error of less than 0.5dB of the peak amplitude at the resonance using one-pole filter. For two-and three-pole filters the error of the measured peak will be less.

2.3.1 Filter time constant factor

For the time constant of the filter, the following relationship may therefore be used according to above argument:

$$\tau \leq 0.1 \times T_{3dB} \tag{2.27}$$

or in terms of the bandwidth of the filter from equation (2.26):

$$B_{3dB} = 0.2 / \tau \geq 2 / T_{3dB} \tag{2.28}$$

where T_{3dB} is the time it takes a particular order to pass through the 3dB bandwidth of the resonance, and B_{3dB} is the 3dB bandwidth of the filter.

2.3.2 Slew rate factor

The time it takes for order number k to sweep through the 3dB bandwidth is:

$$T_{3dB} = \frac{\Delta f_{3dB}}{k \times SR_{Hz}}$$

or

$$T_{3dB} = \frac{60 \times \Delta f_{3dB}}{k \times SR_{RPM}} \tag{2.29}$$

where SR_{Hz} and SR_{RPM} are the sweep rates in Hz/s and RPM/s, respectively. This means that the bandwidth B_{3dB} of the Vold-Kalman filter extracting order number k should follow:

$$B_{3dB} \geq \frac{2 \times k \times SR_{Hz}}{\Delta f_{3dB}}$$

or

$$B_{3dB} \geq \frac{k \times SR_{RPM}}{30 \times \Delta f_{3dB}} \tag{2.30}$$

where Δf_{3dB} is the 3dB bandwidth of the resonance.

2.3.3 System damping condition to determine Δf_{3dB}

From equation (2.30), it can be seen that Δf_{3dB} need to be determined in order to acquire B_{3dB} of Vold-Kalman filter. Heyns (2003) mentions the equation to determine the bandwidth based upon resonance and damping factor, from which Δf_{3dB} can be estimated by

$$\Delta f_{3dB} = 2 \times \xi \times f_n \tag{2.31}$$

where $\xi = C/C_c$, C is the damping coefficient, C_c is the critical damping coefficient and f_n is the natural frequency. Thus the 3dB bandwidth of the resonance can be approximately determined from equation (2.31).

Although the above method is a good method to determine the minimum bandwidth of the Vold-Kalman filter, it still has its limitations. Firstly, since the resonance of the structure usually cannot readily be determined for a real machine, it is a barrier to implement the above procedures to determine the Vold-Kalman filter bandwidth. Under such a condition, a preliminary study of the acquired data can be performed in advance, for instance time-frequency domain data analysis, so that the basic characteristics of the system can be approximately obtained (resonance of system). Secondly, the structure cannot always be treated as lightly damped structure. As a result, the equation (2.31) will not always be valid to estimate so-called 3dB bandwidth of the resonance. In this case, experience is much more important to estimate the filter's bandwidth. In short, choosing a proper bandwidth for the Vold-Kalman filter, some prior information is essential for proper implementation of this technique. This is critical to the implementation. The example in Chapter 3 will theoretically explain this in detail on a simulation model. Finally, Figure 2.4 summarises the procedures for selecting the Vold-Kalman filter bandwidth.

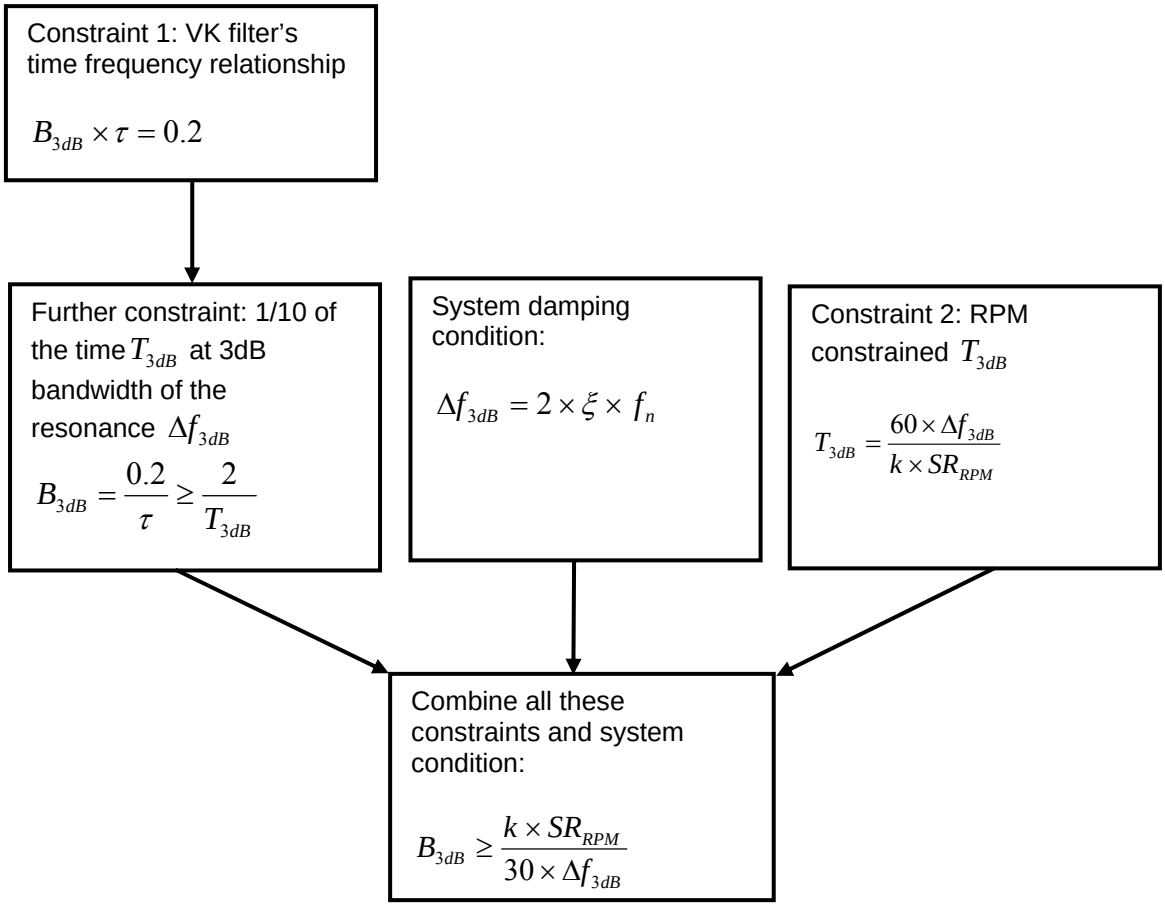

Figure 2.4 Choosing Vold-Kalman filter bandwidth

2.4 Conclusion

In this chapter, a whole package of Vold-Kalman filter application procedures for the selection of filter parameters was presented. Firstly, the basic theory of the Vold-Kalman filter as was introduced by Tuma was explained. The mathematical relationship between the weighting factor r and the relative filter bandwidth was then explored. This forms the basis of the working algorithm of the MATLAB scripts that are used in the Vold-Kalman filtering applications in the following chapters. Secondly, one kind of filter bandwidth choice method was introduced and a mathematical equation also provided, which was established by Herlufsen et al. (1999). Two mind maps for these two parts were developed for the convenience of analysts. Thus a complete package for Vold-Kalman filter choice theory was established.

2.5 Scope of work

Based upon the literature survey presented in chapter 1, bigger picture of condition monitoring techniques as they are applied to electrical machinery, could be obtained. Among these techniques, vibration analysis is proved to be a reliable and practical method.

Within the context of vibration monitoring, the order tracking technique is no doubt overcoming several disadvantages of traditional monitoring methods. It is clear that a specific method –Vold-Kalman filter- makes order tracking even more capable than before. It is also realized from its literature survey that the theory of this capable technique has been available for a long time, but its application to real system remained inaccessible to analysts. This has inhibited the practical exploration of the technique. And only a few papers deal with the abilities of VKF-OT in condition monitoring.

To enhance the understanding of VKF-OT, a simple simulated system with known characteristics is needed to investigate the effect of Vold-Kalman filter parameters. A simple experimental set-up is also required for controlled condition monitoring equipments. This leads to the current research.

Thus, this research presents a MATLAB based simulation model of rotating electrical machinery. By changing the physical parameters to simulate different characteristics of the system, and by suggesting an external excitation force model, which captures typical electrical machine characteristics, the simulation model becomes suitable to experiment with aspects of the application of the Vold-Kalman filter on a known system.

Further, based upon the simulation model, an experimental set-up was established and artificially seeded faults were monitored on a real electrical alternator by using VKF-OT and other conventional order tracking techniques. A comprehensive comparison was made between different order tracking techniques, and the ability of VKF-OT on condition monitoring was demonstrated.

The structure of the dissertation is summarized in Figure 2.5

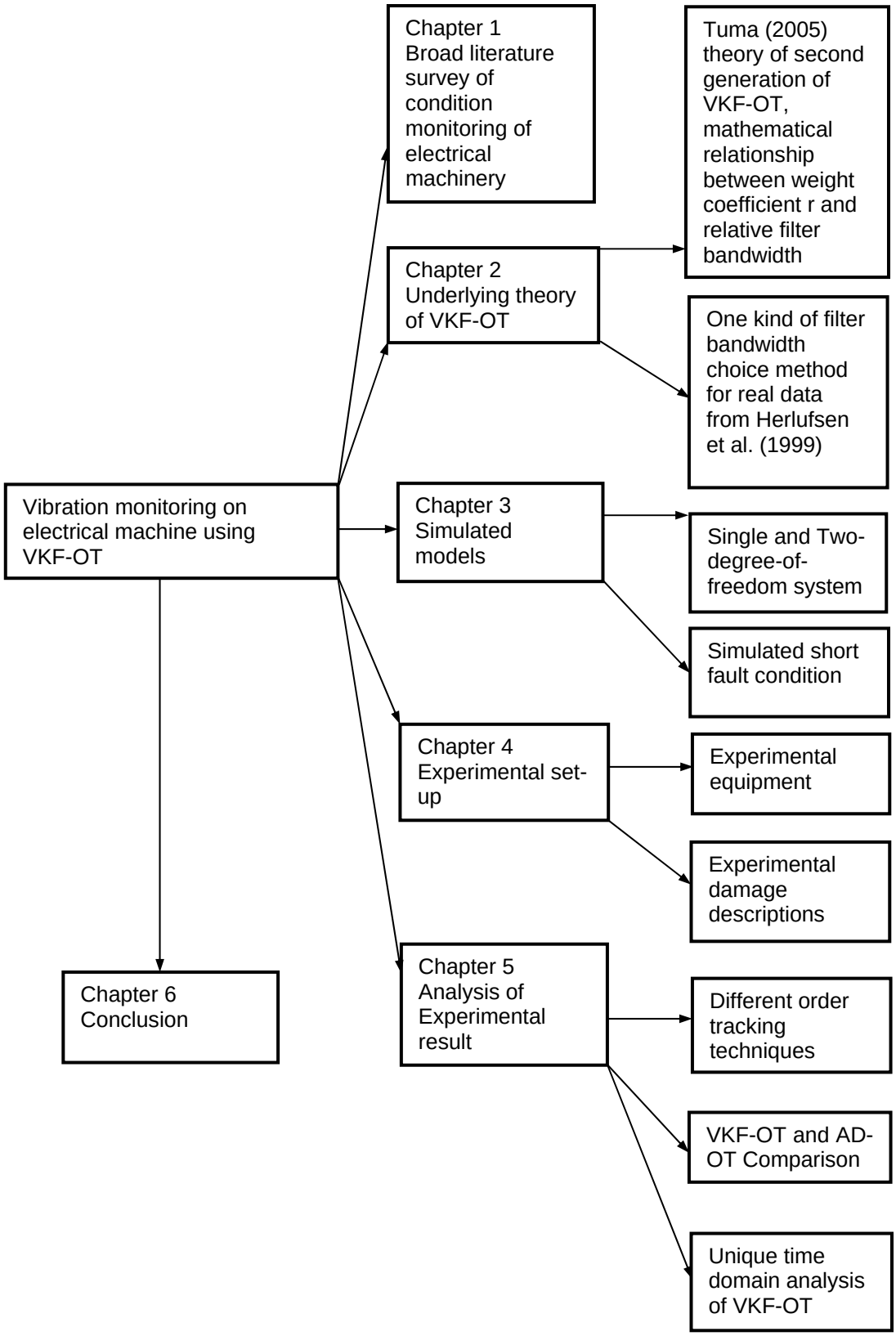

Figure 2.5 Flow diagram for the whole dissertation

Chapter 3 Rotor system simulation study

3.1 Introduction

Rotating electrical machines are complex equipment, because of the electromagnetic field between the rotor and stator, the associated electrical wiring and the mechanical support structures. To simulate such a complex system in detail is not an easy task. In order to gain experience in the implementation of the Vold-Kalman filter order tracking technique in the rotating machine environment, it is appropriate to first construct and then study a simple and well-known system. For this reason, this chapter presents a simulation study in which the entire response of the system under consideration is known. This provides an environment in which the effects of the Vold-Kalman filter characteristics can be investigated, while one has the advantage of full understanding of the system.

Heyns (1989) presented a simplified simulation study of the transient dynamic response of rigid rotors mounted on flexible bearings. In his paper two different models for the lateral response of such systems are presented and applied to study the behaviour of a rotor system, which is subjected to sudden unbalance. Because of its simplicity, this model was adopted and further developed to suit the rotating electrical machines considered in this work. The major difference of this new model with Heyns's rotor models is the addition of more appropriate simulated external excitation forces. In Appendix 1, the external excitation forces for an electrical machine are discussed and a force model is presented.

Using the rotor model, various aspects of the Vold-Kalman filtering process are explored. Filter bandwidth choices, filtered out order signal frequency analysis as well as the resonance effect on Vold-Kalman filter data analysis, are discussed. Finally the use of Vold-Kalman filter time domain analysis for monitoring is attempted, under simulated damage conditions. For this purpose the crest factor, kurtosis value and RMS value are used.

The two simplified models for the Vold-Kalman filter investigation are now presented.

3.2 Single-degree-of-freedom system model

3.2.1 Single-degree-of-freedom system modelling

The first model treats the lateral response of a symmetric rotor as two uncoupled single-degree-of-freedom systems depicted in Figure 3.1. It is assumed that the rotor of mass M is mounted on bearings of total stiffness K and damping coefficient C, in both x-and y-directions. The rotor is assumed to rotate at increasing speed. The external excitation forces described in Appendix 1 are sinusoidal force combinations. In this simulation, order terms 1, 2, 3 and 4 are included in the excitation forces (see Table A1.1 in Appendix 1). The arbitrary system characteristics that will be used for this investigation are listed in Table 3.1.

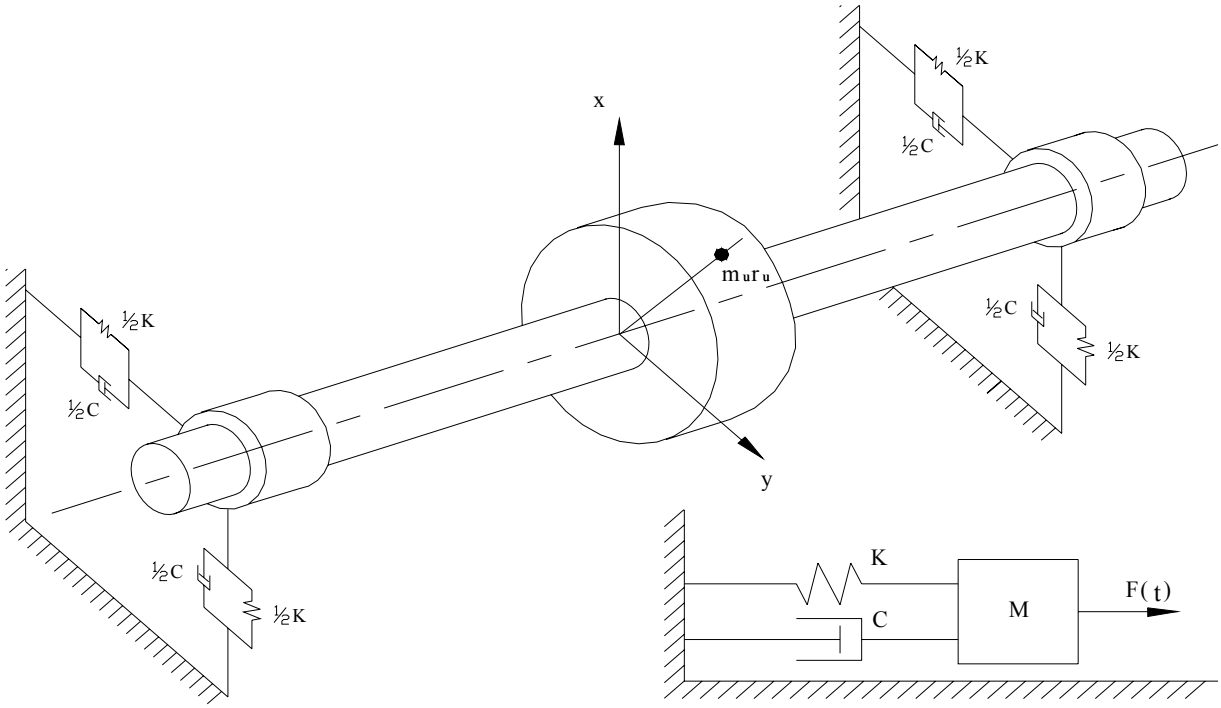

Figure 3.1 Simple symmetric rotor single-degree-of-freedom system

Table 3.1 System characteristics

Parameter	**Value**
Stiffness K	500000 N/m
Rotor mass M	50 kg
Eccentricity r_u	0.1 m
Unbalance mass m_u	0.05 kg
Damping coefficient C	200 Ns/m
Initial time t_0	0 s
Final time t_f	5 s
Time steps	4096
RPM slew rate	200 rpm/s

It can easily be seen that it is simple to tune different parameters of the system in MATLAB. Some critical parameters must be commented on here. Mass and stiffness are two important parameters that will determine the resonance frequency of the system and proportional to the square root of K/M. This system resonance frequency will influence the choice of the Vold-Kalman filter bandwidth. Besides, the damping of system will also influence the choice of the Vold-Kalman filter (see Figure 2.4 in chapter 2). Tuning these three parameters will help in the understanding of the influence of resonance and damping on choosing the appropriate Vold-Kalman filter bandwidth. Further, the excitation forces can be arbitrarily generated in MATLAB. This is the one of biggest advantages of this simulation model, because it makes it possible to include as many orders as desired, as well as simulate any other noise or forces that might exist in real cases. The Runge-Kutta-Gill method was used to integrate the equations of motion for the simulated models.

3.2.2 Equations of motion for the single-degree-of-freedom system

In this rotor model simulation, the viscously damped case is considered and discussed in the following.

Assuming viscous damping the equation of motion is given by

$$M\ddot{X}(t)+C\dot{X}(t)+KX(t)=F(t) \tag{3.1}$$

where $X(t)$ is the system response in x direction, $F(t)$ is the simulated external excitation forces functions, which is developed in Appendix 1. The mathematical expression of simulated force used in the following simulation study can be written as:

$$F(t)=m_u\varpi^2 r_u \sin(\varpi t)+m_u\varpi^2 r_u \sin(2\varpi t)+m_u\varpi^2 r_u \sin(3\varpi t)+m_u\varpi^2 r_u \sin(4\varpi t)$$

where $\varpi=\dfrac{d\theta}{dt}$ is the angular velocity of rotor.

3.2.3 Single-degree-of-freedom system analysis

The system lateral acceleration response under the given external excitation force function in time domain can be calculated as in Figure 3.2.

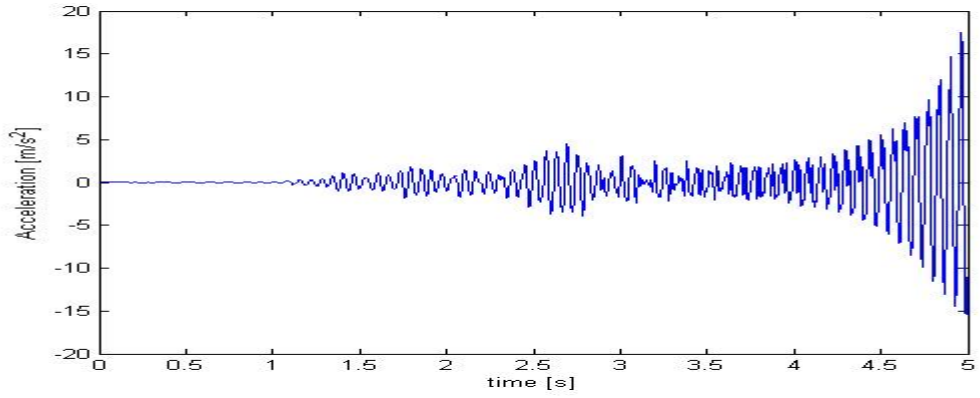

Figure 3.2 System response in x direction

Based upon the choice of the system parameters and external excitation force function, results of the system response can be anticipated. Due to the resonance, there must be a peak at 15.9 Hz in the corresponding spectrum. This can be determined from equation (3.2),

$$f = \frac{1}{2\pi}\sqrt{\frac{K}{M}} \tag{3.2}$$

while orders 1, 2, 3 and 4 due to the external forces must also appear in the response spectrum. In order to see the information in the system response signal clearly, and confirm these expectations, the RPM spectrum map was plotted as shown here in Figure 3.3.

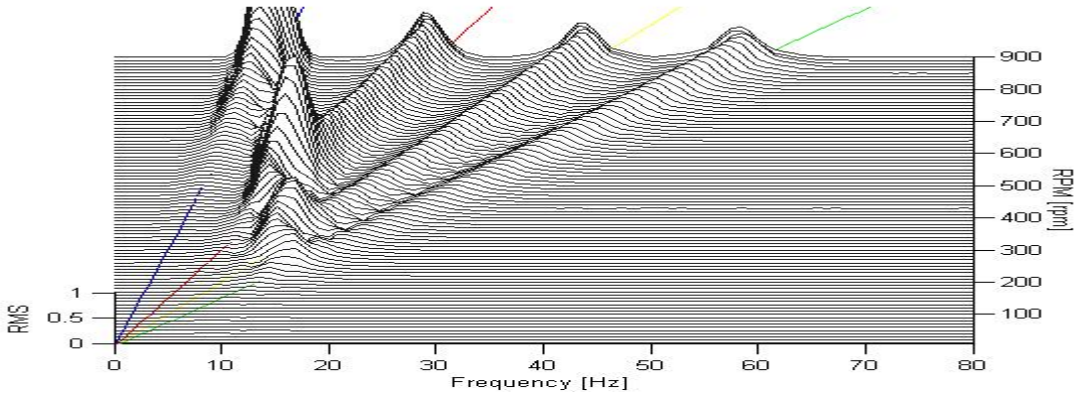

Figure 3.3 RPM spectrum map for system response

Figure 3.3 shows a resonance at 15.9 Hz, which does not change with speed. The order related peaks are marked with blue, red, yellow and green lines, corresponding to orders 1, 2, 3 and 4 respectively.

3.2.4 Vold-Kalman filter application

After obtaining the system response, the order information can now be extracted. Based upon the analysis of chapter 2, the Vold-Kalman filter bandwidth can be determined via the system resonance, damping and the slew rate of the rotor, as was described in Figure 2.4. From equation (2.31), the 3dB bandwidth for the resonance peak can be calculated as

$$\Delta f_{3dB} = 2 \times \xi \times f_n = 2 \times 0.02 \times 15.9 = 0.636 \text{ Hz}$$

where $\xi = \frac{C}{C_C}$, $C_C = 2M\sqrt{K/M}$.

From equation (2.30) the minimum filter bandwidth of order 1 should be chosen as

$$B_{3dB/order1} \geq (k \times SR_{RPM})/(30 \times \Delta f_{3dB}) = (1 \times 200)/(30 \times 0.636) = 10.5 \text{ Hz}$$

By the same token, the minimum filter bandwidth of orders 1, 2, 3, and 4 can be tabulated as in Table 3.2.

Table 3.2 3dB filter bandwidths for orders 1 to 4

Order	Bandwidth [Hz]
1	10.5
2	20.9
3	31.4
4	41.9

In the MATLAB implementation, the script `vktime.m` (MATLAB Vibratools, 2005) will be used to filter the order signal. In this program, several parameters need to be input in the command line -sampling frequency, RPM vector, order to track, type of bandwidth, and bandwidth. Among them, only type of bandwidth and bandwidth are not known yet. Based on ideas presented by Herlufsen et al. (1999), the Vold-Kalman filter bandwidth can be specified in terms of a constant frequency bandwidth or proportional bandwidth. Constant bandwidth is an absolute bandwidth value, but it has its limitations since the filter bandwidth cannot change as the rotating speed varies. Proportional bandwidth is the best choice when analysing over wide RPM ranges or when analysing higher orders. This is so because the proportion of the instantaneous absolute filter bandwidth value to the instantaneous rotating speed frequency is fixed, but during the filtering process, the absolute value of filter bandwidth is varying with the rotating speed increasing or decreasing. From arguments above, it is better to use proportional bandwidth instead of absolute bandwidth for this run-up simulation over a wide range of RPM. In this case, the minimum filter bandwidth values have been calculated as in Table 3.2, thus, percentages of these absolute bandwidth values to resonance frequency (rotating speed frequency at resonance) can also be calculated, in table 3.3

Table 3.3 Minimum proportional bandwidth for orders 1 to 4

Order	Minimum bandwidth percentage
1	65.8%
2	131.6%
3	197.4%
4	263.2%

It is interesting to see that the percentage values for orders 2, 3 and 4 are higher than 100% in Table 3.3. In other words, in this case, the filter bandwidth required to ensure filtering out of the correct amplitude, will be larger than the rotating frequency itself. But Herlufsen et al. (1999) indicated that using a bandwidth of more than 100% cause ripples due to beating interference between orders, even with a three-pole filter. So if the percentage value is beyond 100%, it should be adjusted back less than or equal to 100%. Obviously, at least to some extent, one then loses the correctness at the resonance peak

amplitude, and a compromise is needed between having correctly filtered data at the resonance frequency and avoiding beating interference from other orders.

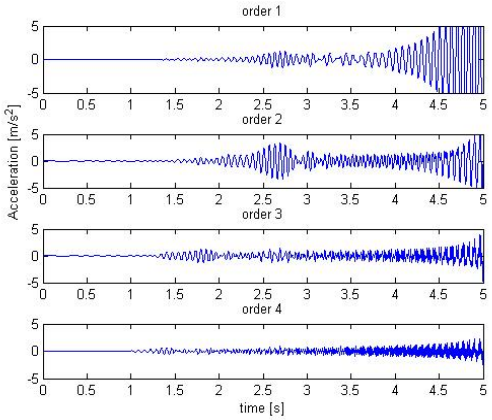

a. Filtered orders waveforms

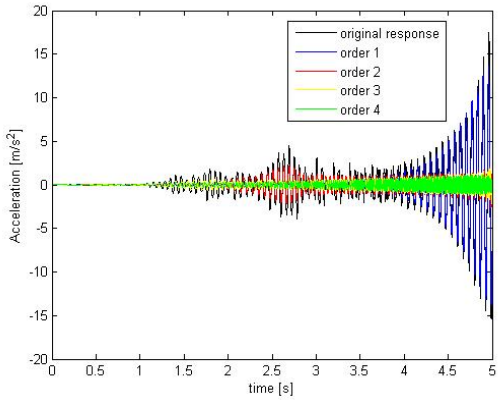

b. Order waveforms and original waveform

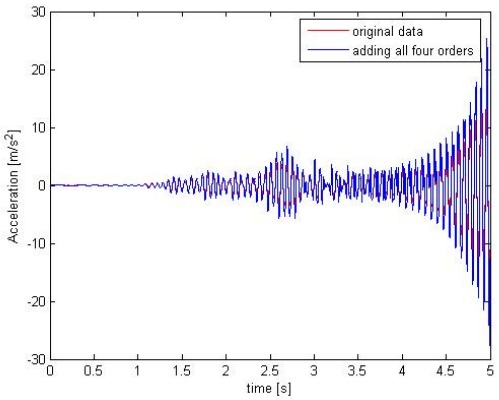

c. Adding all four orders and original data

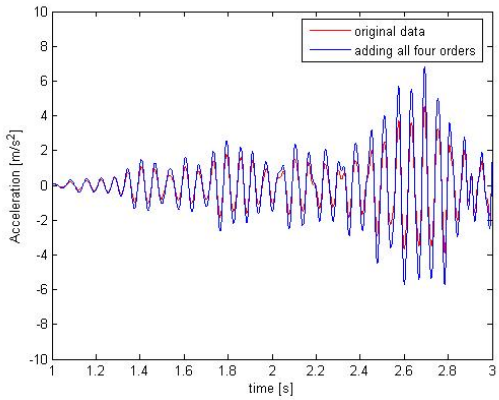

d. zoom in

Figure 3.4 Filtered out order signal in time domain

For convenience we here choose the Vold-Kalman filter proportional bandwidth for each of these 4 orders as 66%. The result is as in Figure 3.4 (a). From Figure 3.4 (a), some observations can be made. Firstly, orders 1 and 2 are higher in amplitude than orders 3 and 4. This is caused by the resonance. If one changes the parameters of the physical system to increase the resonance frequency and influence the higher orders, the amplitude of the filtered signal will correspondingly increase for the higher orders. It can be observed that the waveform shapes are different for the four orders, but all of them appear to feature high amplitude at about 2.6 s, which is the time when resonance occurs. Figure 3.4 (b) is the superimposed figure for all the orders with the original response. If further adding all 4 order waveforms together in the time domain and then comparing the result to Figure 3.2 in the time domain, Figure 3.4 (c) follows. This Figure shows that a fairly good match between the added data and the original data is obtained. After zooming in over a shorter period as in Figure 3.4 (d), it can be seen that the added data is slightly higher than the original data. This is due to the choice of filter bandwidth. In this case 66% filter bandwidth was used for all orders as was discussed above. For the filtering process, a high filter bandwidth can ensure the accuracy of the order amplitude, but it also introduces the interference from other orders, thus it will give rise to this effect. If choosing different filter bandwidths for different orders properly, the added data can approach the original data as closely as possible, but it is a fine-tuning process.

After filtering the orders from the original response, one may ask questions such as: Is this filtered order 1 the real order 1 signal and can this be demonstrated? How do the physical characteristics and filter bandwidth influence the results? Are there some methods that might control the effect of resonance? The simulation model provides ways to solve and better understand these problems.

A frequency analysis of each of the filtered orders and the original response signal renders the following power spectral densities (PSDs) in $m^2/(Hz \cdot s^4)$.

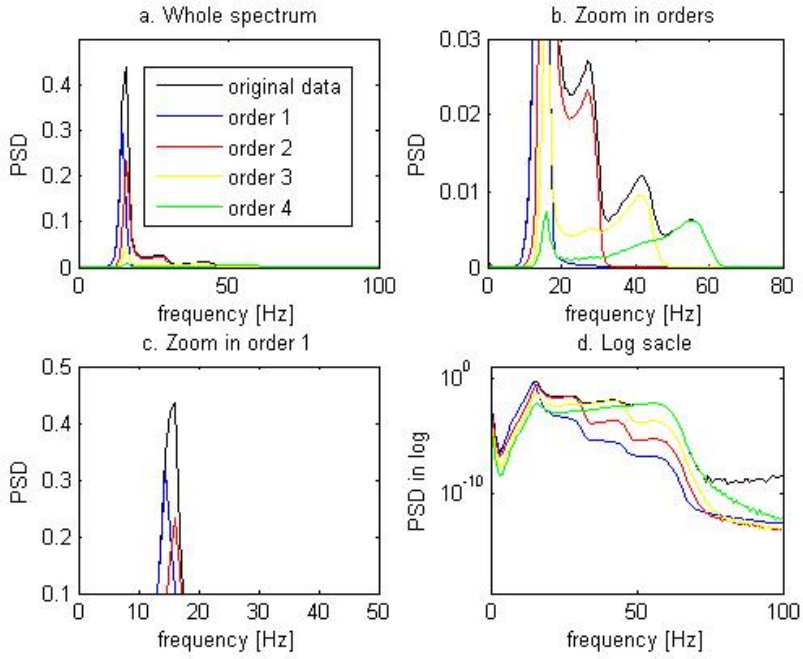

Figure 3.5 Frequency analysis of each order and system response

Figure 3.5 (a) is the whole spectrum for the original response and the separate orders. From this figure, the order 1 and 2 curves are much higher than the other two orders. This corresponds very well to Figure 3.4 (a). Since the resonance peak is very high in Figure 3.5 (a), a log scale figure was plotted as in Figure 3.5 (d). From prior knowledge (and from Figure 3.3), we know that this system has one resonance at 15.9 Hz and 4 orders. These characteristics can also be seen from Figure 3.5 (d). If examining the peak details of order 1 (blue curve) and original response resonance (black curve at 15.9 Hz), the two peaks look like one peak, but they are still different (see Figure 3.5 (c) black and blue curves). From Figure 3.5 (c), order 1 should both appears a resonance peak at 15.9 Hz and an order peak, this can be clearly seen from other order curves. For example, order 4 (green curve in Figure 3.5 (d)), features two peaks at 15.9 Hz, which are at the resonance and around 56 Hz, which is the order peak. But in Figure 3.5 (c) the blue curve does not display the resonance peak, one of the possibilities of this effect is because of the large damping coefficient $C = 200$ Ns/m. A comparison can be made by choosing $C = 20$ Ns/m.

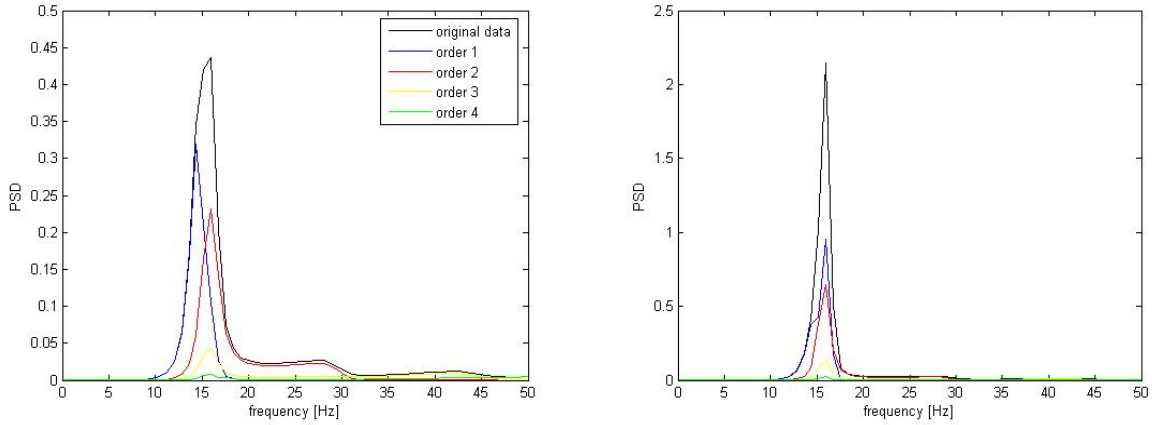

a. $C = 200$ Ns/m b. $C = 20$ Ns/m

Figure 3.6 Different damping values ($C = 200$ Ns/m and $C = 20$ Ns/m)

On Figure 3.6 (b), one can still not see two clear peaks, but this time the higher peak of order 1 switches to the resonance frequency, this is because of the small damping of the system. In addition, the amplitude of original response (black curve) nearly increased 5 times. Hence, Figure 3.6 (b) does still not give a satisfactory result to see the expected two peaks. But it clearly indicates the effect of damping on the filtered data. It is clear that by tuning the damping only is not enough to distinguish the two peaks in this case.

Further the filter bandwidth will also influence the detail of the spectrum. In the following two graphs different filter bandwidths (66% and 20%) are compared for the same $C = 200$Ns/m .

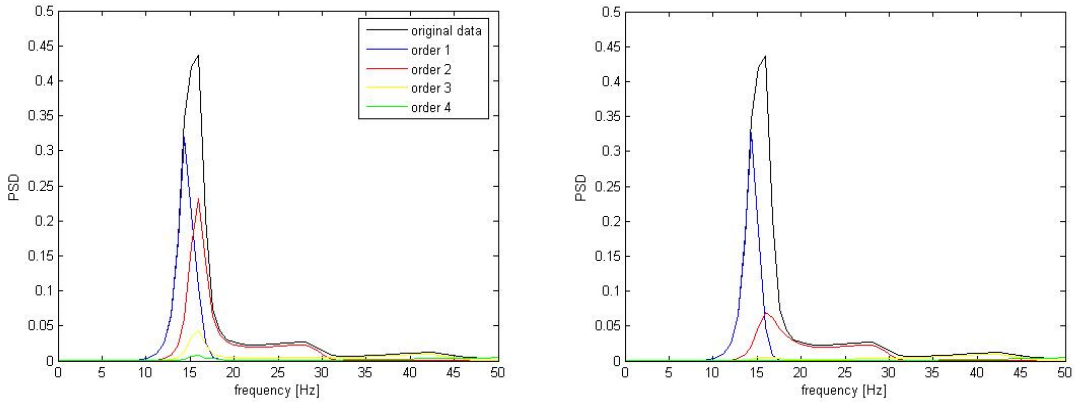

a. 66% filter bandwidth b. 20% filter bandwidth

Figure 3.7 Different filter bandwidths (66% and 20% bandwidths)

From Figure 3.7 (b), it is clear that the 20% filter bandwidth cannot distinguish the two peaks either. As may be expected, all of these orders drop in amplitude due to the decrease of filter bandwidth to 20%. But, in this case, while order 1 does not drop too much in amplitude, orders 2, 3 and 4 decrease tremendously. This means that the filter bandwidth of 20% is too narrow for the higher orders.

The previous experience shows that by tuning only damping or filter bandwidth cannot achieve satisfactory results for this simulated system. If however both the damping coefficient and filter bandwidth are tuned (changed to $C = 20$ Ns/m and filter bandwidth =

20%,) the result is encouraging and two clear peaks appear in the order 1 spectrum in Figure 3.8 (b).

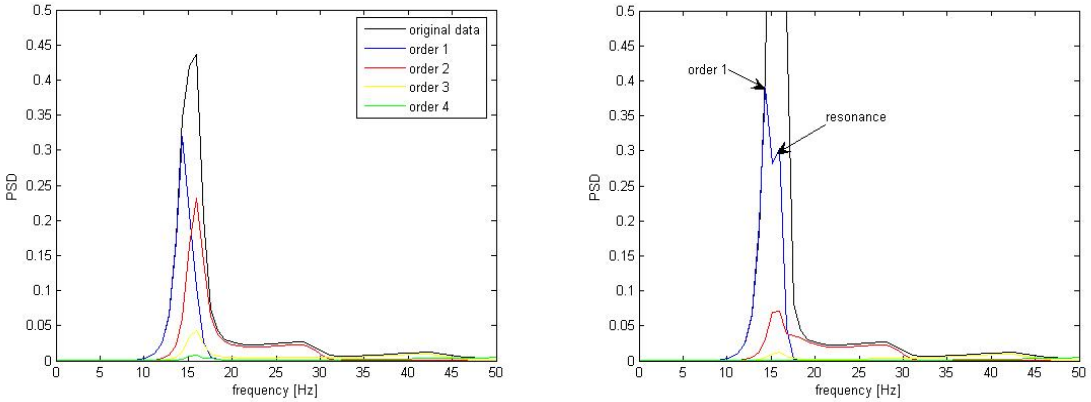

a. $C = 200$ Ns/m ; filter bandwidth = 66% b. $C = 20$ Ns/m ; filter bandwidth = 20%

Figure 3.8 Different damping and filter bandwidth ($C = 20$ Ns/m and 20% bandwidth)

In conclusion: Firstly from the previous frequency analysis, it can be shown that Vold-Kalman filter effectively filters out order information from original data. This can be seen from Figures 3.5 (a) and (d), where the filtered orders show the expected character of one resonance peak and one order peak. These two peaks correspond very well to the known original data. Secondly, both the damping coefficient C and the filter bandwidth will influence the detailed analysis of the spectrum. The narrower the filter bandwidth, the more detailed specific order information might be included, as can be seen in Figure 3.8 (b). But this also brings up the problem of amplitude correctness, as is shown in Figure 3.7 (b). Also as is commonly known, the smaller the damping coefficient C, the sharper the response amplitude peaks will be, this is clearly shown in Figure 3.6 (b). Such a frequency analysis is simple, but significantly enhances a direct understanding of the Vold-Kalman filter's effect, and it can visually verify that the Vold-Kalman filter correctly filters out any order signal in the time domain.

Another question is the elimination of the effect of resonance. In other order tracking techniques, the mathematical algorithm does not allow this. However the unique advantage of the Vold-Kalman filter order tracking over the other techniques lies in the fact that it can filter out certain orders directly from the original response signal. This can also be demonstrated in the simulation model.

Elimination of the resonance can be realized in the Vold-Kalman filter in the following way: Firstly, resonance is not an order, since the resonance frequency will not change with the changing rotational speed. It may however be treated as a special order, which corresponds to an imaginary fixed rotational speed. This may be called a resonance order. For this simulation model, the resonance order's rotation speed should be a constant value - 954 rpm or 15.9 Hz (resonance frequency). A new RPM input can hence be defined to the MATLAB script `vktime.m`. Other parameters will remain unaltered, using a 66% filter bandwidth. Theoretically, in this case, because of a fixed rotating speed was applied, thus, if filtering order 1 from original data, or $1\times$ rotating speed, the resonance data of response will be filtered out. By subtracting this filtered resonance data from the original response data, one is supposed to eliminate the effect of resonance. In doing so, encouraging results can be obtained, which are plotted in RPM spectrum map as Figure 3.9 (a).

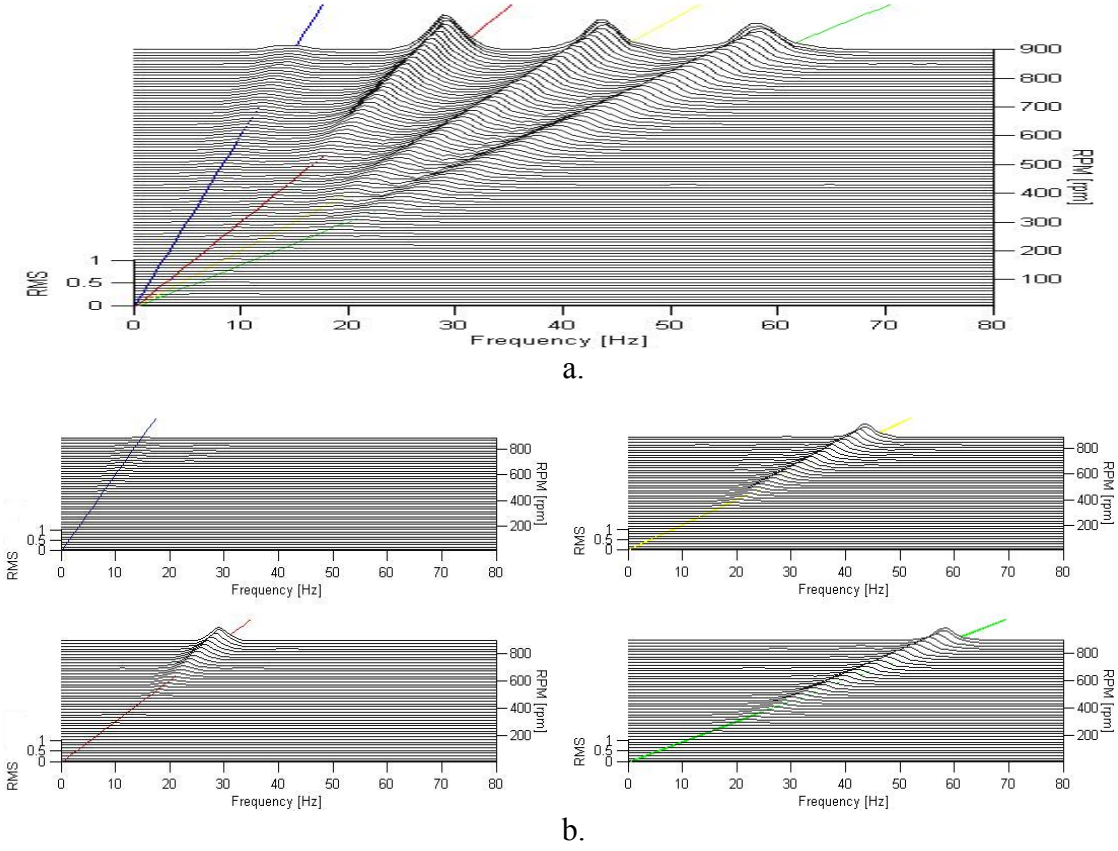

Figure 3.9 RPM Spectrum Map for system response without resonance

Comparing Figures 3.3 and 3.9 (a) clearly shows that the resonance was filtered out. Figure 3.9 (b) shows the RPM spectrum map for each order. Besides, a frequency analysis of the filtered signals without resonance can be seen in Figure 3.10 (b).

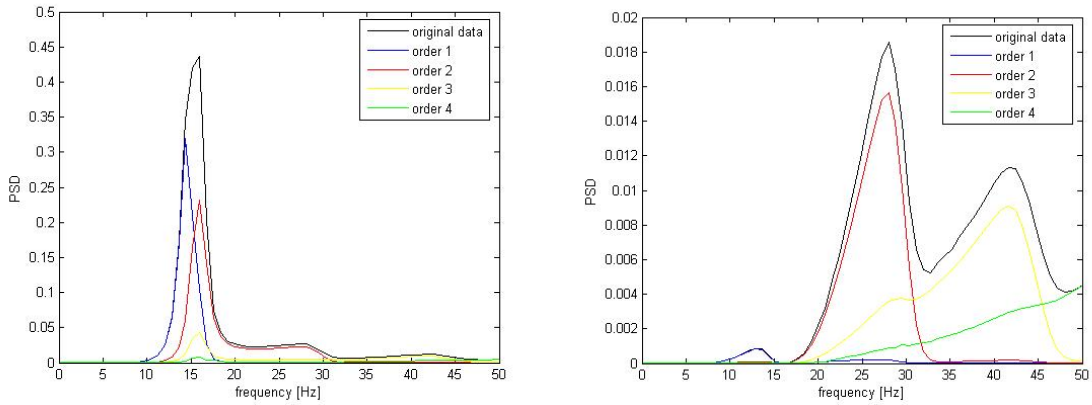

a. Original spectrum b. Filtered out resonance

Figure 3.10 Filtered out resonance order spectrum and original system response

Both the RPM spectrum map (Figure 3.9) and the frequency analysis (Figure 3.10) confirm that the resonance was filtered out. Comparing Figure 3.10 (a) to Figure 3.10 (b), the latter is much clearer in the absence of resonance. The Vold-Kalman filter can therefore provide an advantage to analyse the signal, by eliminating the effect of resonance. Figure 3.11 is the sliced individual orders from RPM spectrum map before and after filtering resonance.

(Sliced order means picking RMS values and corresponding RPM values from RPM spectrum map for a specific order)

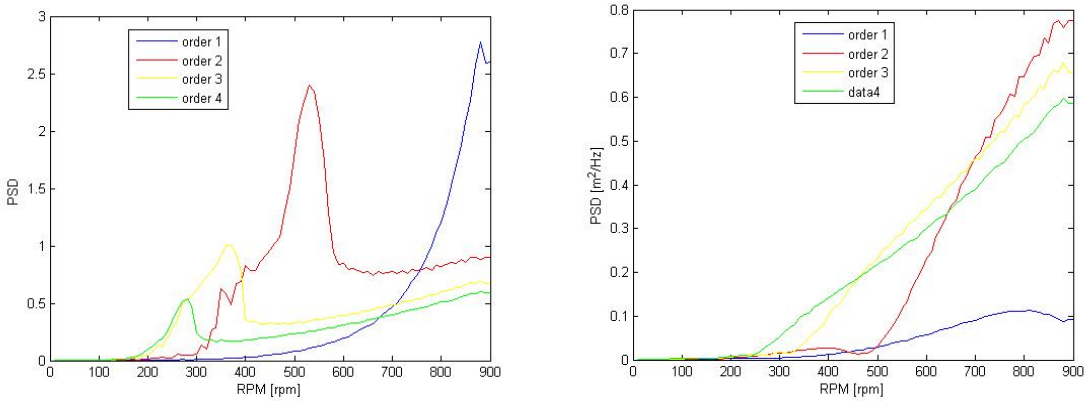

a. Sliced from Figure 3.3 b. Sliced from Figure 3.10 (a)

Figure 3.11 Sliced orders from Figure 3.3 and Figure 3.10 (a)

This figure further confirms the elimination of resonance, but in this case, since order 1 is too close to resonance, the filtering process largely filtered out the order 1 information. Both in Figure 3.10 (b) and Figure 3.11 (b), a 66% filter bandwidth was used to filter out the resonance, thus, in both figures appear low amplitude for order 1. If one narrows the filter bandwidth to 20% when filtering the resonance, Figure 3.12 renders:

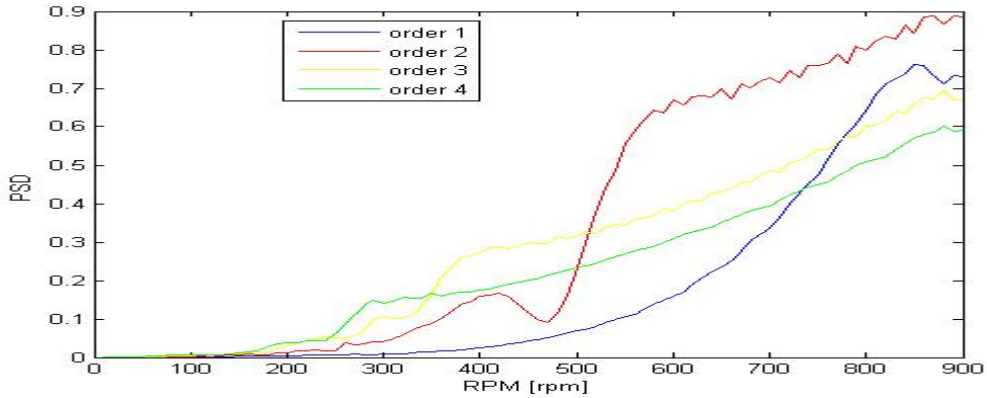

Figure 3.12 Sliced orders using 20% filter bandwidth to filter out resonance

Although Figure 3.12 appears to have a higher order 1 curve than Figure 3.11 (b), due to the narrow filter bandwidth, not all of resonance effects can be filtered out effectively. Therefore there still exist ripples at other orders from 200 RPM to 500 RPM, where the resonance order pass through these orders.

However, this elimination process presents a new perspective on inspecting the system. It is also a unique perspective for the Vold-Kalman filter order tracking technique. The comparison between Figure 3.11 (a) and (b) indicates that the simple and clear sliced curves can be achieved by filtering resonance, so that a clear sliced order can provide a simple indicator for condition monitoring.

In the preceding discussion a simple single-degree-of-freedom system was considered. We now switch to a two-degree-of-freedom system. Since many of the concepts are similar, only a brief explanation is provided in the following.

3.3 Two-degree-of-freedom system model

Generally, rotors are not symmetric around the mid-plane, and the bearings are positioned such that the distances between the bearings and the centre of mass are ℓ_1 and ℓ_2 respectively. The stiffness and damping coefficients for the two bearings may also be different. Such a general rotor model is described by Heyns (1989). In this case both the lateral translation of the centre of mass of the rotor and the rotation of the rotor in the x-z plane, around its centre of mass, will be taken into account. The system is depicted in Figure 3.13 with system characteristics that are listed in Table 3.4.

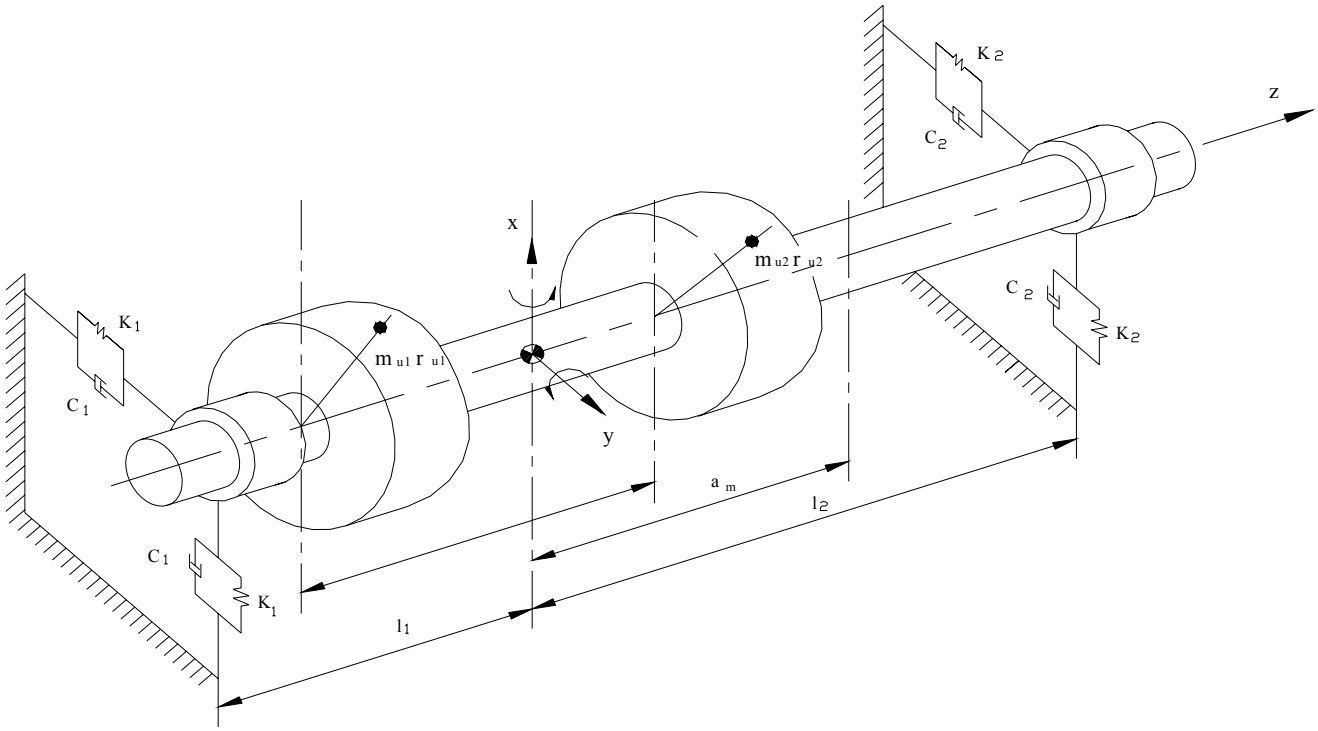

Figure 3.13 Non-symmetric rotor two-degree-of-freedom system

Table 3.4 System characteristics

Parameter	Value
Stiffness K	$K_1 = 100000$ N/m; $K_2 = 10000$ N/m
Rotor mass M	20 kg
Polar moment of inertia of the rotor I_C	0.5 Nm
Eccentricity r_u	0.1m

Unbalance mass m_u	0.05 kg
Damping coefficient C	$C_1 = 35$ Ns/m; $C_2 = 20$ Ns/m
Initial time t_0	0 s
Final time t_f	5 s
Time steps	4096
RPM slew rate	200 rpm/s
Centre to left bearing	$\ell_1 = 0.2$ m
Centre to right bearing	$\ell_2 = 0.3$ m

3.3.1 Equations of motion for the two-degree-of-freedom system

Considering now the rotor of Figure 3.14 at time t with the external forces in the x direction $F_x(t)$, the corresponding resultant moment about the y-axis $M_y(t)$, and the moment of inertia about the centre of mass I_C, the equation of motion in $x-z$ plane may be written as

$$\begin{bmatrix} M & 0 \\ 0 & I_c \end{bmatrix}\begin{Bmatrix} \ddot{x} \\ \ddot{\theta}_y \end{Bmatrix} + \begin{bmatrix} C_1 + C_2 & -C_1\ell_1 + C_2\ell_2 \\ -C_1\ell_1 + C_2\ell_2 & C_1\ell_1^{\,2} + C_2\ell_2^{\,2} \end{bmatrix}\begin{Bmatrix} \dot{x} \\ \dot{\theta}_y \end{Bmatrix}$$

$$+\begin{bmatrix} K_1 + K_2 & -K_1\ell_1 + K_2\ell_2 \\ -K_1\ell_1 + K_2\ell_2 & K_1\ell_1^{\,2} + K_2\ell_2^{\,2} \end{bmatrix}\begin{Bmatrix} x \\ \theta_y \end{Bmatrix} = \begin{Bmatrix} F_x(t) \\ M_y(t) \end{Bmatrix} \quad (3.3)$$

or

$$M\begin{Bmatrix} \ddot{x} \\ \ddot{\theta}_y \end{Bmatrix} + C\begin{Bmatrix} \dot{x} \\ \dot{\theta}_y \end{Bmatrix} + K\begin{Bmatrix} x \\ \theta_y \end{Bmatrix} = \begin{Bmatrix} F_x(t) \\ M_y(t) \end{Bmatrix} \quad (3.4)$$

From this it follows that

$$\begin{Bmatrix} \ddot{x} \\ \ddot{\theta}_y \end{Bmatrix} = -M^{-1}C\begin{Bmatrix} \dot{x} \\ \dot{\theta}_y \end{Bmatrix} - M^{-1}K\begin{Bmatrix} x \\ \theta_y \end{Bmatrix} + M^{-1}\begin{Bmatrix} F_x(t) \\ M_y(t) \end{Bmatrix} \quad (3.5)$$

With the state vector defined as

$$q = \begin{Bmatrix} x \\ \theta_y \\ \dot{x} \\ \dot{\theta}_y \end{Bmatrix} \quad (3.6)$$

it follows that

$$\dot{q} = \begin{bmatrix} O & I \\ -M^{-1}K & -M^{-1}C \end{bmatrix} q + \begin{Bmatrix} 0 \\ 0 \\ M^{-1}\begin{Bmatrix} F_x(t) \\ M_y(t) \end{Bmatrix} \end{Bmatrix} \tag{3.7}$$

with I the unit matrix.

In equation (3.7)

$$-M^{-1}K = \begin{bmatrix} -(K_1 + K_2)/M & (K_1\ell_1 - K_2\ell_2)/M \\ (K_1\ell_1 - K_2\ell_2)/I_c & -(K_1\ell_1^{\,2} + K_2\ell_2^{\,2})/I_c \end{bmatrix} \tag{3.8}$$

and

$$-M^{-1}C = \begin{bmatrix} -(C_1 + C_2)/M & (C_1\ell_1 - C_2\ell_2)/M \\ (C_1\ell_1 - C_2\ell_2)/I_c & -(C_1\ell_1^{\,2} + C_2\ell_2^{\,2})/I_c \end{bmatrix} \tag{3.9}$$

3.3.2 Two-degree-of-freedom system analysis

a. Typical response of two-degree-of freedom system

Figures 3.14 and 3.15 depict the lateral and angular accelerations in the time domain, and the RPM spectrum map respectively. The amplitude of rotational response in Figure 3.15 is much higher than lateral response, it can also see from Figure 3.15 RMS value of RPM spectrum map.

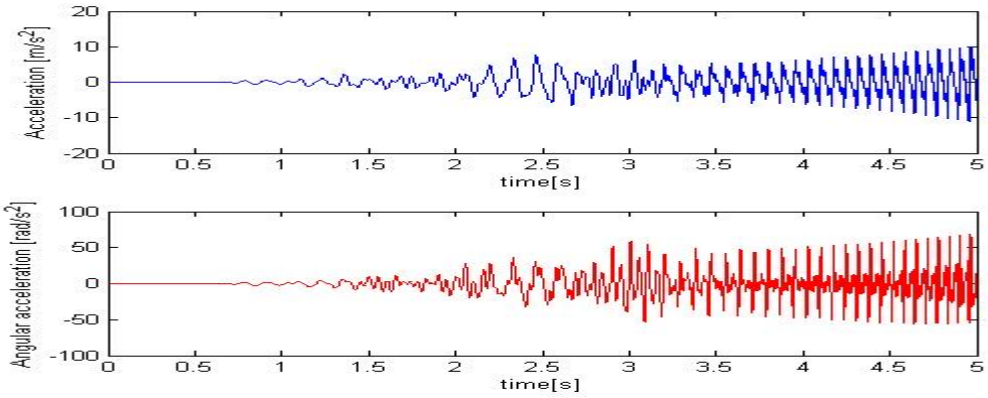

Figure 3.14 System responses in lateral and rotational directions

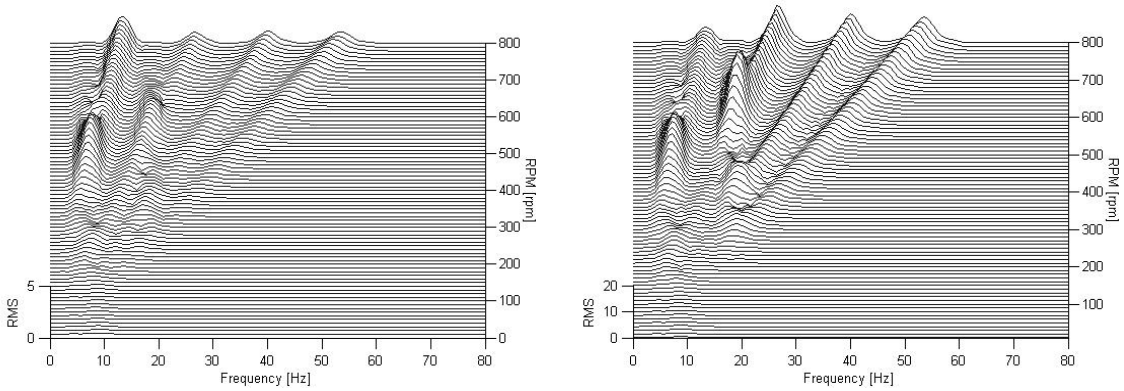

a. Lateral response b. Rotational response

Figure 3.15 RPM spectrum map for two-degree-of-freedom system

By the same token, as has been done for the single-degree-of-freedom system, the filtered order time domain waveforms can be added together and compared to the original responses. For the illustration purposes, the rotational responses were used as the example:

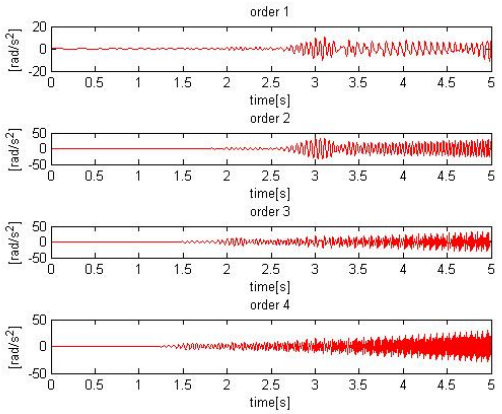

a. Filtered orders waveform

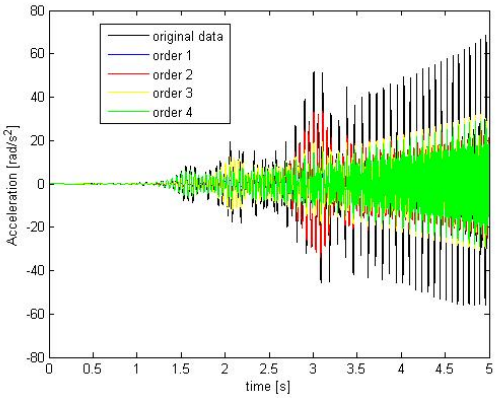

b. Order waveforms and original waveform

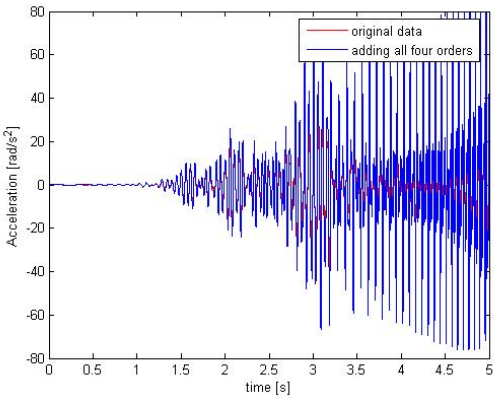

c. Adding all four orders and original data

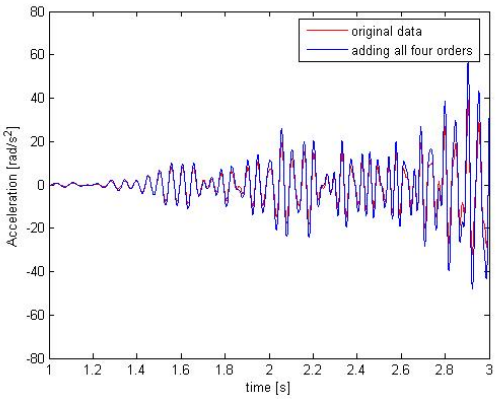

d. zoom in

Figure 3.16 Filtered out order signal in time domain

Figures 3.16 (a) are the filtered order waveforms for all four orders. Figure 3.16 (b) is the superposition of all the order waveforms with the original waveform. Figures 3.16 (c) and

(d) show the effect of adding all the order time domain data together and superimposing on the original waveform. It can be seen that these two curves match very well, with the added data slightly higher than the original data. This also happened in the single-degree-of-freedom-system, due to the choice of filter bandwidth.

b. System resonance analysis

For the two-degree-of-freedom system, the system resonance can be seen clearly by plotting the frequency response function (FRF), so that system resonance can be easily identified. Equation 3.10 from Heyns (2003) can be used to evaluate the FRF of a multi-degree-of-freedom system under a unit harmonic excitation force

$$[X(i\omega)] = [H(i\omega)][F(i\omega)] \tag{3.10}$$

For the two-degree-of-freedom system under consideration

$$[H(i\omega)] = \begin{bmatrix} \alpha_{11} & \alpha_{12} \\ \alpha_{21} & \alpha_{22} \end{bmatrix} \tag{3.11}$$

where 1 corresponds to the lateral degree of freedom and 2 to the rotational degree of freedom.

A general element in the receptance FRF matrix $H_{jk}(i\omega)$ with response at j and excitation at k, is defined as

$$H_{jk}(i\omega) = \alpha_{jk}(i\omega) = \left(\frac{x_j}{f_k}\right)_{f_m=0;m=1,N;m\neq k} \tag{3.12}$$

These elements are plotted in Figure 3.17.

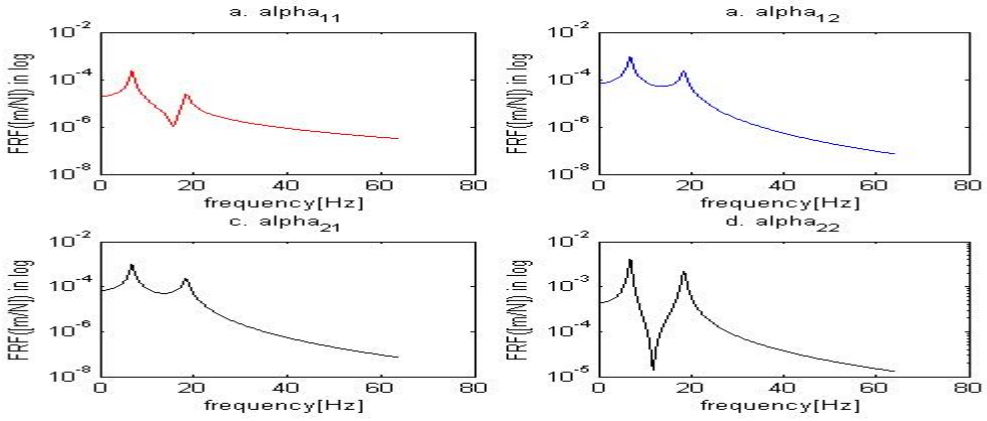

Figure 3.17 FRF for the system

Due to the choice of parameters, for the two-degree-of-freedom system, there are two clear resonances appearing in the spectrum at 6.9 Hz and 18.5 Hz. Both of these influence the lateral and rotational responses. Thus clear resonance information was obtained, it is very useful for the following Vold-Kalman order tracking application.

3.3.3 Vold-Kalman filter application in two-degree-of-freedom system

Procedures similar to those followed with the single-degree-of-freedom system, may be applied for this two-degree-of-freedom system. There is however a difference in the choice of the filter bandwidth, simply because the two resonances and two damping ratios ξ will be included. These parameters therefore need to be calculated by solving the eigenproblem associated with the equation of motion. The two resonances are 6.9 Hz and 18.5 Hz respectively and, the corresponding two damping ratios are 0.042 and 0.024. The Vold-Kalman filter bandwidth will be chosen according to these results, and are tabulated as in Table 3.5

Table 3.5 3dB filter bandwidths for orders 1 to 4

Order	Minimum bandwidth (Hz) (resonance=6.9 Hz)	Minimum bandwidth (Hz) (resonance=18.5 Hz)	Percentage (6.9 Hz)	Percentage (18.5 Hz)
1	11.6	7.6	63%	41%
2	23.2	15.1	126%	82%
3	34.8	22.7	189%	123%
4	46.5	30.2	252%	164%

An initial filter bandwidth can be chosen as 66%, as have been chosen in the single degree-of-freedom system. But it must be borne in mind that in order to achieve the correct amplitude at resonance peak, the above table gives the minimum filter bandwidth for each order. The Vold-Kalman filter may now be applied to the two-degree-of-freedom system. The rotational response is considered to perform the analysis. The result of order 1 and the overall response over a period of 5 s can be plotted as

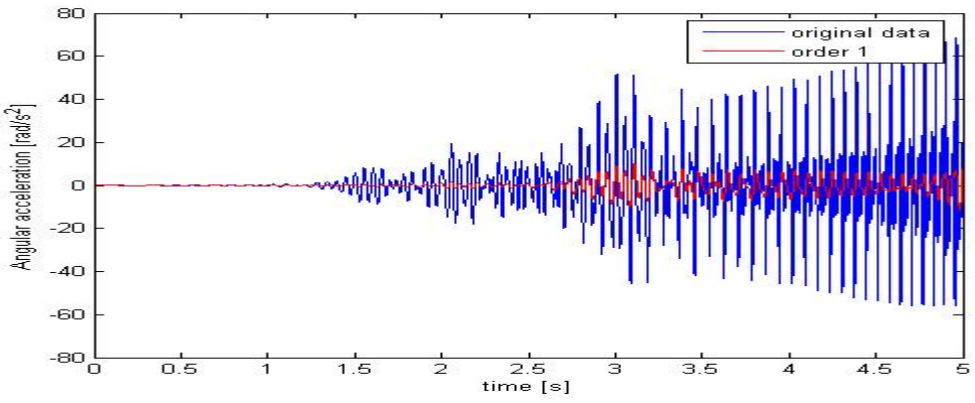

Figure 3.18 Overall rotational response and order 1

A frequency analysis of the response and all the orders renders the following:

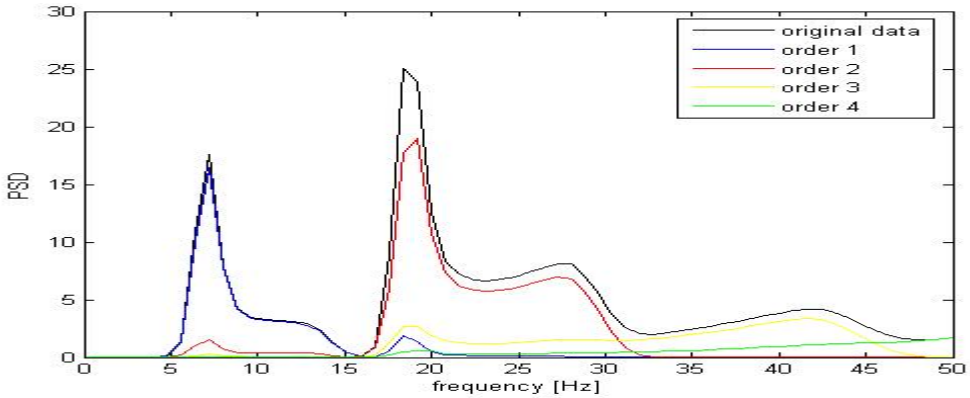

Figure 3.19 Frequency analysis of response and orders

In Figure 3.19, the response displays 6 peaks. The two highest peaks are the system resonances at 6.9 and 18.5 Hz respectively, and the others are the orders. These are less sharp compared to the resonances.

In the same way as was done for the single-degree-of-freedom system, the resonances can also be filtered out from original data. The results with one resonance filtered out and with both of them filtered out on the response, can be plotted as:

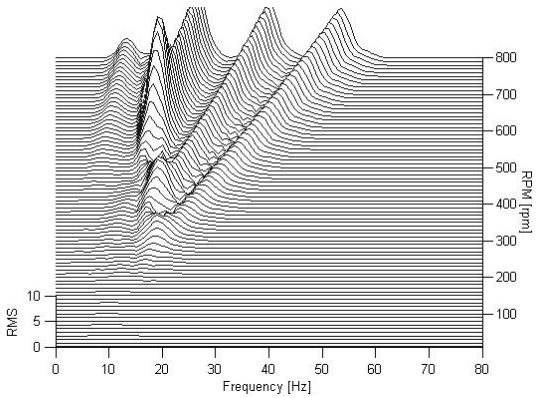

a. 6.9 Hz resonance filtered out

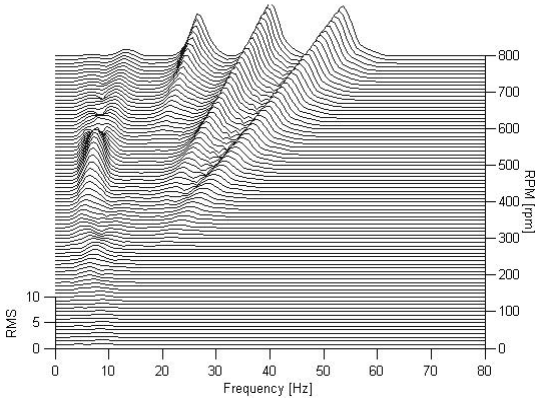

b. 18.5 Hz resonance filtered out

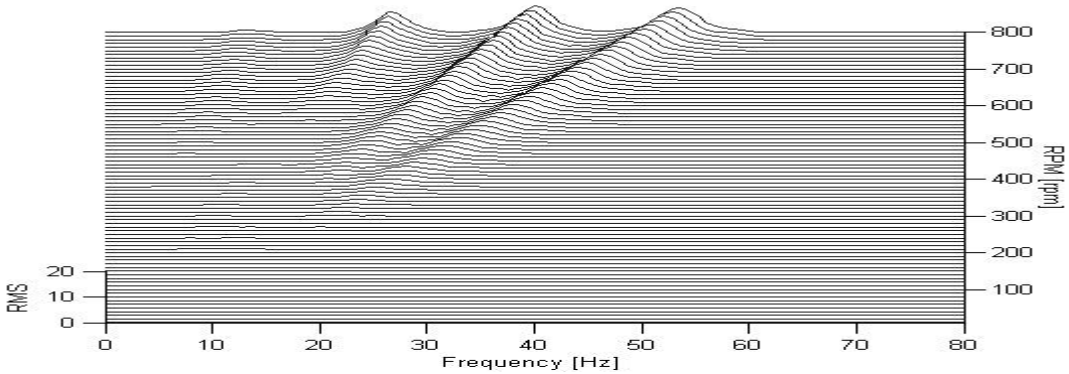

c. Both 18.5 Hz and 6.5 Hz resonance filtered out

Figure 3.20 Filtering of system resonance

From comparisons between Figures 3.15 (b) and 3.20, it is clear that both of the resonances or each resonance can be filtered out. In Figure 3.20 (c), the fact that all of these orders

become smaller in amplitude, it is due to the effect of filtering the resonances. The sliced order curves are plotted in Figure 3.21. In Figure 3.21 (a), the peak of order 2 is higher both in RPM and RMS value than order 1. If the system only has one resonance, the peak of order 1 should appear at higher RPM than order 2, as can be seen in the single-degree-of-freedom system, Figure 3.11 (a). But this is two-degree-of-freedom system and there are two system resonances, both of which will influence the sliced order curves. By examining Figure 3.15 (b) and Figure 3.21 (a), it can be concluded that the highest peak of order 1 is excited by the resonance at 6.9 Hz at around 500 rpm, while the highest peak of order 2 is excited by the resonance at 18.5 Hz at around 700 rpm. At the same time, Figure 3.21(b) shows the sliced orders for the filtered out resonance in the two-degree-of-freedom system. This can also provide a clear indicator for condition monitoring.

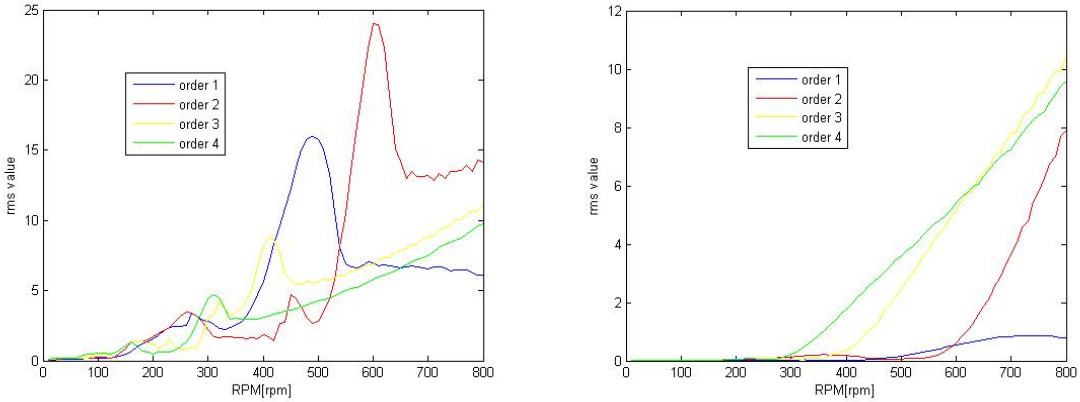

a. Sliced from Figure 3.15 (b) without filtering resonance

b. Sliced from Figure 3.20 (c) with filtering out resonance

Figure 3.21 Sliced orders of system

3.4 Simulated damage and its analysis via Vold-Kalman filter

3.4.1 Simulated damage

As was discussed in paragraph 1.2.1-c, electrical machinery – especially for high rating generators or motors – experience the problem of winding looseness or shorts due to excessive vibration. This may eventually result in fatigue failure of winding components or even worse consequences. Thus, condition monitoring of this kind of failure is of great practical importance. In this study, the Vold-Kalman filter will be used to test its capability of detecting such kinds of failure in electrical machinery. The failure mechanism will be briefly analysed and approximately simulated in the simulation model.

A short is an abnormal connection of relatively low resistance between two points of a circuit. The result is excess (often damaging) current between these points. For instance, conductors from different phases either touch or come closer than the minimum spacing allowed during the design. Sottile et al. (2001) presented an experimental and theoretical analysis used to establish electrical features that can be utilized as indicators of stator winding deterioration. In their study, they indicate that when inter-turn stator deterioration such as that represented by R_{sh} in Figure 3.22 occurs, the circulating current in this loop

produces a mechanical magnetic force (MMF) distribution across the air gap of the machine.

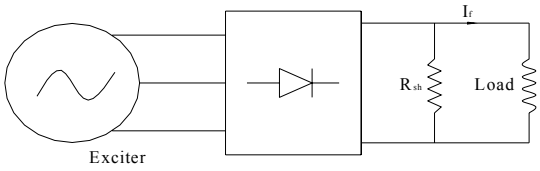

Figure 3.22 Simplified inter-turn short circuit for electrical generator

This MMF is in addition to the normal MMF that is due to the three-phase stator winding currents. This normal MMF is rotating at synchronous speed in the direction of the rotor rotation. On the other hand, the MMF produced by the inter-turn fault is centred on the axis of the fault coil, it is stationary in space, and its amplitude will be pulsating sinusoidally in time at the rated frequency. Mathematically, the pulsating flux density distribution due to the fault current MMF may be represented as the summation of two rotating magnetic flux density waves

$$B(\theta,t) = B_{+}\cos(\omega t - \theta) + B_{-}\cos(\omega t + \theta) \tag{3.13}$$

where B is flux density, θ is the electrical space angle and ω is the electrical angular frequency in radians/second, $\pm$ is the direction of rotor rotation.

The first term in this summation represents a magnetic flux density distribution travelling at synchronous speed in the direction of rotor rotation and the second term represents a similar distribution travelling at synchronous speed opposite to the direction of rotation. The first term therefore should not induce any voltage in the field coil, while the oppositely rotating component should induce a voltage of twice the electrical angular frequency in the field circuit. This induced voltage should cause an alternating current of frequency 2ω to flow in the field circuit, in addition to the normal DC field excitation, such that the excitation current I_f in Figure 3.22 would have a double frequency component.

Based upon the above analysis, an inter-turn short can cause an excitation with a frequency of twice the rated frequency, for the electrical rotating machine. The rated frequency is closely related with rotating frequency, therefore, an inter-turn short will be closely related with rotating speed. Thus, it is reasonable to simulate the forces like sinusoidal forces. In order to simplify the simulation, two cycles sinusoidal forces with amplitude of 10 N per revolution will be added in the main excitation force, the mathematical expression for this force is listed in Appendix 1, Table A1.1. Thus, in the analysis process, the presence of the second order will signify this type of fault.

3.4.2 Condition monitoring of fault condition

Figure 3.23 (a) illustrates the excitation force on the rotor for an undamaged stator, assuming a 4- pole motor with one cycle of excitation per revolution. Assuming damage due to a short on one stator winding, two sinusoidal impulses are now added on every revolution. If a constant force amplitude of 10 N is assumed, the excitation forces might be simulated as represented in Figure 3.23 (a) for the undamaged case and 3.23 (b) for the damaged case.

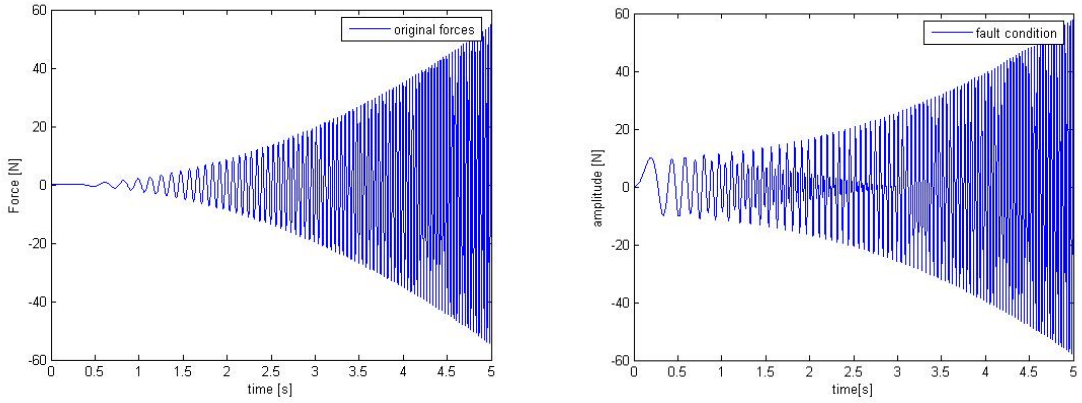

a. Without sinusoidal impulse b. With sinusoidal impulse

Figure 3.23 External excitation forces without and with impulses

The simulated lateral acceleration responses for the undamaged and damaged excitation models are shown in Figures 3.24 (a) and (b).

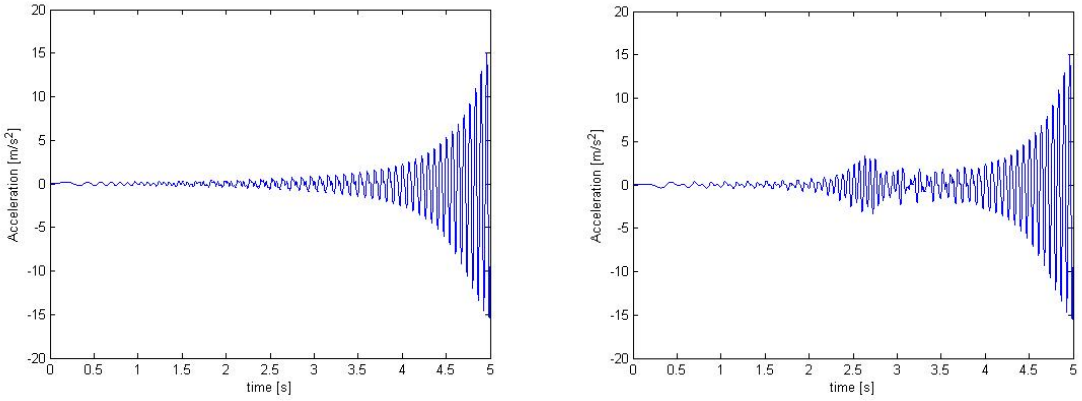

a. Undamaged b. Damaged

Figure 3.24 Simulated displacement response

Then, the Vold-Kalman filter may be used to filter the order 2 signal in time domain (66% filter bandwidth assumed). As was discussed above, order 2 will be the indicator of fault

condition. The filtered order 2 for the undamaged and damaged cases are shown in Figure 3.25

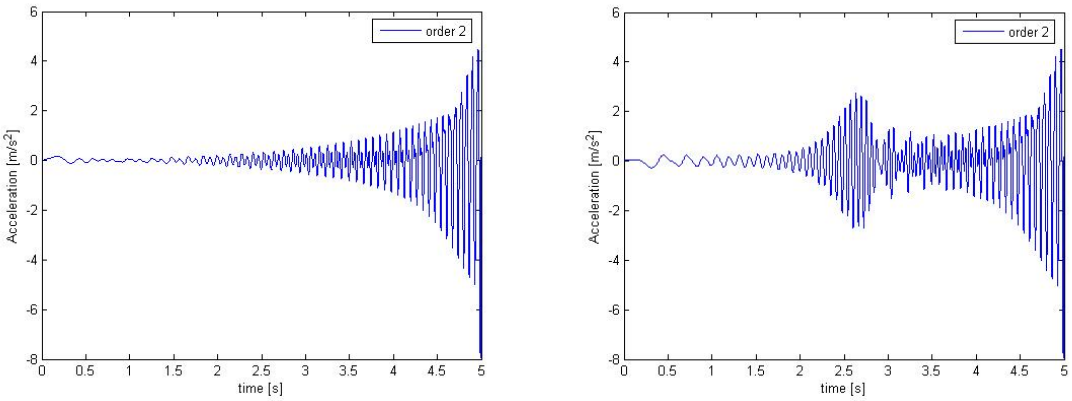

a. Undamaged b. Damaged

Figure 3.25 Filtered order 2 displacement response

One of the advantages of the Vold-Kalman filter is its time domain ability. This is the unique advantage over the other order tracking techniques. Thus, it is very meaningful to investigate its ability to detect failure of electrical machine in time domain.

Crest factor, kurtosis value and RMS value are commonly used as condition monitoring features in time domain data analysis. The crest factor is a measure of the impulsiveness of a vibration signal. Kurtosis is the fourth statistical moment, which is used to define the shape of the probability density distribution. They are often used when dealing with shocks, impulse noise and short events. The RMS value is based on calculating the root mean square value of the data vector, and is widely used in industry for general monitoring purposes. Therefore, filtered data from Vold-Kalman filter will be analysed by these common techniques. MATLAB scripts `crest.m`, `kurtosis.m and rms.m` were used to compare the results for the damaged and undamaged cases, as in table 3.6

Table 3.6 Crest factor and kurtosis value for filtered order 1 and 2

Orders	**Indicator values**	**Undamaged**	**Damaged**		
		$F_{original}$	$F_{original} + F_{10}$	$F_{original} + F_{50}$	$F_{original} + F_{100}$
1	Crest factor	5.94	5.92	5.40	4.40
	Kurtosis value	14.82	14.59	10.45	5.78
	RMS value	2.56	2.57	2.83	3.50
2	Crest factor	8.78	7.42	4.40	4.56
	Kurtosis value	18.72	10.60	7.93	9.03
	RMS value	0.90	1.07	2.88	5.50

In Table 3.6, different damage levels with force amplitudes of 10 N, 50 N and 100 N, were used to apply to the simulation model. F_{10} is the sinusoidal force with amplitude of 10 N, F_{50} is the sinusoidal force with amplitude of 50 N and F_{100} is the sinusoidal force with amplitude of 100 N. $F_{original}$ is the undamaged excitation force.

The table indicates a rough trend of the three factors with the damage condition deteriorating. It is clear that with the damage condition deteriorating (amplitude of damage force level increasing), crest factor and kurtosis value will become smaller, but RMS value will become bigger. This is also clearly seen in Figure 3.26, which is based on Table 3.6.

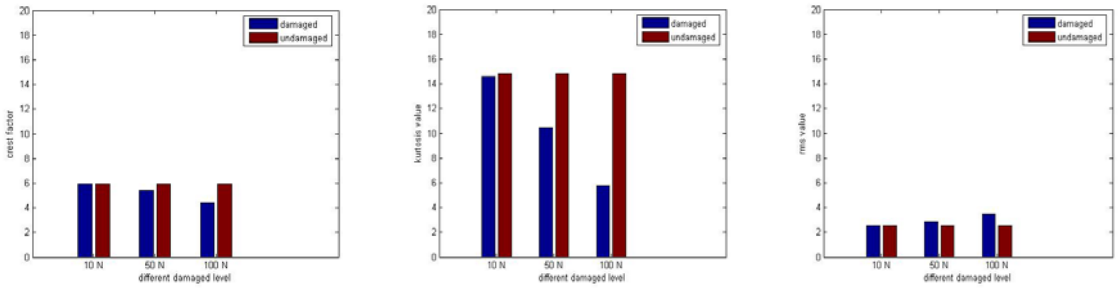

a. Crest factor-order 1 b. Kurtosis value-order 1 c. RMS value-order 1

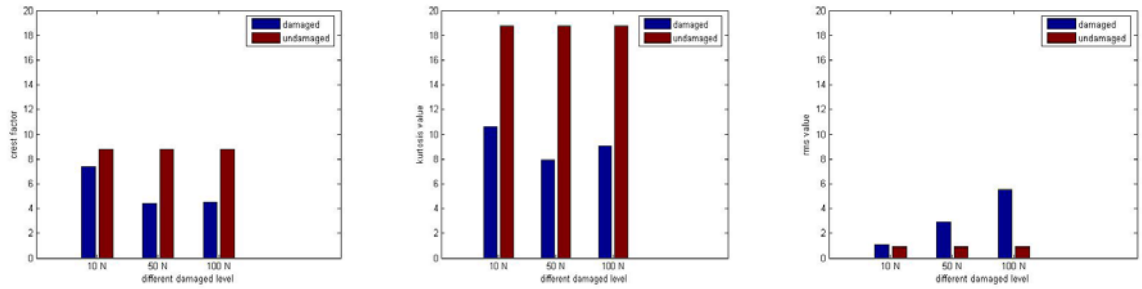

e. Crest factor-order 2 f. Kurtosis value-order 2 g. RMS value-order 2

Figure 3.26 Filtered order 1 and 2 crest factors, kurtosis values and RMS values comparison

From Figure 3.26, after analysing the data using the Vold-Kalman filter and then considering order 1 and order 2 separately, it is fairly clear that crest factor, kurtosis value and RMS value is effective in identifying the damage due to a simulated short.

Due to a fault excitation force with twice the frequency of the fundamental frequency was included in the external excitation force function, which can be expressed mathematically as (see Appendix 1, Table A1.1)

$$F(t) = m_u \varpi r_u^{\,2} \sin(\varpi t) + 10\sin(2\varpi t)$$

therefore, in the system responses, clear data changes with twice fundamental frequency are expected to appear, or order 2.

Figure 3.26 (a), (b) and(c) are figures for order 1, while Figure 3.26 (e), (f) and (g) correspond to order 2. It can clearly be seen from the figures for order 2, that there are much bigger differences in the indicators than for order 1. Thus, from the simulation model analysis, these three time domain analysis techniques seem to be promising indictors for condition monitoring.

In conclusion, data filtered with the Vold-Kalman filter can be trended using the crest factor, kurtosis value and RMS value on a simulated model, to provide simple condition monitoring indicators. The unique advantage of this time domain filtered data analysis is that it does not determine the analysis features such as crest factor or kurtosis value on the overall measured data, but for specific orders. This allows the analyst to focus on the change of a specific order rather than the whole system. In chapter 5, similar damage was introduced on actual alternator stator windings. The real experimental data will be filtered via Vold-Kalman filter and analysed by crest factor and kurtosis value. This theoretical simulation provides a good reference for the subsequent real experimental data analysis.

3.5 Conclusion

In this chapter, a single and a two-degree-of-freedom simulated rotor model were constructed. The system response was in both cases generated via Runge-Kutta-Gill integration of the equations of motion. The Vold-Kalman filter was subsequently applied to the two simulated responses. Possible condition monitoring strategies were investigated by using the Vold-Kalman filter on both systems. The unique ability of Vold-Kalman filter in time domain was explored. Filtered data were analysed by using crest factor, kurtosis value and RMS value. This provides a good indicator for condition monitoring of an inter-turn short in the stator windings.

Chapter 4 Experimental set-up selection and monitoring equipment

4.1 Introduction

In order to implement the order tracking technique on a real electrical rotating machine, a proper experimental set-up needed to be established. The most important design aspect would be that results obtained from the experimental set-up must be representative of real industrial electrical machinery. For this purpose the experimental set-up had to comply with the following specifications:

- Variable speed must be available to perform different tests.
- Since a key element of the set-up is that it must be easy to be damaged, disassembled and again reassembled at reasonable cost, a component such as automotive alternator, would be most appropriate. This is similar to real industrial electrical machines while still very affordable.
- The experimental set-up must be easy to monitor, in other words, it must be easy to place sensors on the key component.
- A load bank must be used to simulate real working conditions.
- The set-up should provide for growth in future research.

It was recognised at early stage that this research would focus on the implementation of the Vold-Kalman filter order tracking technique in electrical machine monitoring, and that proper data had to be acquired on a comparatively stable and simple experimental set-up. For this reason, a laboratory scale experimental set-up comprising the monitoring of a universal automotive alternator was designed and constructed.

This specially designed experimental set-up satisfies the above requirements. It also provides a very appropriate and simple experimental model for the power dissipation. Some experiments that cannot easily be performed in a real big industrial generator can easily be conducted on this simple experimental set-up. Various kinds of damage, which are representative of real damage on industrial systems may be artificially induced for monitoring purposes. For this work, the case of a stator winding short was considered.

The main focus in the current work will be on the application of the Vold-Kalman filter order tracking technique and its comparison with other order tracking techniques. This experimental set-up can however be used as a very good platform for the future research.

4.2 Experimental set-up

The experimental set-up is shown as in Figure 4.1 and the monitoring process is schematically represented in Figure 4.2**.** The key components of the experimental set-up are the alternator, the variable speed motor, the controller and the battery. The alternator is driven by a variable speed induction motor via a normal V-belt. The variable speed motor

is controlled by a DC controller. The alternator will charge the normal automotive battery that, in this case, is used as the system load.

The monitoring equipment for this experimental set-up, comprise an accelerometer and a shaft encoder, with a National Instruments Board (NIB) and computer. The accelerometer is mounted on the outer surface of the alternator, and the acquired signal is amplified and transferred through a PCB amplifier and NIB to the computer. The rotational speed signal is monitored simultaneously through the shaft encoder, which was mounted on a specially made rotor shaft extender. The acquired signal first goes to the shaft encoder signal transfer box and then to the NIB before it finally also reaches the computer.

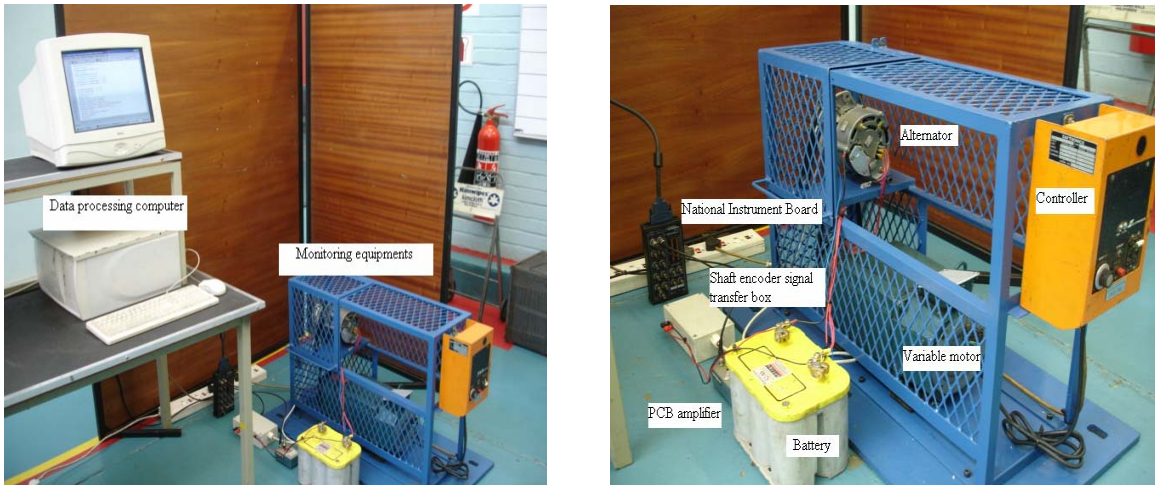

a. Experimental set-up b. Zoomed detail

Figure 4.1 Experimental set-up

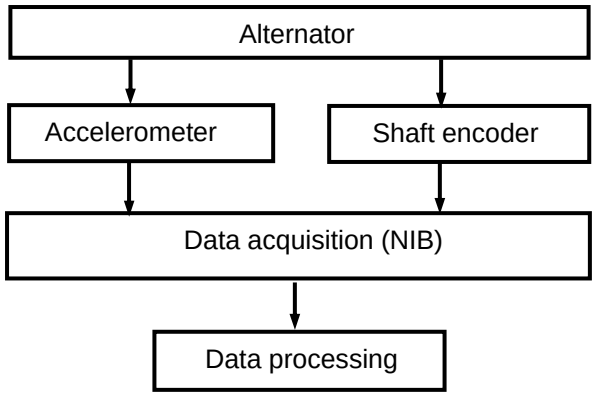

Figure 4.2 Monitoring process

4.2.1 Controller and data acquisitioning

a) Speed controller, NIB and accelerometer

A speed controller was used to control the variable motor. The variable motor speed can be tuned by tuning its controller button manually. This controller can be seen in Figure 4.1 (b). Its specifications are listed in Table 4.1.

Table 4.1 Controller specifications

Type	DC controller	Maker	Saftronics
	Rated input	Rated output	
Frequency	50-60Hz		
Voltage	220V	180V	
Current	15A	12A	

In order to acquire a valid encoder signal, a high sampling frequency was required. Thus the NIB was used to sample the data (see Figure 4.1(b)). The model of this card is BNC-2110, and the highest sampling frequency of this model is 2 MHz. If shared between two simultaneous channels the highest sampling frequency for each channel drops to 1 MHz. For the vibration signal acquisition, an accelerometer was used to acquire the data, its specifications are listed in Table 4.2.

Table 4.2 Accelerometer specifications

Model	M353B18
Sensitivity	10.13 mV/g
Range	1-10 kHz

b) Shaft encoder and its assembly

One of the most important factors that influence the performance of the order tracking technique is to acquire a clean rotating speed signal. There are various kinds of monitoring equipment for acquiring the speed data. In this experimental set-up, a precise shaft encoder, made by Hengstler, was mounted onto the alternator shaft extender (Figure 4.3). Its specifications are listed in Table 4.3

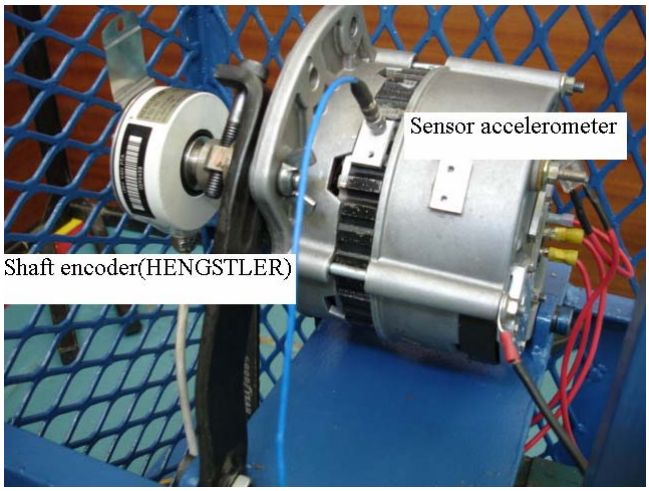

Figure 4.3 Shaft encoder and accelerometer

Table 4.3 Shaft encoder specifications

Type	RI 76 TD
Pulses/ revolution	1 or 1024 pulses/ revolution
Shaft diameter	20mm
Mounting	Front clamping ring
Supply voltage	10-30 VDC
Operating temperature	-25 to…+100°C
Absolute maximum speed	3600 RPM (at 70°C)

In order to mount the shaft encoder properly on the alternator, a specially designed shaft extender was manufactured (Figure 4.4). The prime design consideration was to shorten the distance between the encoder and the alternator, and therefore the dimensions were determined by the space available. Due to the extension of rotor shaft, the centre between the rotor shaft and the shaft extender could not be manufactured perfectly in line, under conditions of separate manufacturing. For this reason, the rotor was taken out of the alternator and the shaft extender was turned on a lathe together with the rotor shaft, to get the best possible alignment. See Appendix 3 for more details.

Figure 4.4 Shaft extender

4.2.2 Variable speed motor and alternator

a) Variable speed motor

The purpose of this experiment is to measure the radial vibration of the alternator under conditions of variable speed. Therefore a variable motor was equipped to be the driving equipment in the whole test rig, its specifications are listed in table 4.4. For an assembly photograph see Figure 4.5 (a).

Table 4.4 Variable motor specifications

RPM	1750 rpm
Armature voltage	180V
Armature current	9.5A
Field voltage	100/200V
Field maximum current	1.7/8.5A

b) Alternator

The equipment that will be monitored in this experimental set-up is the alternator. A universal automotive alternator was used as the key component of the whole test rig. As has been mentioned as previous chapters, the main purpose of this research is to investigate the use of the Vold-Kalman filter order tracking technique for monitoring of electrical machine faults. Since alternators are very common electrical machines, and because of its low price and ease of artificially inducing damage, it was selected as very suitable for the monitoring investigations on the experimental set-up. Its specifications are listed in table 4.5. An assembly photograph see Figure 4.5 (b).

Table 4.5 Alternator specifications

Stator bars	36 bars
Claw rotor	12 claws
Output	12 V
Max current	65 A

a. Variable motor b. Alternator

Figure 4.5 Variable motor and alternator

4.2.3 V-belt, pulley selection and tension mechanism

a) V-belt and pulley

A simple V-belt was used to transmit the power from the motor to the alternator. This emulates aspects of a real generation system, because, from turbine blades to generator rotors, the real rotational speed can be expected to vary continuously. For the two pulleys of the motor and the alternator shaft, a 1.5:1 ratio was used, so that the maximum speed that the alternator can attain is given by, $RPM_{\max} = 1.5 \times 1750 = 2625$ rpm. Both pulleys and the V-belt were bought from a hardware shop as standard parts.

b) Tension mechanism

An automotive alternator tensioning mechanism was used in this test rig, to tension the belt (Figure 4.6). The belt provides the connection between the driving and the driven equipments and the tensioning mechanism is very important to get a comparatively stable transmission.

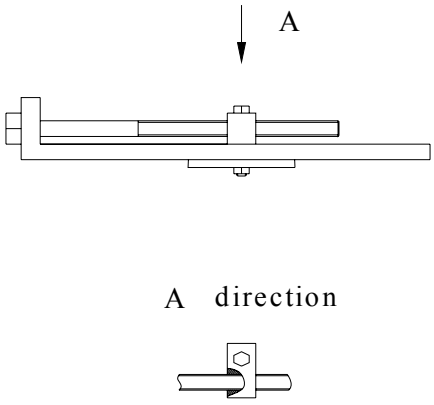

Figure 4.6 Tension mechanisms

This tensioning mechanism is very simple and easy to be adjusted. Two screws are employed to adjust the tension. Obviously it was necessary to keep the tension repeatable during various experiments. This was done by marking the position of adjusting screws so as to maintain constant tension in the belt. After a few experiments, one had to check the position of both screws in the vertical and horizontal directions to ensure adequate tension (Figure 4.7).

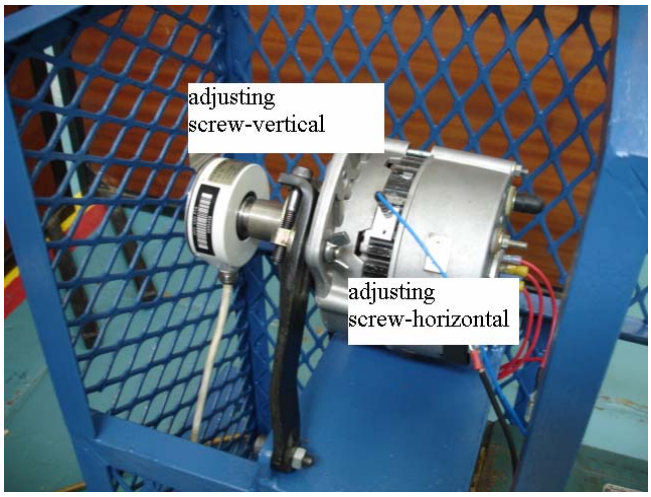

Figure 4.7 Tensioning devices

4.2.4 Battery and battery charging process

a) Battery

A 12 V car battery is used to supply the starting power, as well as to act as a load by charging the battery during the operating cycle. In this sense, the battery acts as a load bank (Figure 4.1 (b)).

b) Battery charging process

The operational condition of the alternator influences the observed vibration response of the system. Figure 4.8 shows an electrical diagram of the three-phase diode bridge rectifier used for charging a constant voltage battery. This is typically used in battery charger/power supply systems such as are employed in automotive applications. This circuit is used in this experimental alternator as well. In Figure 4.8, v_{sa}, v_{sb} and v_{sc} are AC source voltage, the AC voltage is rectified into DC voltage by the diode bridge, after which the average charging circuit current becomes equal to i_o, and the battery is properly charged. (Caliskan, 1999).

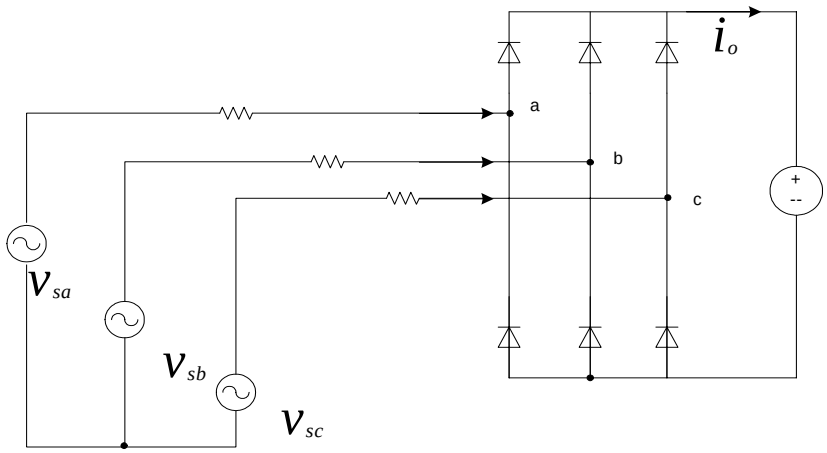

Figure 4.8 A three-phase diode bridge rectifier

During experiments, it is necessary to control the factors that will affect the vibration signal. Caliskan et al. (1999) presented a quantitative analysis of the operating characteristics of three-phase bridge rectifiers with AC-side reactance and constant–voltage loads. They provide a mathematical relationship between the line current and various system parameters, so that it helps to understand the influence from various experimental factors with respect to the vibration signal.

One of the most important equations that have been derived in their paper is

$$I_{s1} = \frac{\sqrt{V_s^{\,2} - \left(4V_O^{\,'}/\pi\right)^2}}{\omega L_S}$$

$$\tilde{i}_o \approx \frac{2}{\pi} I_{s1} \qquad (4.1)$$

where I_{s1} is the magnitude of the fundamental of the line current, V_s is the source voltage, $V_o^{'}$ is output voltage, ω is the source frequency ($\omega = 2\pi f$), L_s is the line inductance and $\tilde{i}_o$ is the average output current. Clearly, the monitored system vibration signal will be influenced when the average output current varies. From the above equation, one can see that V_s, V_o', ω and L_s will influence the magnitude of the fundamental of the line current. Among these factors, L_s can be treated as a fixed value, since the electrical machine is

common for all experiments. V_o' can be treated as a manually controlled semi-fixed value, since the voltage of the battery in each experiment can be controlled and read by voltmeter before monitoring (the battery voltage range from 11.5 to 11.6 V during experiments). ω and V_s can also be treated as manually controlled semi-fixed values, since ω and V_s are closely related to the rotating speed, which can be manually controlled by the variable speed motor controller.

In short, this mathematical relationship suggests that during each individual experiment, the following should be kept constant as far as possible:

Same load condition, keep battery voltage constant,
Same speed varying condition, motor speed control need to be consistent,
Same experimental subject, each experiment for the same machine only.

4.2.5 Connection of monitoring equipments

The connection of the monitoring equipments can be seen clearly in the Figure 4.9

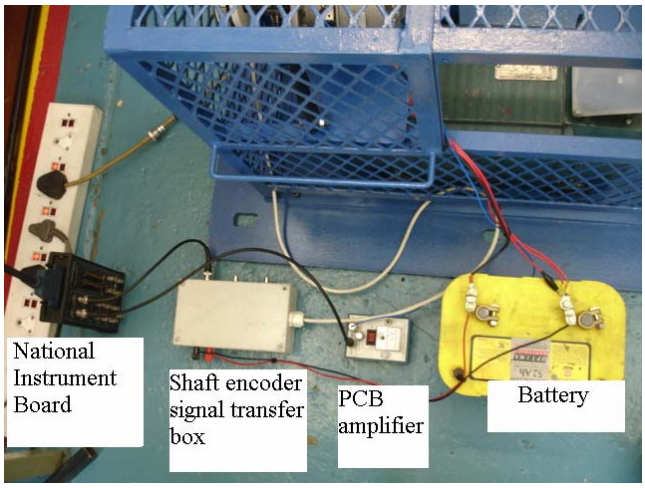

Figure 4.9 Connection of monitoring equipments

This kind of monitoring system was used to obtain the following two sets of data:

Vibration signal – the accelerometer sensor signal goes to the PCB amplifier, from the amplifier the signal goes to the NIB from where this signal will be stored in the computer.

Rotational tachometer signal – shaft encoder signal goes to shaft encoder transfer box, after transferring, it will go to the NIB, and then it goes to computer.

Both signals were monitored simultaneously.

4.2.6 Frame structure design

The frame structure of the experimental set-up was designed to include all these components in a two-level structure. This design mainly considers the economical use in space and compactness of the experimental set-up assembly. But undoubtedly, it will introduce certain structural natural frequencies while the motor is running. Therefore, a

simple modal test using an impact hammer on the frame structure was performed. To approximate free-free support conditions, the frame structure was put on a tyre inner tube, as is shown in Figure 4.11

Figure 4.11 Modal analysis of frame structure

Due to the complexity of structure, the FRF graph acquired from the modal test shows several structural natural frequencies in the spectrum (Figure 4.12). This will gave rise to significant noises during the experiment. This is also happened in the real electrical machine working environment.

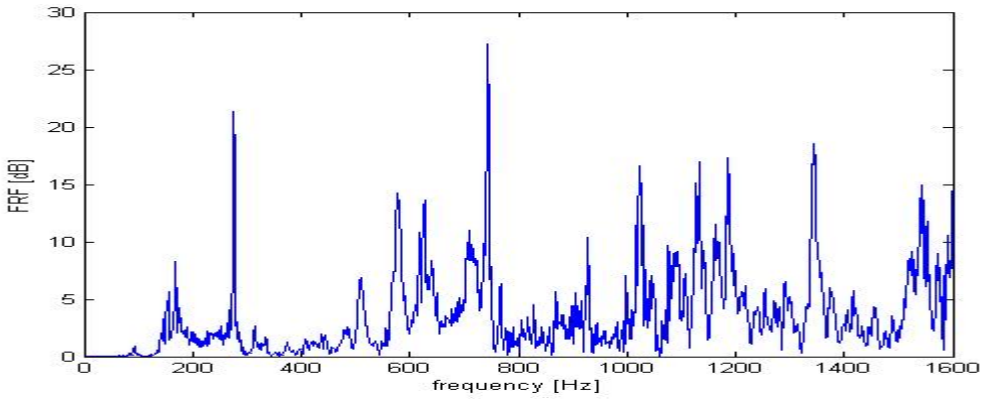

Figure 4.12 FRF acquired from modal analysis

A photo of the set-up structure can be seen in Figure 4.13 and schematically in Figure 4.14

Figure 4.13 Frame structure of experimental set-up

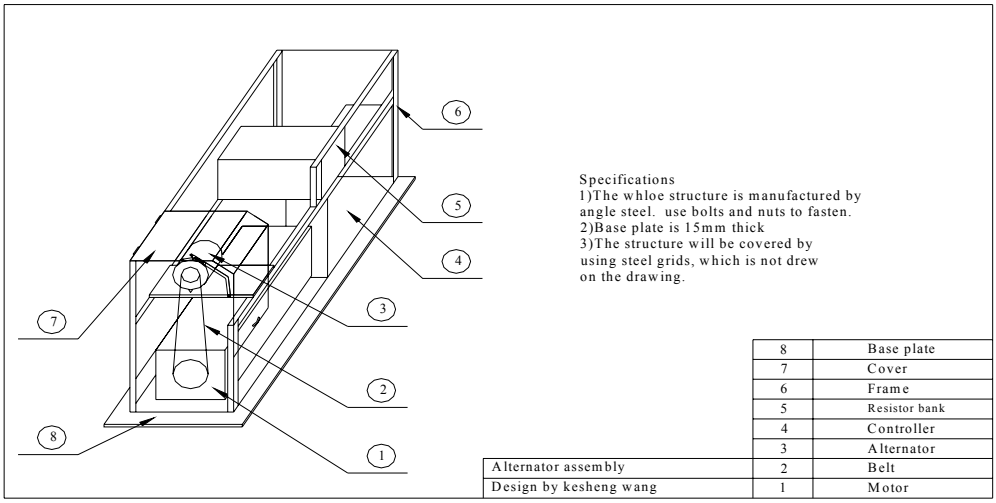

Figure 4.14 Structural design of the experimental set-up

4.3 Damage description

One of the purpose of this research is to investigate the effectiveness of Vold-Kalman filter order tracking in condition monitoring. Thus, a specific electrical machine fault condition should be artificially introduced into the system for condition monitoring purposes. As was stated in paragraph 1.2.1-c. of the literature survey, generator stator windings short damage due to excessive vibration is one of the main problems experienced by electrical machines in industry. To simulate such a fault, the stator windings were artificially damaged in this experimental set-up. (Figure 4.15(b)).

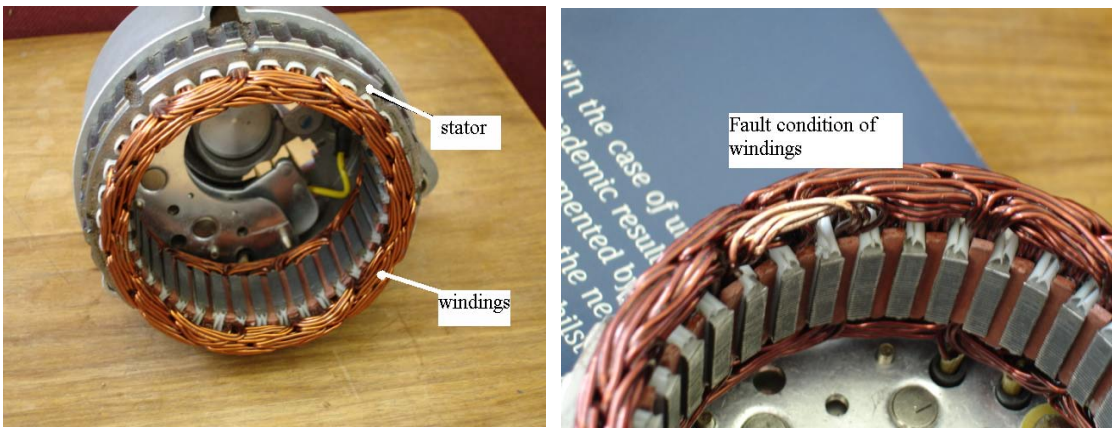

a. Good condition windings b. Fault condition windings

Figure 4.15 Alternator stator windings and the fault condition

Figures 4.15 (a) and 4.15 (b) show the alternator before and after introducing the damage respectively. In this alternator, there are 36 stator bars on which windings are wound. A small knife was used to scratch out the outer isolation layer resin of windings at the location shown in Figure 4.15 (b). This introduced a short between the windings. Due to the 36 winding bars, theoretically, this fault may be expected to influence the related orders, which are multiples of order 36. Thus, order 36 and multiples thereof will be the focus in the experimental results.

Chapter 5 Experimental data analysis using conventional monitoring order tracking techniques and Vold-Kalman filter order tracking

5.1 Experimental data analysis using order tracking techniques

The discussion on the monitoring data analysis is divided into three parts: The first part discusses the different order tracking methods applied to the same set of good condition data. The advantages and disadvantages as well as effectiveness are compared and evaluated. The second part focus on the effectiveness of order tracking techniques to detect fault conditions, and a comparison of fault condition detection is made between the Vold-Kalman Filter Order Tracking (VKF-OT) and the Angle Domain Sampling Based Order Tracking (AD-OT). Finally, the unique Vold-Kalman filter time domain filtered data are used to apply crest factor and kurtosis value under both good and fault conditions, to test their ability for condition monitoring on filtered data.

5.1.1 Different order tracking techniques for good condition data

In this section, acquired data are analysed comprehensively by using the three basic order tracking methods. As was mentioned in the literature survey, these order tracking methods are applied by using good condition monitoring data sampled from the experimental set-up. They are the Fourier Transform Based Order Tracking (FT-OT), AD-OT and VKF-OT. The data acquired from the experimental set-up comprise both vibration and tachometer signals during a run-up as are shown in Figure 5.1. In this figure the tachometer signal gives one pulse per revolution (it can also output 1024 pulses per revolution for the tachometer used in this experimental set-up). The following section examines the three basic order tracking techniques.

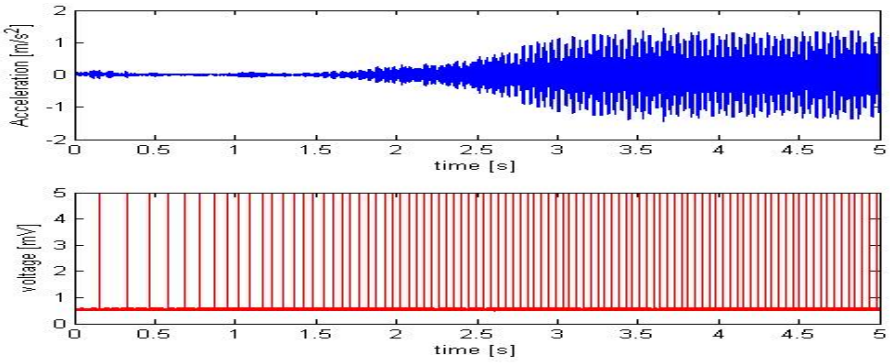

Figure 5.1 Acquired data from experimental set-up

a. Fourier Transform Based Order Tracking

i) Time spectrum map order tracking

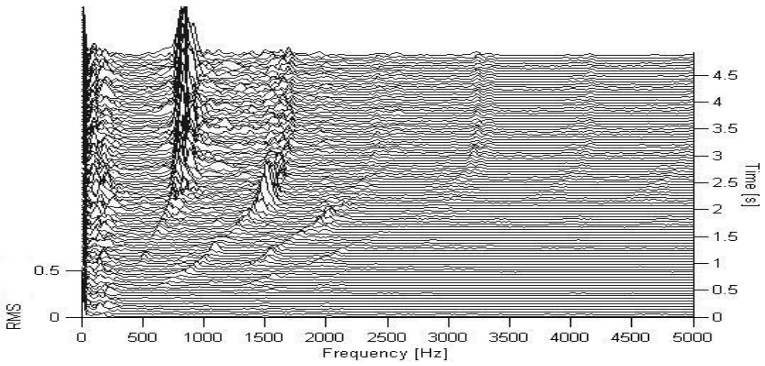

Figure 5.2 Time spectrum map

Figure 5.2 shows typical acceleration data acquired from the experimental set-up, which was subsequently analysed in the time-frequency domain using FT-OT analysis. From this map, important information about the system can be estimated. Before examining the figure, order 36 and its multiple orders are expected to appear in the figure due to the physical configuration of alternator (36 stator bars). It is clear that there are at least two high spikes through out the time. If one examines the second highest spike, it can be seen that at about time 2.2-2.5s, there is a high peak. After and before this period of time the spectral amplitude is smaller. In other words, one of the resonances in the system happened at about 2.2-2.5 sec, which is corresponding to about 1400-1700 Hz. Further, the range of order number of this second spike can be determined by combined analysis of its RPM curve (see Figure 5.3) and the time spectrum map.

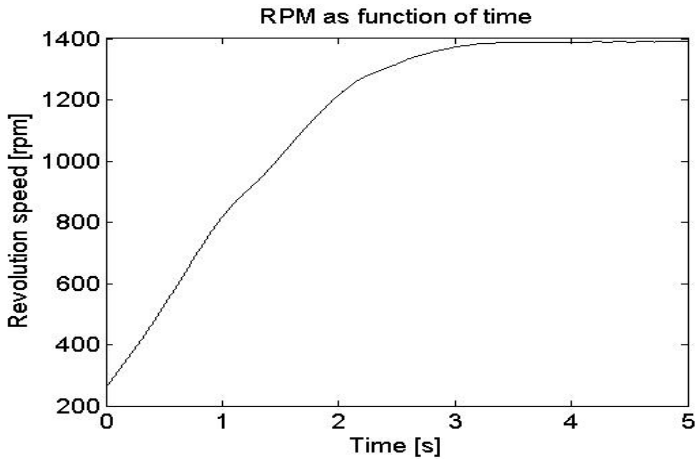

Figure 5.3 RPM curve

Figure 5.3 shows that the rotating speed is 1269 and 1316 rpm at 2.2 and 2.5s respectively, or 21.15 Hz and 21.9 Hz. Then, the corresponding order can be roughly determined from

$$order = \frac{f}{f_{rpm}} = \frac{1400}{21.15} \approx 66$$

$$order = \frac{f}{f_{rpm}} = \frac{1700}{21.9} \approx 77$$

Thus, based upon the physical structure of the alternator (36 stator bars), order 72 is the interesting order of that spike. These two graphs can be used together to determine any other orders by the same procedures. The first spike in Figure 5.2 can also be demonstrated to correspond to order 36. The above analysis calculated at one of the resonances of the system, this information will be useful to roughly estimate system damping ratio, which will be used for the choice of Vold-Kalman filter bandwidth as described in Appendix 2.

ii) RPM spectrum map order tracking

Figure 5.1 gives several spikes in the time spectrum map, but it needs an additional RPM curve to assist determining these order numbers associated with spikes on the spectrum map. Another most popular order tracking method is RPM spectrum map order tracking. It combines the RPM curve and time spectrum map together so that one can determine the order number within one map. This time, each Fourier transform is based upon a record length of 81.9 ms giving a line spacing of 19.6 rpm. (Note that the entire RPM spectrum map in the following analysis used the same resolution.) A typical RPM spectrum map is depicted in Figure 5.4, the same acceleration data was used.

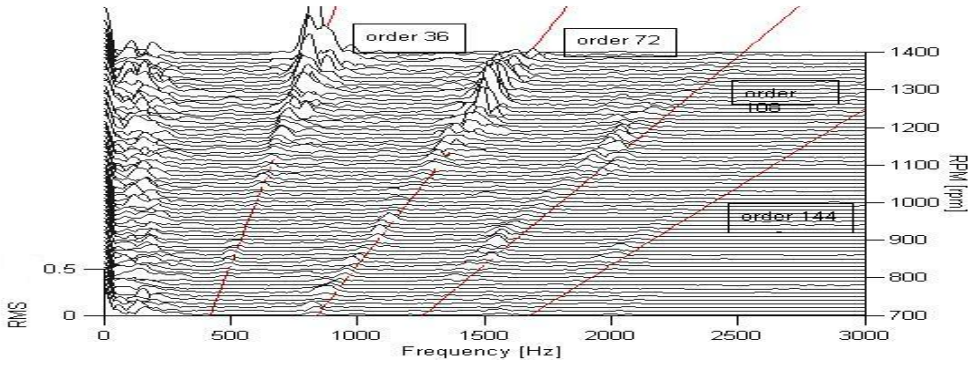

Figure 5.4 RPM spectrum map

The red lines on the map are specific orders, from the left to the right, they are orders 36, 72, 108 and 144. The equation for determining order can be defined by

$$RPM = \frac{60 \times f}{order} \qquad (5.2)$$

where f is the frequency in Hz. This representation technique is much more effective than the time spectrum map order tracking depicted in Figure 5.2.

b. Angle Domain Sampling Based Order Tracking

AD-OT has the advantage that it can overcome the frequency changing as function of time, as was stated in the literature survey. The typical AD-OT RPM spectrum map using the same set of data as above, can be plotted in Figure 5.5 (a). As was stated the AD-OT overcome the frequency changing as function of time. Figure 5.5 (a) gives a very good

visual explanation of this advantage. Each Fourier transform is based upon a record length of 0.09 orders giving a line spacing of 19.6 rpm. Compared to Figure 5.4, there are clear straight order spikes in the spectrum. Besides, since the abscissa is transformed to the order domain, a specific order will relate to a specific physical characteristic of the machine. Therefore, this type of order tracking provides a clear and simple tool to examine the changes associated with these orders. It becomes much clearer in the order domain than in the normal spectrum domain. In this sense, AD-OT becomes a good tool to detect machine faults. It must however be realised that this technique can still not overcome the amplitude varying as a function of time, during the process of Fast Fourier Transform. Therefore, the accuracy of the amplitude change of this technique is still not an ideal indicator. But this shortcoming can also be suppressed by applying a special order tracking technique – a rotation domain averaging technique, which combines the ability of order tracking and time domain averaging to suppress the spectrum smearing effect caused by fluctuation in speed, as well as to suppress the amplitude of vibration which is not synchronous with the rotation of the shaft. This technique was described by Stander et al. (2005). In this paper, only the conventional AD-OT will be discussed. Figure 5.5(b) shows the traditional angle domain order tracking analysis with several clear peaks in the spectrum, which are respectively at orders 36, 72, 108 and 144. These higher vibratory energies on orders, such as 36 and 72, are this alternator's main characteristics. Observing the changes on these orders, might provide an indication for the fault condition of this alternator.

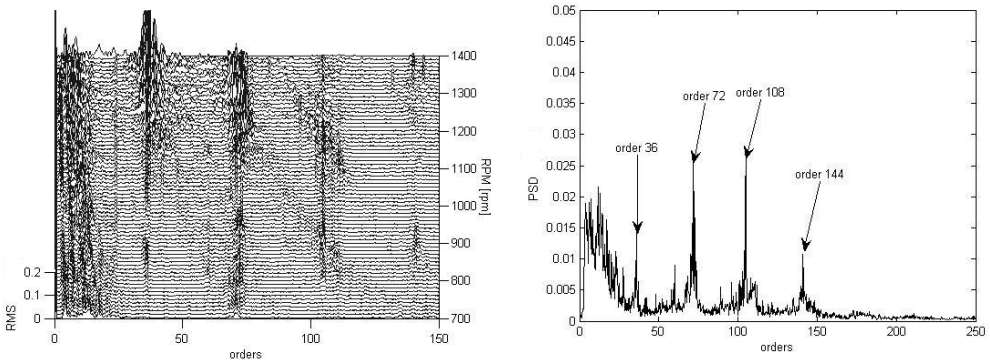

a. RPM spectrum map b. Order domain spectrum

Figure 5.5 Angle Domain Sampling Based Order Tracking

For comparison purposes, a normal spectrum map of the same set of data can be plotted as shown in Figure 5.6.

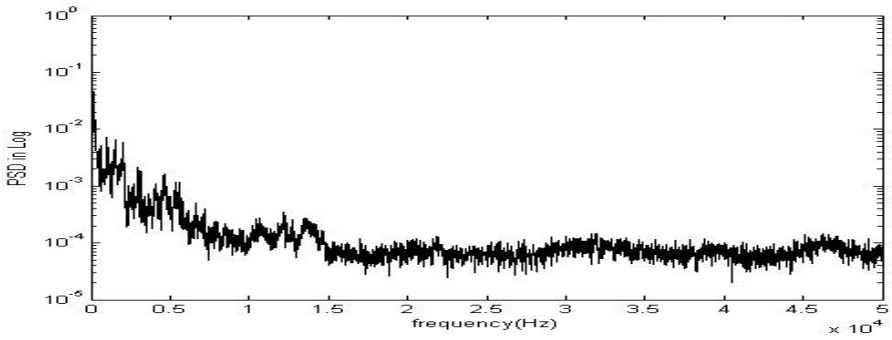

Figure 5.6 Frequency spectrum of data

Figure 5.6 shows that it is fairly difficult to find any dominant peaks by only performing frequency analysis, while the angle domain sampling order tracking rearranged the data and present a unique advantage over the normal spectrum analysis for the transient data.

On the experimental set-up used for research purposes it is possible to fix the speed, and then, to obtain averaged data at constant speed. Under these circumstances, the spectrum will not look like Figure 5.6 and some clear peaks will appear as seen in Figure 5.7 (figure acquired from Diagnostic Instruments PL202). Certain frequencies and their harmonics, for instance the marked red lines in Figure 5.7, will dominate the spectrum. Thus, the cepstrum technique could also be employed in this case to analyse the data. Fixed speed is however usually not easy to attain on industrial machines and machine speed may vary significantly. Therefore only transient monitoring techniques will be focused on in this research.

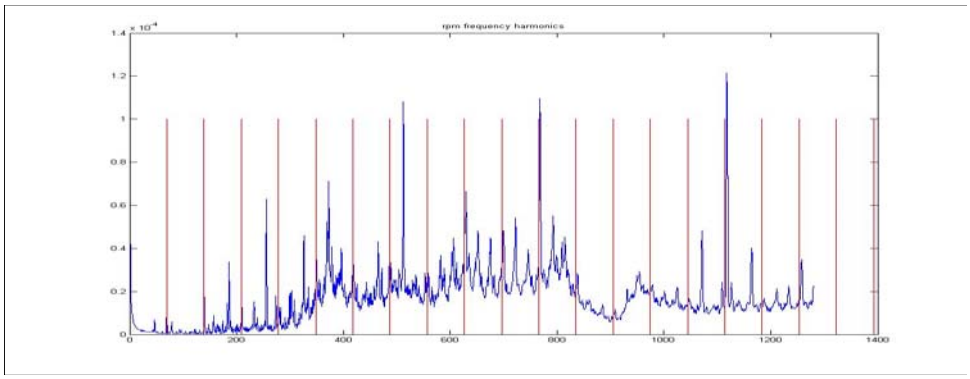

Figure 5.7 Averaged spectrum based on 50 averages

c. Vold-Kalman Filter Order Tracking

Vold-Kalman Filter Order Tracking is certainly one of the most effective OT techniques to extract order waveform. By way of example, Figure 5.8 gives a Vold-Kalman filter result for orders 36 and 72 respectively of this experimental set-up data. (See Appendix 2 for the choice of the filter bandwidth.)

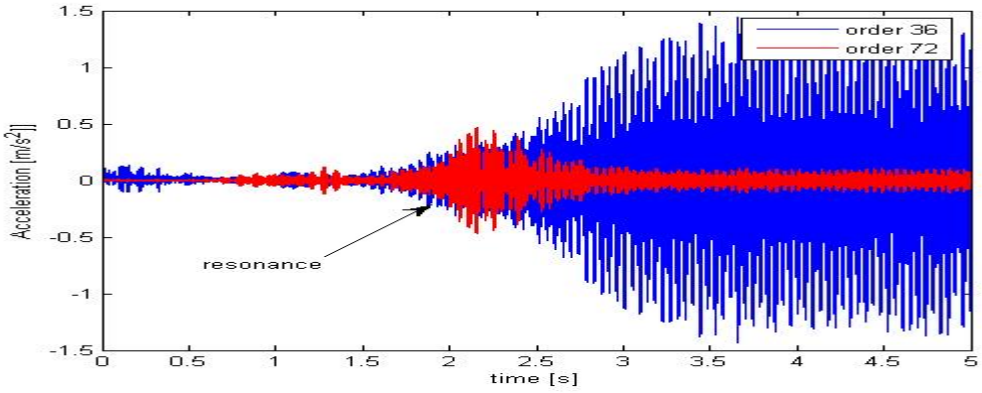

Figure 5.8 Filtered out order 36 and order 72

It is very interesting to see that at about 2.2-2.5 second, the time wave form of these orders also present a resonance which corresponds very well with what was observed with the other techniques discussed above. This filtered time domain data can also be plotted into a RPM spectrum map, which will exclude all the other orders. This allows focus on a specific order in the frequency domain. This can be seen in the following figures.

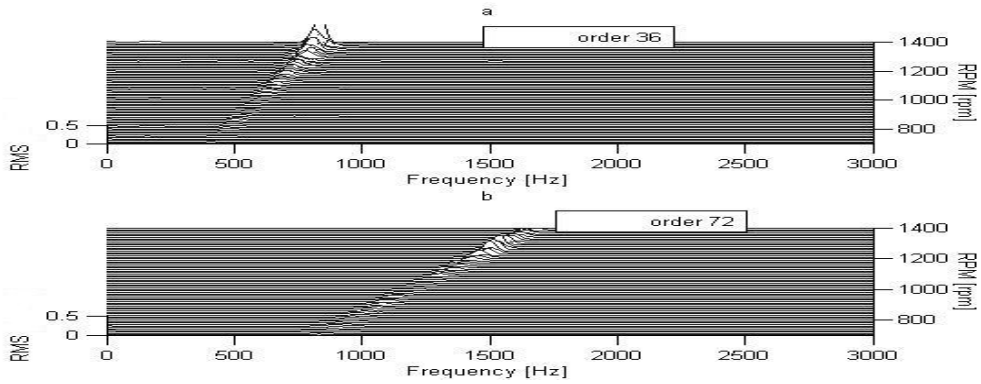

Figure 5.9 RPM spectrum map of order 36 and order 72

Figure 5.9 depicts the filtered out orders 36 and 72, which have been plotted into a RPM spectrum map. Comparing Figures 5.4 and 5.9, it is clear that orders 36 and 72 have been isolated out from the original signal. Vold–Kalman filtering also provides the ability to filter out a certain order as shown in the next figure.

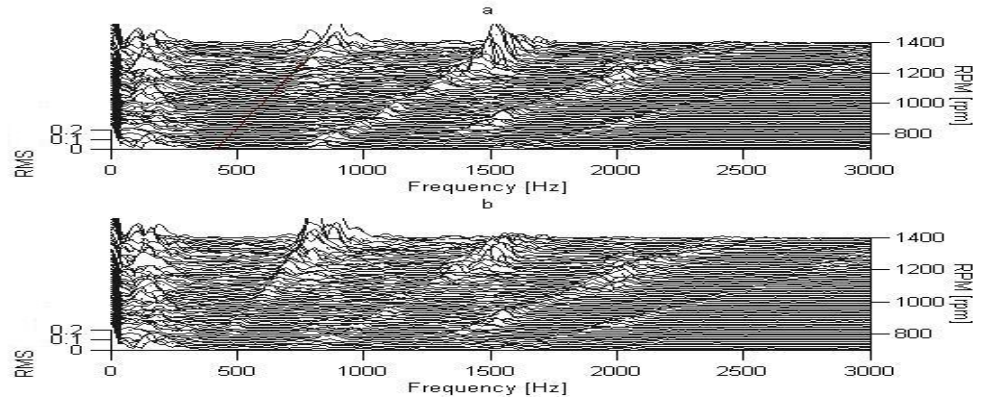

Figure 5.10 RPM spectrum map of filtering out order 36

In Figure 5.10 (a), order 36 (marked by the red line) has been filtered out. Figure 5.10 (b) is the original rpm spectrum map with order 36 still present. This leads to the question of what will be the advantage of filtered data and how the filter bandwidth affects filtering process. This is explored in Figure 5.11, which focuses on order 36.

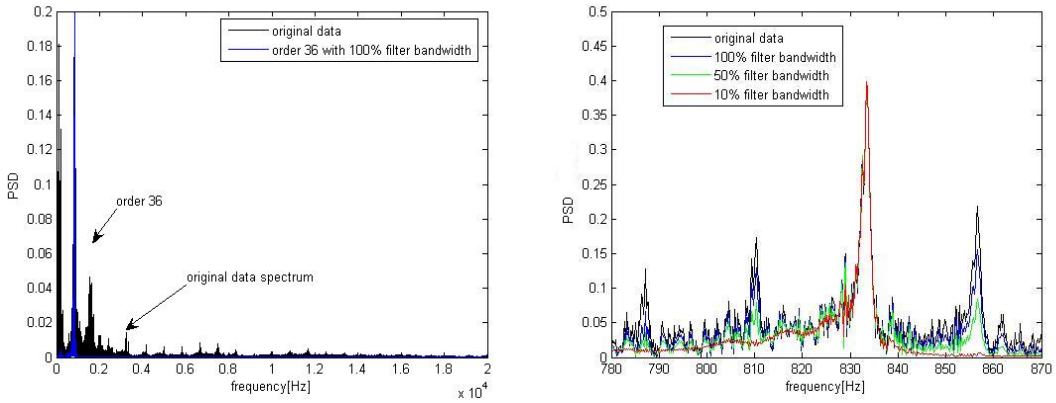

a. b.

Figure 5.11 Spectrum analysis of original data and order 36 with 100%, 50% and 10% filter bandwidth

Figure 5.11 shows another feature of Vold-Kalman filtering technique. Vold-Kalman filtering can help to understand the frequency peaks of original data frequency analysis. If one performs frequency analysis on the filtered out data, and superimpose this graph on the original frequency spectrum graph, a better understanding of original spectrum can be achieved. From Figure 5.11 (a), it can clearly be seen that the frequency peak, which relates to order 36 only, corresponds to one peak among the peaks of original spectrum map. This unique feature helps analysts to fully understand the whole spectrum. Figure 5.11 (b) is the frequency analysis of order 36 by using different filter bandwidths and comparing with original data frequency analysis graph, it is zoomed in the frequency range of 780 Hz – 870 Hz. From the comparison, it can be clearly seen that using 100% and 50% filter bandwidths, order 36 frequency peak appears at about 833 Hz, but it still includes too many sidebands, as can be seen in the Figure 5.11 (b) blue and green curves. Further, narrowing the filter bandwidth to be 10%, the result gives a clear red peak in frequency spectrum at 833 Hz, which separate order 36 effectively in spectrum map. For different filter bandwidths, Figure 5.11 (b) gives a clear illustration of the effect of filter bandwidth. The Vold-Kalman filter therefore presents a very good tool for maintenance engineers to fully understand the whole spectrum. This unique feature of Vold-Kalman filter might be used when the spectrum peaks are very close and many harmonics appear in the spectrum. With regards to the VKF-OT, one more comparison needs to be presented here:

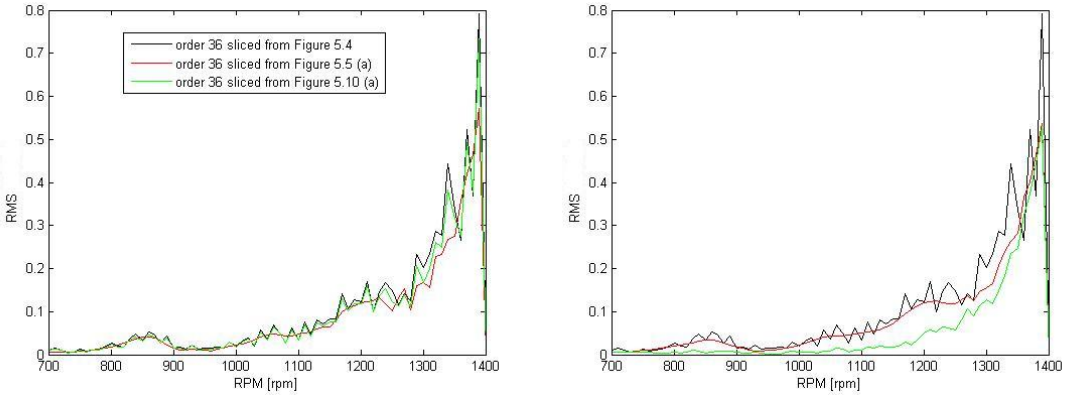

a. Vold-Kalman filter bandwidth 100% b. Vold-Kalman filter bandwidth 10%

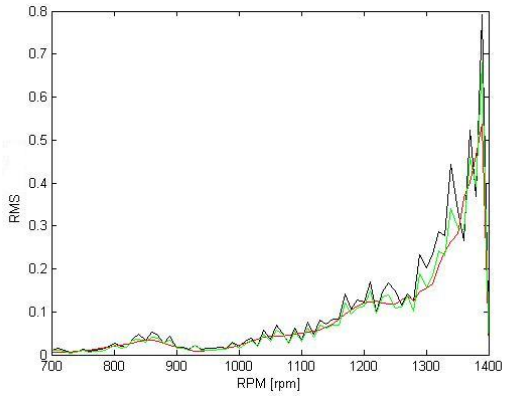

c. Vold-Kalman filter bandwidth 62%

Figure 5.12 Order 36 sliced curves

Figure 5.12 (a) depicts three sliced curves from different order tracking maps. The black curve corresponds to order 36 sliced from Figure 5.4 (RPM spectrum map), the red curve is the order 36 sliced from Figure 5.5 (a) (Angle Domain Sampling Based Order Tracking RPM spectrum map) and the green curve is the order sliced from Figure 5.9 (a) (filtered order 36 RPM spectral map). It is very interesting to see that, three of them correspond very well, especially the order sliced from RPM spectral map (black curve) and filtered order 36 RPM spectrum map (green curve). The sliced order from angle domain sampling RPM spectrum map appears smoother and lower in amplitude than another two. In other words, the angle domain sampling algorithm rearranged the original data, and it is not hundred percent true to the original data. But it does provide a good approximation and smooth curves. For Vold-Kalman filter order tracking, an important conclusion can be made based upon Figure 5.12 (a). The Vold-Kalman filter does not rearrange the original data, it provides higher fidelity to the original data than the AD-OT, in this sense, VKF-OT is more useful for examining the detail changes in the spectrum than the rearranged angle domain method. Again as has been experienced on the simulated rotor model, the Vold-Kalman filter bandwidth will also influence the result of amplitude accuracy. If a 10% filter bandwidth is applied to the data, the order 36 sliced curves will change to Figure 5.12 (b). As discussed in Appendix 2, the filter bandwidth should be at least 62% for order 36. This was applied to the data and rendered Figure 5.12 (c). Comparing the three figures, it is clear that the 62% filter bandwidth is very close to the case of 100%. In other words, filter bandwidth from 62% to 100%, the filtered results are similar. But Figure 5.12 (b) shows a clear drop in amplitude by choosing 10% filter bandwidth, so if one chooses filter bandwidth in the range of 10% to 62%, the Vold-Kalman filter will not give a stable result with this specific data. Hence, it is crucial to choose the proper filter bandwidth to perform VKF-OT. Although the choice of Vold-Kalman filter bandwidth is not a standard procedure, the proposed procedures in chapter 2 and applied in appendix 2 for the experimental data, show that this kind of procedure can be a good start for choosing the proper filter bandwidth. It is worthwhile for the inexperienced analyst to initiate the application of Vold-Kalman filter.

The preceding descriptions mainly focus on order tracking techniques and demonstrate their capabilities. Now, the effectiveness of these techniques with respect to the identification of machine faults will be further investigated.

5.1.2 Fault condition monitoring by using Vold-Kalman Filter Order Tracking technique and comparison with Angle Domain Sampling Based Order Tracking method

In this part, fault condition of alternator described in chapter 4 will be monitored via VKF-OT and AD-OT. The following monitoring techniques and comparison will be made, which are listed in table 5.1.

Table 5.1 Monitoring techniques and comparison

Monitoring techniques	Comparison
a) Angle Domain Sampling Based Order Tracking (AD-OT) b) Vold-Kalman Filter Order Tacking (VKF-OT) c) Crest factor and Kurtosis value analysis	Comparison between AD-OT and VKF-OT

a. Angle domain sampling Based Order Tracking and Vold-Kalman Filter Order tracking spectrum peak picking

For the purpose of comparison, four sets of good and fault condition data were acquired from experimental set-up. Firstly, analysing these data via AD-OT, figures like Figure 5.5 (b) for each individual test can be obtained, by using the `ginput.m` command in MATLAB, the peak values corresponding to each order can be found, so that the order 36 and other order peak values may be compared before and after fault conditions. Using the AD-OT method leads to Figure 5.13.

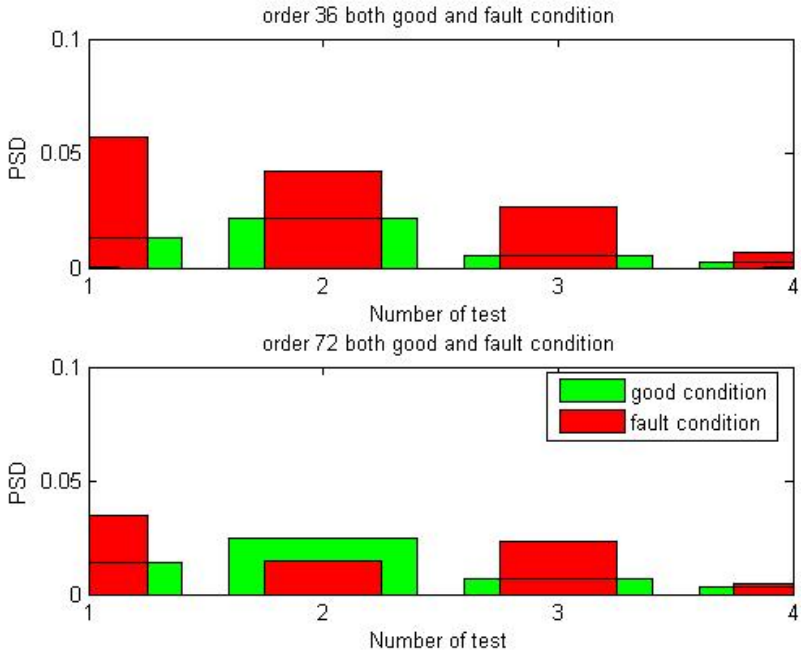

Figure 5.13 Angle domain sampling peak picking results for order 36 and 72

.
From Figure 5.13, it can be seen that order 36 gives a clear difference between good and fault condition, but order 72, at test 2, good condition value even higher than fault condition. It cannot give a consistent trend of the system, this will give rise to trouble to indicate the fault condition.

Secondly, using same sets of data, let's look at the counter part in this comparison-Vold-Kalman filter. The Vold-Kalman filter can filter out order data in time domain, and then these time domain data can be analysed into frequency domain as was presented in Figure 5.11 (a). If one chooses the proper filter bandwidth (in this case, using 100% filter bandwidth) and performs frequency analysis of each order. Again to use `ginput.m` command to pick the peak values in the each order data spectrum, Figure 5.14 can be resulted.

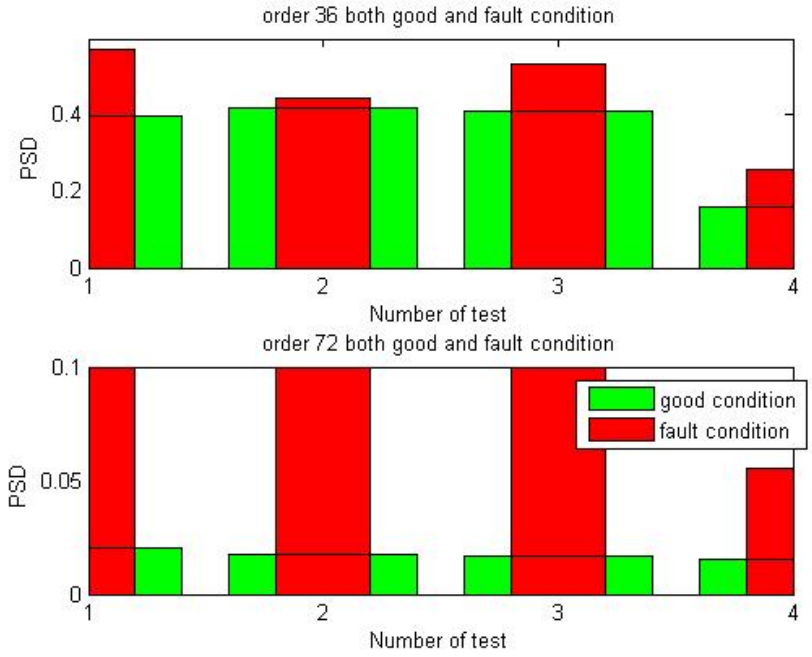

Figure 5.14 Vold-Kalman filter peak picking results for order 36 and 72

Comparing Figures 5.13 and 5.14, Figure 5.14 gives a much clearer indication that fault condition peak values are overwhelmed in both order 36 and 72, in other words, using the same four sets of data, the Vold-Kalman filter can more effectively detect the changes of the system. Examining the details of Figure 5.14, there is a consistent large difference in the peak amplitude on order 72 between the good and fault conditions. But this does not appear in Figure 5.13. The reason for the large differences observed on order 72 is that, (as was discussed in paragraph 3.4.1), the stator windings inter-turn fault excitation forces will be pulsating sinusoidally in time, at a frequency of twice the rated electrical frequency in the field circuit. For this experimental alternator, the sensor was put directly on the outer surface of stator bar (36 bars), on which the windings are wound and the field current flow through these windings. Thus, the fault excitation forces will correspond to twice the number of stator bars, which is order 72. Therefore, with the help of the simulated damage model analysis, the real experimental data can be explained reasonably and confidently.

In conclusion, the VKF-OT has an advantage over the AD-OT in indicating the fault condition. In this case, it gives a very clear indication that something went wrong in the

machine, which relates to order 72. From the arguments presented in chapter 4 this can be tied to a stator winding short. This conclusion can be reached effectively from the Vold-Kalman filter order tracking.

b. Time domain unique advantage attempt for Vold-Kalman Filter Order Tracking

As observed in the simulated damage study and analysis via Vold-Kalman filter (paragraph 3.4.2), the crest factor, kurtosis value and RMS value can be a good indicator to monitor the machine fault of stator windings short. In this case, crest factor and Kurtosis value will be applied in real experimental data in the following.
Crest factor and kurtosis value are widely used in machine diagnosis, and are defined as follows:
Crest factor: Crest factor is defined as the peak amplitude of a waveform divided by its RMS value:

$$\text{Crest factor} = \frac{\textit{Peak amplitude of a waveform}}{\textit{RMS value}} \qquad (3)$$

Kurtosis value: For univariate data $x_1, x_2, \ldots, x_N$, the formula for kurtosis is**:**

$$kurtosis = \frac{\sum_{i=1}^{N}(x_i - \bar{x})^4}{(N-1)s^4} \qquad (4)$$

Where $\bar{x}$ is the mean, s is the standard deviation, and N is the number of data points.
The purpose of the crest factor calculation is to give an analyst a quick idea of how much impacting is occurring in a waveform. Kurtosis is a measure of whether the data are peaked or flat relative to a normal distribution. Data sets with high kurtosis tend to have a distinct peak near the mean, the corresponding normal distribution decline rather rapidly, and have heavy tails. Data sets with low kurtosis tend to have a flat top near the mean rather than a sharp peak. Both of these factors are sensitive to impact related changes in the data sets.

But for the seeded fault as was introduced on the alternator stator in the experimental test rig, the inter-turn short will not cause high amplitude impacts on the system, but rather give rise to a synchronous excitation force with lower amplitude compared with the dominant magnetic force. Thus, this fault scenario is not associated with significant impact in the system signals, but rather a comparatively low amplitude synchronous force which actually increases the value of the RMS, but not the peak amplitude of the data. By way of example: From Eq. (3) it is clear that if the peak value remains stable as the RMS value increases, the crest factor will become smaller.

To make this point clearer, a simple example is presented here:

Consider a simple sinusoidal wave (amplitude $1m$, frequency $1/2\pi$ Hz) with a single high peak at $10m$. For this system the RMS = 0.7159 and the Peak amplitude = $10m$ (Figure 1(a)). If a sinusoidal wave (amplitude $0.5m$ and frequency $1/\pi$ Hz) is added to this system the RMS = 0.7986 and the peak amplitude remains = $10m$ (Figure 1(b)).

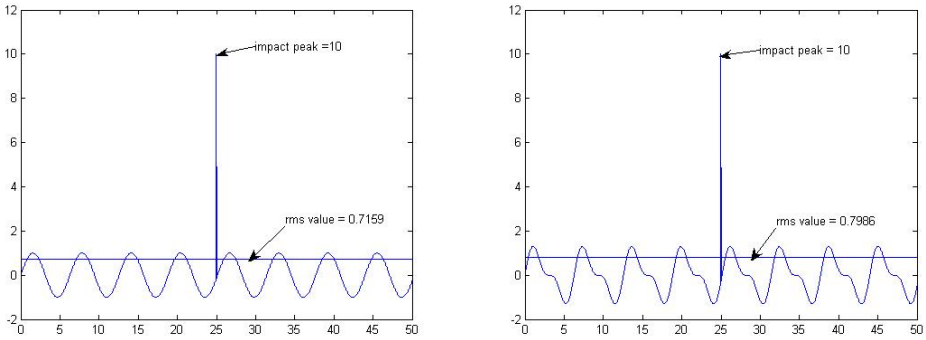

a. b.

Figure 1 Sinusoidal wave and peak

It is clear that with the introduction of the smaller amplitude sinusoidal wave, the RMS value increased from 0.7159 to 0.7986. Hence, the corresponding crest factors for the two scenarios are 13.97 and 12.52. This is the reason why the value decreased as the short fault occurs in the alternator stator windings.

Thus, the same sets of data as were used above before and after introducing short damage in alternator stator windings, two factors (crest factor and Kurtosis) were compared at two orders namely 36 and 72.

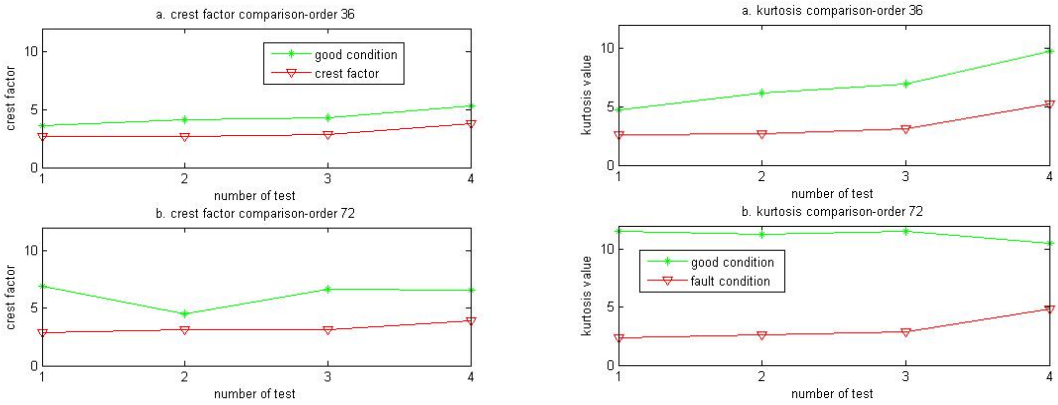

a. Crest factor comparison b. Kurtosis values comparison

Figure 5.15 crest factor and Kurtosis value comparison for order 36 and 72

From Figure 5.15, it is very clear to see that, both crest and kurtosis values have a clear difference before and after introducing damage for order 36 and 72. As can be expected that, for the inter-turn short condition, both crest factor and kurtosis values are lower than the good condition, this also happened in the simulated discussion in chapter 3. Thus, the simulated fault condition discussed in chapter 3 and this real fault condition results confirm the validity of this method both in theory and practice. Besides, from previous frequency peak discussion, especially from Figure 5.14, order 72 relates to the inter-turn short damage, in Figure 5.15, it also indicates that order 72 appears bigger difference both in crest factors and kurtosis values. In the end, this is the unique analysis for the Vold-Kalman filter order tracking technique, and no other order tracking methods can perform time domain analysis like this so far.

Chapter 6 Conclusion

This dissertation entails a study of condition monitoring on electrical machinery and particularly explores the advantages of the Vold-Kalman filtering. The choice of the Vold-Kalman filter bandwidth for real data, as well as the basic theory of this technique was described. In order to gain experience in the implementation of the Vold-Kalman filter order tracking technique in the rotating machine environment, a simulation study of electrical machinery was performed by using a single and a two-degree-of-freedom system, in which the entire response of the system and system characteristics under consideration are known. Further, a proper experimental set-up was established. Vibration and tachometer data were monitored simultaneously for both good and fault conditions, VKF-OT as well as other order tracking techniques were applied on these data, and the unique abilities of VKF-OT were demonstrated.

In chapter 1, condition monitoring techniques on electrical machinery were firstly surveyed from electrical, vibratory, thermal and chemical prospectives. Three basic order tracking techniques, namely, Fourier Transform Based Order Tracking (FT-OT), Angle Domain Sampling Based Order Tracking (AD-OT) and Vold-Kalman Filter Order Tracking (VKF-OT), were discussed and compared.

In chapter 2, the second generation Vold-Kalman filter underlying theory based on Tuma's (2005) work and one method to choose the Vold-Kalman filter bandwidth for application on real data (as developed by Herlufsen et al. (1999)) were summarized together as a package. This provides the basic theory of simulation model application of Vold-Kalman filter technique as well as the basic theory of MATLAB program of Vold-Kalman filter.

In chapter 3, a single and a two-degree-of-freedom system rotor models were subsequently introduced with simplified simulated electrical machine external excitation forces. In this way simulated electrical rotor systems with known characteristics were established. The Vold-Kalman filter was applied on these models. The known model characteristics were used to demonstrate the validity of a Vold-Kalman filter MATLAB program. Further, Vold-Kalman filter relative bandwidth choice developed in chapter 2 was applied to choose the proper filter bandwidth for filtering. System damping and Vold-Kalman filter bandwidth effects were investigated on the known simulated system. It was shown that both these factors will influence the filter results. The higher the damping of the system, the narrower of Vold-Kalman filter should be chosen in order to achieve the proper filtered data. The unique ability of Vold-Kalman filter to filter out resonance of the system and time domain data analysis ability was explored. It was shown that after filtering the resonance of simulated system, the sliced order from RPM spectrum map becomes a clearer indicator for condition monitoring. The crest factor, kurtosis value and RMS value are effective to detect the simulated damage of the system, and also provide a theoretical basis for the further experimental analysis.

In chapter 4, a simple experimental set-up was constructed. It provides a practical platform for condition monitoring of electrical machinery. A simple stator inter-turn short was introduced into the system for condition monitoring purposes. Electrical influence factors on each experiment were discussed via a mathematical relationship. Two signals from

electrical alternator were acquired simultaneously, namely, rotating tachometer signal and stator vibration signal for performing order tracking analysis.

In chapter 5, experimental results were acquired from the set-up. Three different order tracking techniques were applied on the same set of experimental data. A comparison between them was made. The sliced curves from three order tracking techniques' RPM spectrum map show that the popular AD-OT is not perfectly true to the original data due to the re-sampling process, but the Vold-Kalman filter method is much more true to the original data in this sense. The Vold-Kalman filter bandwidth effect on experimental data was also explored via the sliced order curves. It shows that the proposed filter bandwidth choice method is a good initial choice for the application of Vold-Kalman filtering. Further, fault condition monitoring stator inter-turn short shows that the Vold-Kalman filter is more capable to give clear indications for the fault condition than the AD-OT did by using the same sets of data. Unique time domain filtered order data also shows that crest factor and kurtosis value are capable to provide a clear indicator of system fault condition via analysing filtered order data.

References

Albright, D. R. (1971). Inter-turn short circuit detector for turbine generator rotor windings. *IEEE Trans. Power Appl*. And Sys. Vol., PAS-50, 1971,PP478-483.

Albright M. F. and Qian Sh. (2001) A comparison of the newly proposed Gabor order tracking technique vs. other order tracking methods. *SAE paper*, No.2001-01-1471

Arshad, M. (2004). Turbo generator stator winding condition assessment. *Power System Technology, 2004. PowerCon 2004. 2004 International Conference*. Nov. 2004, Vol. 2, pp1399-1403.

Barber, A. (1992). *Handbook of noise and vibration control,* 6th edition, Elsevier.

Blough, J. R. (2003a). Development and analysis of time variant discrete Fourier transform order tracking. *Mechanical and Systems and Signal Processing* (2003) 17(b), pp1185-1199.

Blough, J. R. (2003) A survey of DSP methods for rotating machinery analysis, what is needed, what is available. *Journal of Sound and Vibration* 262(2003), pp707-720.

Brandt, A., Thomas, L., Ahlin, K. and Tuma, J. (2005). Main principles and limitations of current order tracking methods. *Sound and Vibration*, March 2005.

Brüel and Kjær (1980). Measuring Vibration, Brüel and Kjær, Naerum, 1980.

Brüel and Kjær (1984). Brüel and Kjær: machine health monitoring Brüel and Kjær, Naerum, 1984.

Buckley, G. W. (1982). The effects of rotor inter-turn short circuits on voltage imbalance and circulating currents in large generator stator windings, *Proc. Of Int. Conf. On Electrical Machines - Design and Applications*, *IEE*, London, Conference Publn. 213, July 1982, pp206-211.

Cameron, J. R., Thompson, W. T. and Dow, A. B. (1985). Vibration and current monitoring for detecting air gap eccentricity in large induction motors, *Proc. Of Int. Conf. On Electrical Machines- Design and applications*, *IEE*, London, September, Publn. 254, pp173-179.

Caliskan V., Perreault, D.J., Jahns, T.M., and Kassakian, J.G. (2003). Analysis of three-phase rectifiers with constant-voltage loads. *IEEE Transaction on circuits and systems-1: Fundamental theory and applications*, Vol 50, No.9, September 2003.

Carson, C. C., Barton, S. C. and Crobel, L. P. (1971). Immediate detection of overheating in gas-cooled electrical machines, *IEEE PES Winter Power Meeting*, January 1971, Paper 71.

Carson, C. C., Barton, S. C. and Echeverria, F. S. (1973). Immediate warning or local overheating in electrical machines by the detection of pyrolysis products, *IEEE Trans. Pow. Appl. & Sys.*, Vol. PAS-92, January/June 1973, pp533-542.

Carson, C. C, Barton, S. C. and Gill, R. S. (1978). The occurrence and control of interference from oil-mist in the detection of overheating in a generator. *IEE, Trans. Pow. App. & Sys.*, Vol. PAS-57, No. 5, Sept/Oct. 1978, pp1590-1514.

Caryn, M. R. (1998). A method for sensorless on-line vibration monitoring of induction machines. *IEEE, Transaction on Industry Applications*, Vol. 3, No.6.

Conolly, H. M., Jackson, R. J., Lodge, I. And Roberts, I. A. (1985). Detection of shorted turns in generator rotor windings using air gap search coils. *Proc. Of Int. Conf. On Electrical Machine- Design and Applications*, *IEE*, London, Conference Publn. 254, September 1985, pp11-15.

De Mello, F. P. (1994). Measurement of synchronous rotor angle from analysis of zero sequence harmonic components of machine terminal voltage. *Power Delivery, IEEE Transaction*, and Vol. 9, pp1770-1777.

Electrical training manual, ESKOM (undated study notes) Power station electrical plant module 3-Generator.

Emery, F. T., Lenderking, B. N., Couch, R. D. (1981). Turbine generator on-line diagnostics using RF monitoring, *IEEE Trans. On power appl. And Sys*, Vol. PAS-100, No. 12, December 1981, pp4974-4982.

Erskine, J. B. (1978). A user's view of noise and vibration aspects of A.C. induction motors. *IEE Colloquium on Design Applications and Maintenance of Large Industrial Drives*.

Erlicki, M. S., Porat, Y. and Alexandrovltz, A. (1971). Leakage field changes of an induction motor as indication of non-symmetric supply. *IEEE Trans. Gen. Appl.*, Vol. IGA-7, No.6, Nov./Dec, pp 713-717.

Feldbauer, Ch. And Holdrich, R. (2000) Realisation of a Vold-Kalman Tracking Filter – A Least Square Problem, *Proceedings of the COST G-6 Conference on Digital Audio Effects*, DAFX 1-4, Verona Italy, December 7-9.

Fischer, D. (2002). Using a Bayes classifier to optimize alarm generation to electric power generator stator overheating. *Virtual and intelligent Measurement System*, *2002. VIMS'02. 2002 IEEE International Symposium*. May 2002, pp 140-145.

Fyfe, K. R. and Munck, E. D. S. (1997). Analysis of computed order tracking. *Mechanical Systems and Signal Processing*, 1997, 11(2), pp187-205.

Gade, S., Herlufsen, H., Konstantin-Hansen, H. and Vold, H. (1999). Characteristics of the Vold-Kalman order tracking filter, *Brüel and Kjær Technical review*, 1999.

Gaydon, B. G., Hopgood, D. J. (1979). Filtering pulse can reveal an ailing motor, *Electrical Review*, Vol.205, No. 14, October 1979, pp 37-38.

Gaydon, B. G. (1979). An instrument to detect induction motor rotor circuit defects by speed fluctuation measurements, *Testmex Conference*, *IEE* Wembley, June 1979, Conference Publn.174, pp5-8.

Greg, C. (1995). In-service evaluation of Motor and Generator stator windings using Partial Discharge Tests, *IEEE Transaction on industrial applications*, Vol. 31 No.2 March/April 1995.

Geszti, P. (1986). Test system for measuring rotor temperature using contactless signal transmission. *Conf. On Evolution and Modern Aspects of Induction Machines*, Turin, Italy, July 8-11,1986.

Green, V. (2005). Summary of industry practices, guides and standards related to on-line partial discharge monitoring of stator insulation condition. *Petroleum and Chemical Industry Conference*, 2005. Industry Applications Society 52nd Annual, pp359-365

Hargis, C., Gaydon, B. G. and Kamash, K. (1982). The detection of rotor defects in induction motors. *Proc. Int. Conf. On Electrical Machines, Design and Applications*, *IEE*, London May 1982, Publn. 213. July 1982, page 216-220.

Hargis, C., Muhlhaus, J., Roberts, I.A. and Sutton, J. (1985). Turbo-generator rotor earth fault monitoring and protection, *Pro. Of Int. Conf. On Electrical Machines- Design and Applications, IEE*, London, Confernece Publ. 254, September 1985, pp6-10.

Hewlett Packard (1983). Application Note 243-1: Dynamic signal analyzer applications, Palo Alto, 1983.

Herlufsen Henerik, Gade Svend and Konstantin-Hansen H. (1999). Characteristics of the Vold/Kalman order tracking filter. *17th International Modal Analysis Conference*, Kissimmee, FL, Feb. 1999.

Heyns, P. S. (1989). Transient dynamics of rigid rotors on flexible bearings. *International Journal of Mechanical Engineering Education* Vol. 17 No.3.

Heyns, P. S. (2003). *Study guide: Mechanical vibration*. Study notes of Mechanical vibration course in University of Pretoria.

Khudabashev, K. A. (1961). Effect of turn short-circuits in a turbo-generator rotor on its state of vibration, *Elekt Stantsii (Russian)*, No. 7,1961, pp40-45.

Kliman, G. B. (1996). A new approach on-line turn fault detection in AC motors. *Industry Applications Conference*, *1996, Thirty-first IAS Annual Meeting, IAS' 96., conference Record of the 1996 IEEE*, Vol. 1, pp687-693.

Kryukhin, S. S. (1972). A new principle for synchronous machine protection from rotor winding inter-turn and double earth faults. *Elect. Technol. USSR*, Vol. 2, 1972, pp47-59.

Ksala, G. F. (1966). The ion chamber detector as a monitor of thermally produced particulates. *J.de Res. Atmos*, 1966, April/Sept.

Kurtz, M., and Stone, C. C. (1979). In-service partial discharge testing of generator insulation, *IEEE Trans. of Electr. Insul*. Vol. EI-14, No. 2, April 1979, pp 94-100.

Kurtz, M, Stone, C. C., Freeman, D., Mulhall, V. R., Lonseth, P. (1980). Diagnostic testing of generator insulation without service interruption. *CIGRE*, Paris 1980, paper 11-09.

Leger A.C. Szylowicz, N. (1997). Modelling the vibration behaviour of stator end windings. *Electrical Machines and Drives, 1997 Eighth International Conference* (Conf. Publ. No.444), Sept. 1997, pp160-164.

Leonard, R. A. and Thompson, W. T. (1984). Vibration and stray flux monitoring for unbalanced supply and inter-turn winding fault diagnosis in induction motors. *Proc. 1st U.K. International Conf. On condition Monitoring Swansea*, pp340-354.

Li X. (2004). Application of UHF on partial discharge detection in generator stator bar. Solid Dielectrics, 2004. ICSD 2004. *Proceeding of the 2004 IEEE International Conference*, July 2004 Vol. 2, pp 676-678.

Lodge, I. (1982). Prevention of catastrophic failure of large generators by early detection of overheating. *Proc. Int. Conf. Of Electrical Machines –Design and Applications*, *IEE*, London, Conference Publn. 213 .1982, pp123-130.

Makel, D. (1986). Thermal design and development of actively cooled brushes for compact homopolar generators. *Magnetics IEEE Transactions*, Nov. 1986, Vol. 22, pp 1603-1608.

Malik, A. K., Cook, R. F. and Tavner, P. J. (1985). The detection of discharges in alternators using wideband radio frequency techniques. *Proc. Of Int. Conf. On electrical Machines – Design and applications IEE*, London, September 1985, Conference Publn. 254, pp 121-125.

Maxwell, J. H. (1983). Induction motor magnetic vibration. *Proc. Vibration institute, Machinery Vibration Monitoring and Analysis Meeting*, Houston, Texas.

Mayes, I. W., Steer, A. G. and Thomas, G. B. (1981). The application of vibration monitoring for fault diagnosis in large turbo-generators. *6th Thermal Generation Specialists Meeting*, Madrid, 5-6 May.

McDonald, J. R. (1991). Advanced condition monitoring and fault diagnosis of turbo-alternators using an embedded expert system. *Advanced Condition Monitoring System for Power Generation, IEE Colloquium*. Oct. 1991, pp9/1-9/4.

Mchiguchi, Y., Tonisaka, S., Izumi, S., Watanabe, T. and Miyashita, I. (1983). Development of a collector ring monitor for sparking detection on generators. *IEEE Trans. Power Appl. And Sys.*, Vol. PAS-102, No. 4,1983, pp928-933.

Mellor, P. H., Turner, D. R. and Roberts, D. (1985). Microprocessor based induction motor thermal protection. *Proc. Int. Conf. Electrical Machines, Design and Applications*, *IEE*, London, 1985, Publn. 254.

Munlhaus, J., Ward, D. M. and Lodge, I. (1985). The detection of shorted turns in generator rotor windings by measurement of circulating stator currents. *Proc. Of Int. Conf. On Electrical Machines- Design and Applications*, *IEE*, London, Conference Publn. 254, September 1985, pp100-103.

Neale, M. and associates (1979). A guide to the condition monitoring of machinery, HMSO Publication.

Norton, M. P. (1989). *Fundamentals of noise and vibration analysis engineers*. New York: Cambridge university press, 1989.

Pan, M. Ch. and Lin Y. F. (2006). Further exploration of Vold-Kalman-filtering order tracking with shaft –speed information. *Mechanical Systems and Signal processing* 20 (2006) 1410-1428.

Pan, M. Ch., Liao, Sh. W. and Chiu, Ch. Ch.(2006) Improvement on Gabor order tracking and objective comparison with Vold-Kalman filtering order tracking. *Mechanical Systems and Signal processing* 21 (2006) 653-667.

Pan, M. Ch. and Wu, Ch. X. (2007) Adaptive Vold-Kalman filtering order tracking. *Mechanical Systems and Signal processing*. Doi:10.1016/j.ymssp.2007.06.002

Penman, J., Hadwick, J. G. and Stronach, A. F. (1980). Protection strategy against the occurrence of faults in electrical machines. *Proc. Of 2nd Int. Conf. On Developments in Power System Protection IEE*, London, Conference Publn. 185, June 1980, pp54-58.

Penman, J., Tait, A. J., Smith, J. R. and Bryan, W. E. (1985). The development of a machine condition monitoring system for electrical drives. *Proc. Of Conf. On Drives, Motors and controls*.

Poyhonen, S. (2004). Signal processing of vibrations for condition monitoring of an induction motor. *Control, Communications and Signal Processing*, 2004. First International Symposium, pp499-50.

Rai, R. B. (1974). Air gap eccentricity in induction motors, *ERA Report*, pp1174-1188.

Ramsden, D. and Dring, E. (1966). Thermal protection of small and medium size low tension induction motors. *LSE Engineering Bulletin*, Vol. 9, No. 2, October 1966, pp1-20.

Randall, R. B. (1980). Ceptrum analysis and gearbox fault diagnosis, *Brüel and Kjær Publications*, Application Note 233.

Rankin, D. R. Wilson, I. (1995). The use of shaft voltage to detect air gap eccentricity and shorted turns in salient pole alternators. *Electrical Machines and Drives, 1995, Seventh International Conference* (Conf. Publ. No. 412), Sep. 1995, pp194-197.

Rickson, C. D. (1983). Protecting motors from overload due to asymmetrical fault conditions. *Electrical Review*, 7th December, pp778-780.

Rosenberg, L. T. (1978). Influence of shorted turns on thermal unbalance in large generators *IEEE*, *PES Summer Meeting,* Los Angeles, July 1978, paper A78, 587-8.

Rogers, A. J. (1982). Optical temperature sensor for high voltage applications. *Applied Optics*, Vol. 21, No.5, March 1982, pp882-885.

Rusche, P. A. E. (1985). Torsional monitoring for diagnosis and surveillance: utility experience. *EPRI Workshop*, USA, pp 52-66.

Say, M. G. (1976). Alternating Current Machines. *Pitman Publishing*, London, 1976, p137.

Shao, H., Jin. W. and Qian, Sh. (2003) Order tracking by discrete Gabor expansion. *IEEE Transactions on instrumentation and measurement* . Vol. 52. No. 3, June 2003

Shoel, E. O. Shoel, E. D. (1984). Shock pulse as a measure of the lubricant film thickness in roller element bearings. *Condition Monitoring '84, Ed. M.H. Jones, Pub. Pineridge Press*, Swansea, pp148-161.

Showalter, A. (1999). In-service winding failure of newly installed replacement stator. *Electric Machines and Drives*, *1999. International Conference IEMD '99*, pp797-799.

Siyambalapitiya, D. J. T., Mclaren, P. G. and Acarnley, P. P. (1986). A rotor condition monitor for squirrel cage induction machines, *IEEE Industrial Applications Society Annual Meeting*, Denver, U.S.A., Sept. 1986.

Sottile, J., Trutt, F. C., Leady, A. W. (2001). Condition monitoring of brushless three-phase synchronous generators with stator winding or rotor circuit deterioration. *Industry Application conference*, *thirty-sixth IAS Annual meeting conference record of the 2001 IEEE*. Vol. 3, pp1587-1594.

Stander C. J., Heyns, P. S. (2005) Condition monitoring of gearboxes operating under fluctuating load conditions. Pretoria: University of Pretoria.

Steqemann, D. (1998). Monitoring and vibration diagnostic of rotating machinery in power plants. Power Station Maintenance- Profitability Through Reliability, 1998, First *IEE/ImechE International Conference*, pp39-44.

Stone, G., Kapler, J. (1998). Stator winding monitoring. *Industry Applications Magazine*, *IEEE*, Sep.-Oct. 1998, Vol. 4, Issue: 5, pp15-20.

Stone, G. C. (2003). Recent important changes in IEEE motor and generator winding insulation diagnostic testing standards. *Petroleum and Chemical Industry Conference*, 2003. Record of Conference Papers. IEEE Industry Applications Society 50th Annual. pp101-110.

Subhasis Nandi (2005). Stator fault detection in induction machines using triple harmonics at motor terminal voltage after switch-off. *Power Engineering Society General Meeting*, *2005, IEEE*., pp 1897-1902.

Tavner, P. J., Penman, J. (1987). *Condition monitoring of electrical machines*. Publisher: Research studies press Ltd.

Trutt, F. C. (2002). Condition monitoring of induction motor windings using electrically excited vibrations. *Industry Applications Conference*, 2002. 37th IAS Annual Meeting. Confernece Record, Vol. 4, pp2301-2305

Tuma, J. (2005). Setting the pass bandwidth in the Vold-Kalman order tracking filter. *Twelfth International Congress on Sound and Vibration,* Lisbon, Jul. 2005.

Tuma, J. (undated study notes). *Vold-Kalman Order Tracking Filteration*. Faculty of Mechanical Engineering, Department of Control Systems and Instrumentation.

Vold, H., Herlufson H., Mains, M., Corwin-Renner, D. (1997). Multi axle order tracking with the Vold-Kalman tracking filter. *Sound and Vibration magazine,* 13(5)(1997) 30-34.

Vold, H., Mains, M. and Blough, J. (1997). Theoretical foundations for high performance order tracking with the Vold-Kalman filter. *Proc. SAE Noise & Vibration Conference*, Traverse City, MI, 1997.

Warrington, A. W., Van C. (1982). Protective relays, their theory and practice. Champman and Hall Ltd., London 1982.

Watson, J. F. (1999). The use of finite element methods to improve techniques for the early detection of faults in 3-phase induction motors. *Energy Conversion, IEEE Transactions*, Vol. 14, issue: 3, pp655-660.

Wilson, A., Nye, A. E. T. and Hopgood, D. J. (1982). On-line detection of partial discharge in hv plant. *4th BEAMA International Electrical Insulation Conference*, Brighton, UK, May 1982,pp 233-239.

Wood, J. W., Ryan, M. J., Gallagher, P. and Gunton, D. (1982). Condition monitoring of turbo-generators. *Proc. Int. Conf. Of Electrical machines- Design and Applications*, *IEE*, London, 13-15 July 1982, conference Publn. 213, pp131-135.

Wu, K. (2005). Influence of mechanical vibration on the behaviour of partial discharges in generator stator windings. Electrical Insulation Materials, 2005. (ISEIM 2005). *Proceeding of 2005 International Symposium*, June 2005, Vol. 1, pp281-284.

Appendix 1 External excitation force simulation

In this research, simulated electrical machine rotor models have been introduced in chapter 3. Appropriate external excitation force models are discussed in the following.

External excitation force simulation for a simulated electrical machine rotor

a. Principal vibration sources

An electrical machine with its associated support structures, form a complex mechanical and electrical system. It is free to vibrate at its own natural frequencies or can be forced at many different excitation frequencies. The forces may result in responses that are unacceptably high and lead to progressive mechanical damage that may end in a total machine failure.

Consequently a great deal of effort has been applied to determine the principal sources of vibration in electrical machines. Noise and vibration sources in electrical machine are fairly complicated. By way of example, the vibration sources in electrical motors can be divided into (i) electrical, (ii) aerodynamic or (iii) electromagnetic (see Figure A1.1):

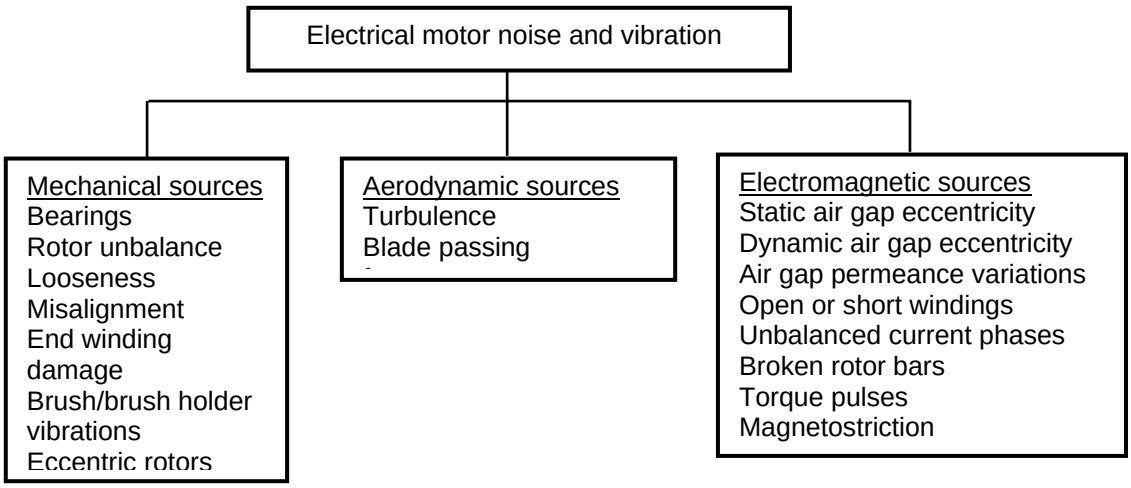

Figure A1.1 Major sources of electrical motor noise and vibration (from, Norton, 1989)

Mechanical vibrations are generally associated with bearing damage, mechanical looseness, rotor problems, stator end winding damage due to mechanical shock, impact or fretting, etc. Aerodynamic problems are generally connected with ventilation fans, broadband turbulence and resonant volume excitations within the motor housing, etc. Noise and vibrations that are related to electrical problems are generally due to unequal electromagnetic forces acting on the stator and rotor. Broken rotor bars, static and/or dynamic air gap eccentricity, uneven air gap flux distribution, open or shorted rotor and stator windings and other inter-turn winding faults, unbalanced current phases, torque oscillations or pulses, and magnetostriction can all result in electromagnetic forces.

b. Characteristics of excitation forces for simulation

Vibration excitation sources are complicated for electrical machines, but most of these vibration sources are related to the common characteristic: rotating speed. Mechanical vibration sources such as bearing damage, rotor problems or stator end winding problems, are all related to rotor rotating speed, and their vibration frequencies will invariably be multiples of rotating frequency. Aerodynamic problems that come from ventilation fans are also in closely related to rotating speed. Most of the electromagnetic forces coming from the rotor or stator are all closely connected to the rotating speed as well, because the rotating speed is closely related with the rated current in the windings and the rated current determines the electromagnetic field. Using an electrical motor as an example, that electrical supply current flow through the stator windings will determine the rotor speed, this can be mathematically expressed as (In ideal condition, slip is neglected):

$$f_s = \frac{2 f_c}{p} \qquad \text{A1.1}$$

where f_s is the shaft rotating frequency, f_c is electrical supply frequency and p is the number of magnetic poles.

For the case of a generator, this is a reversed process, the current flow in the stator field windings will be determined by the shaft rotating frequency. Based upon such a close relationship, problems such as broken rotor bars, shorted rotors, stator inter-turn winding faults, and unbalanced current phase, etc. will all be related with the rotating speed. For a given electrical generator, the number of magnetic poles is a constant number, therefore, the rotating speed will dominantly influence the magnetic force.

c. External excitation force simulation

Although the forces acting on the system might seem complicated to model, most of these forces have the one common characteristic that they are related to the rotating speed of the rotor, as has been discussed above. In this simulation study, we focus on the magnetic force of an electrical machine. The magnetic force will vary as the speed varies, with a fixed number of force cycles per revolution (for instance 2 or 4 cycles per revolution). The specific number of force cycles per revolution is determined by the physical and electrical parameters of the machine. Forces due to bearing damage, the brush box and the forces generated by a stator inter-turn short, are all linked to the rotational speed with a fixed number of cycles per revolution. This is the fundamental to the success of order tracking for monitoring purposes.

For modelling of the external force exerted on the rotor, the force amplitude will be simulated as a normal force. This is not to say that all the force components will obey the law of normal force in reality. But for simplicity, the mathematical expression for normal force is assumed to be:

$$F_{normal} = m_u \times \varpi^2 \times r_u \qquad \text{A1.2}$$

where m_u is the mass unit, r_u is the distance from the centre to the mass unit and $\varpi = \frac{d\theta}{dt}$ is the angular velocity of rotor.

A common characteristic for these magnetic forces is that the fixed number of force cycles per revolution for each magnetic force. This can be simulated by unit sinusoidal force at multiple frequencies of fundamental rotating frequency. Combining both the force amplitude simulation and different unit sinusoidal force, it come to the final force for each order, this can be seen in Figure A1.2

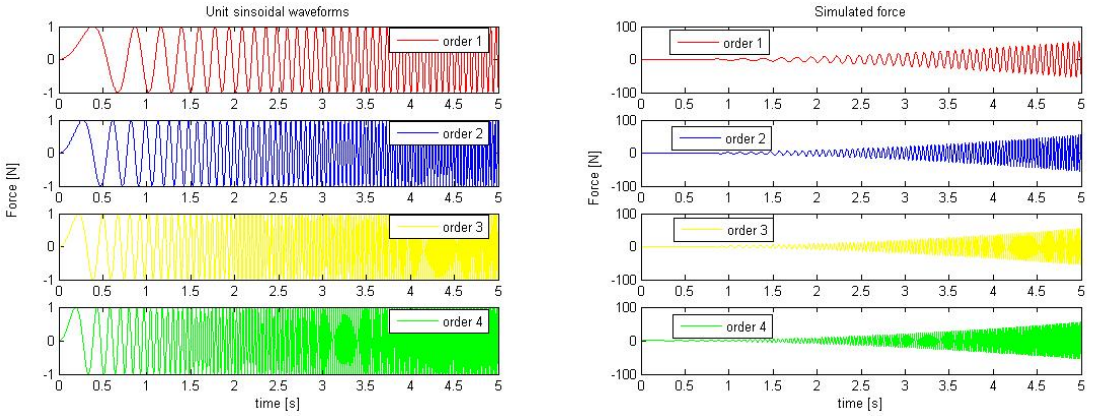

a. Unit sinusoidal order waveforms b. Simulated external force for each order

Figure A1.2 Final external excitation force for each order

Figure A1.2 (a) shows unit sinusoidal force for each order, Figure A1.2 (b) is the modulation of unit sinusoidal force with force amplitude. Combining these forces together, the final external excitation force used in chapter 3 will be resulted as is shown in Figure A1.3.

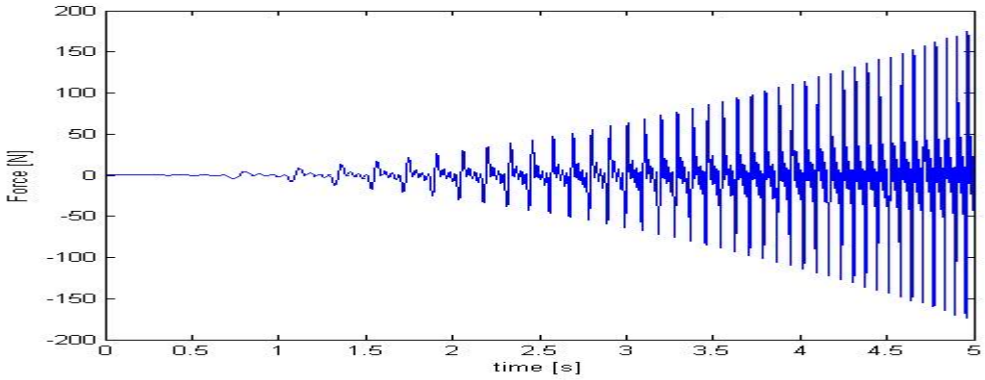

Figure A1.3 Simulated external excitation force

The mathematical expression of the external excitation force and simulated stator inter-turn short excitation force are listed in Table A1.1.

Table A1.1 External excitation forces used in Chapter 3

Model	External excitation force
Single and two-degree-of-freedom system	$F(t) = m_u \omega^2 r_u \sin(\omega t) + m_u \omega^2 r_u \sin(2\omega t) + m_u \omega^2 r_u \sin(3\omega t) + m_u \omega^2 r_u \sin(4\omega t)$
Simulated stator inter-turn short damaged system	$F(t) = m_u \omega^2 r_u \sin(\omega t) + 10\sin(2\omega t)$

Appendix 2 Vold-Kalman filter bandwidth choice for real experimental data

The choice of the Vold-Kalman filter bandwidth is a tuning process. Blough (2003) mentioned that one of the largest disadvantages of Vold-Kalman filter is the experience required to get accurate results. In real application processes, this will mainly present on the choice of filter bandwidth.

In this research, real experimental data were acquired from the experimental set-up. The MATLAB Vold-Kalman filter scripts, developed by Tuma, were used to perform Vold-Kalman filter order tracking. The choice of Vold-Kalman filter bandwidth of this experimental data was studied as follows.

To begin with the choice of filter bandwidth, the theoretical analysis should be used as the point of departure. Figure 2.4 gives clear steps for the choice of filter bandwidth based upon the system resonance, slew rate, system damping and the time frequency relationship. This is however not ideal for finding the Vold-Kalman filter bandwidth for the experimental data, simply because all of these parameters either are not fixed or very difficult to determine precisely. However, to begin with a rough estimation of minimum filter bandwidth is worthwhile.

With regard to the experimental data analysed in Chapter 5, the minimum Vold-Kalman filter bandwidth can be roughly estimated by calculation methods similar to that done in the simulated model. From previous analysis of FT-OT in paragraph 5.1.1 (a), it is not very difficult to roughly determine the system resonance. So that a similar procedure as have been done in paragraph 3.2.4 can be implemented in this real experimental data as follows:

Using order 36 as an example, the 3dB bandwidth for the resonance peak can be calculated from $\Delta f_{3dB} = 2 \times \xi \times f_n$. In this equation ξ is unknown, and f_n is located at about 702 – 840 Hz, this is reached similar as the analysis of paragraph 5.1.1 (a). Heyns (2003) describes an estimated method to determine the damping ratio of a lightly damped system at the resonance peak, which can be expressed as

$$\xi = \frac{f_2 - f_1}{2 \times f_n}$$

where f_n is the resonance frequency, f_1 and f_2 are half power points frequency.

The same procedures can be used to roughly estimate the value of experimental system's damping ratio at the resonance of order 36. In Figure A 2.1, a 3dB line was drawn on the original data spectrum under the resonance peak value ($f_n = 833.49$ Hz), another two frequency values on the 3dB line (half power point line) were picked by using `ginput.m`, namely $f_1 = 833.09$ Hz and $f_2 = 834.03$ Hz, see in Figure A 2.1.

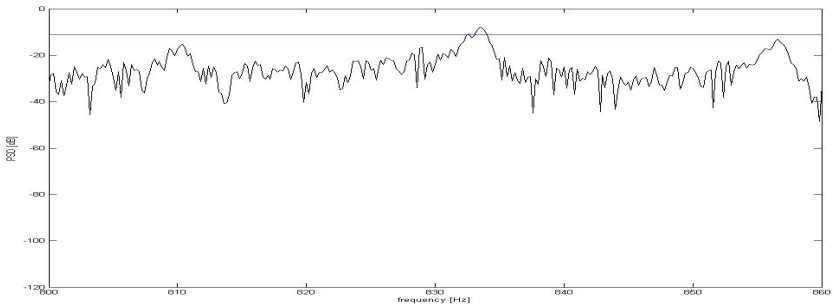

Figure A 2.1 Estimation of damping ratio

Then, ξ can be estimated by $\xi = \frac{f_2 - f_1}{2 \times f_n} = 0.00056$, therefore,

$$\Delta f_{3dB} = 2 \times \xi \times f_n = 2 \times 0.00056 \times 833.49 = 0.93 \text{ Hz}$$

$$B_{3dB/order36} \geq (k \times SR_{RPM}) / (30 \times \Delta f_{3dB}) = (36 \times 400) / (30 \times 0.93) = 516.13 \text{ Hz}$$

(Note: SR_{RPM} can be estimated from RPM graph in Figure 5.4, during the period of 2 – 3 seconds, it is about 400 rpm/s).

Finally, the proportional bandwidth $\geq \frac{B_{3dB/order36}}{f_n} = \frac{516.13}{833} = 0.6196 \approx 62\%$.

This is a very rough calculation for initiating the choice of filter bandwidth. But it is a reasonable beginning for implementing the Vold-Kalman filter. Therefore, to ensure the correctness of the resonance amplitude value, the minimum proportional bandwidth for order 36 is about 62%. By using the same procedures, the minimum proportional bandwidth for order 72 is about 15%. In chapter 5, peak values will be used to compare the effectiveness of different order tracking techniques, thus a higher filter bandwidth is preferred to acquire the accurate peak value. But, Herlufsen et al. (1999) stated that a filter bandwidth of more than 100% would give rise to the beating interference between orders. In the end, a 100% filter bandwidth was chosen to be the proportional filter bandwidth for this experimental data.

Appendix 3 Shaft encoder extender manufacture

In order to properly mount the shaft encoder onto the alternator, a specially designed shaft encoder extender was used to assemble the shaft encoder properly (Figure A3.1).

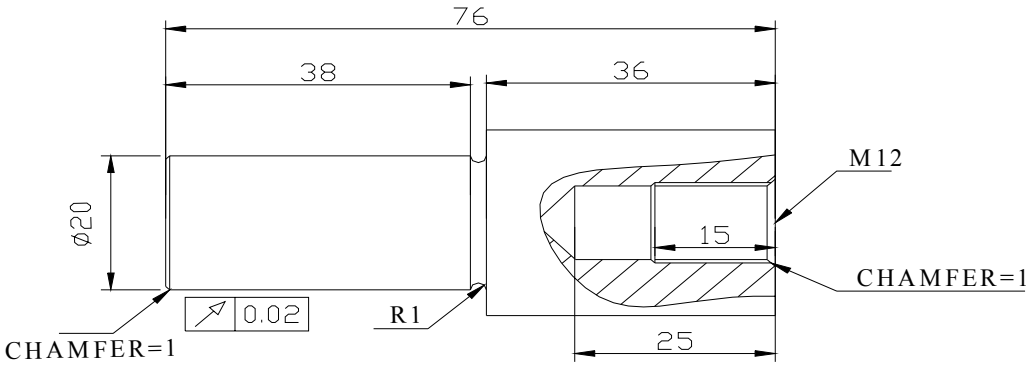

Figure A3.1 Shaft encoder extender

This shaft encoder extender was manufactured together with alternator rotor set on the lathe (Figure A3.2).

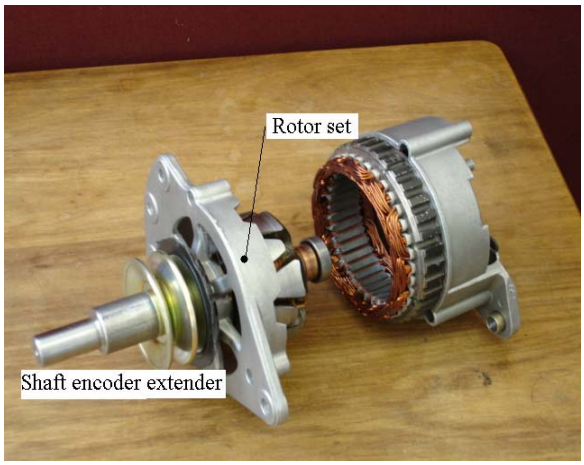

a. Shaft encoder extender

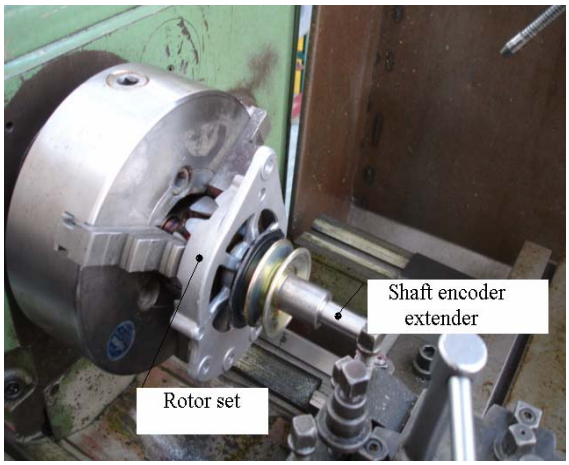

b. Manufacturing process

Figure A3.2 Shaft extender manufacturing

Appendix 4 MATLAB programmes

This appendix provides details on the MATLAB scripts used for analysing the simulated models and real experimental data. It is divided into two parts, one for the simulated models and the other for the experimental data.

A3.1 Simulated models

A3.1.1 Single-degree-of-freedom system

The programme logic is shown in Figure A3.1:

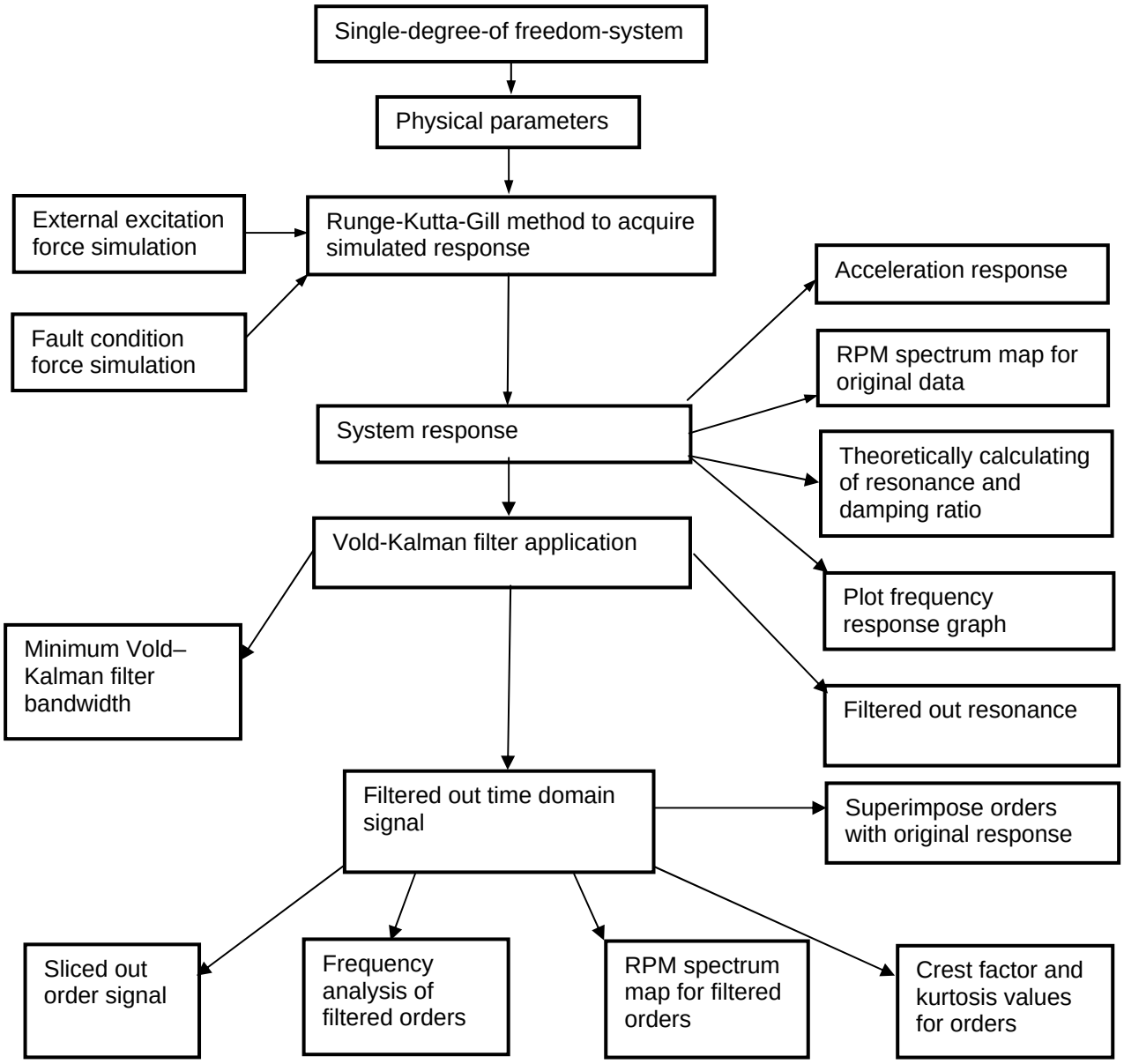

Figure A3.1 Single-degree-of-freedom MATLAB programme flow chat

```
clear all,close all,clc
% Univ.of Pretoria,Department of Mechanical and Aeronautical Engineering
% K. Wang
% Student number: 24494225
% March 2007
%**************************************************************************
%Using Runge-Kutta-Gill method to simulate the vibration response under
%the known system, Vold-Kalman filter order tracking was performed for
%the single-degree-of-freedom system
%**************************************************************************
%Physical parameters
global m k c mu ru fs
k=500000;                                   %stiffness
m=50;                                       %mass of rotor
mu=0.05;                                    %unbalance mass
c=200;                                      %damping
ru=0.1;                                     %normal force distance to centre
t0=0;                                       %initial time
tf=5;                                       %final time
N=4096;                                     %points
g=9.81                                      %constant
co=200;                                     %RPM sweep rate
fs=N/(tf-t0);                               %sampling frequency
%
%Runge-Kutta solution to acquire simulated response
%
x0=[0 0]';
tspan=linspace(t0,tf,N);
[t,x]=ode45('vkfiltattemptmorepoints',tspan,x0);
rpm=co*t;                                   %constant sweep rate rpm
%
%Plot rpm graph
%
figure(1)
plot(t,rpm);xlabel('time [s]');ylabel('RPM [rpm]')
%
%External excitation forces simulation
%
co1=co*0.5;
co3=1.5*co;
co4=2*co;
F=1*mu*(2*pi*((co*t)/60)).^2*ru.*sin((2*pi*((co*t)/60)).*t)+...
    1*mu*(2*pi*((co*t)/60)).^2*ru.*sin((2*pi*((co1*t)/60)).*t)...
    +mu*(2*pi*((co*t)/60)).^2*ru.*sin((2*pi*((co3*t)/60)).*t)...
    +mu*(2*pi*((co*t)/60)).^2*ru.*sin((2*pi*((co4*t)/60)).*t);
%
% %Fault condition force simulation
% %
% F=mu*(2*pi*((co*t)/60)).^2*ru.*sin((2*pi*((co1*t)/60)).*t;
% df=10*sin((pi*2*((co*t)/60)).*t);
% F=F+df;
% %
FO=F;
%
%External forces plot
%
% figure(2)
% subplot (2,1,1);plot(t,FO,'b');title('original forces');
% xlabel ('time [s]')
% ylabel ('force [N]')
% subplot(2,1,2);plot(t,F,'b');title('add damage force per revolution')
% xlabel('time[s]')
% ylabel('force [N]')
```

```
%
%System response: vel-velocity response; dip-displacement
%Response; vibacc-acceleration response
%
vel=x(:,2);
dip=x(:,1);
vibacc=(-c/m)*vel-(k/m)*dip+F/m;
y=vibacc;
fs=length(y)/(tf-t0);               %sampling frequency
RPM=rpm;
%
%Acceleration response
%
figure(3)
plot(t,y,'b');xlabel('time [s]');ylabel('Acceleration [m/s^2]')
%
%RPM spectrum map for original data
%
fsrpm=fs;
figure(4)
[M,F,R] = rpmmap(y,fs,rpm,fsrpm,10,10,co*5*0.9,1024,0,80,1);
%Draw order lines on RPM spectrum map
hold on;plot(F,60*F/1,'b')
hold on;plot(F,60*F/2,'r')
hold on;plot(F,60*F/3,'y')
hold on;plot(F,60*F/4,'g');hold off;
%
%Vold-Kalman application
%
%Plot frequency response graph to visually see resonance of system
%
fn=linspace(0,100,2000);ww=2*pi*fn;
FRF=1./((k-m*ww.^2)+i*ww.*c);
figure(5)
subplot(2,1,1);plot(fn,20*log10(abs(FRF)),'k');hold on;
ylabel('Acceleration [dB]')
subplot(2,1,2);plot(fn,angle(FRF));hold off
xlabel('frequency (Hz)')
ylabel('Phase [deg]')
%
%Theoretically calculating of resonance and damping ratio
%
sr=co;                          %slew rate of RPM
ff=(1/(2*pi))*sqrt(k/m);        %resonance frequency theoretical
Cc=2*sqrt(m*k);                 %critical damping
zeta=c/Cc;                      %damping ratio
%
%Vold-Kalman filter application
%
%Minimum Vold-Kalman filter bandwidth
%
Reband=2*zeta*ff;               %resonance 3dB bandwidth
korder=1;                       %filtered order
fh=(korder*sr)/(30*Reband);     %minimun VK-filter bandwidth
%
% % Filted out resonance
%
%  for i=1:N
%  rpmre(i)=ff*60;
%  end
%  rpmre=rpmre';
%  order1=1;type=0;
%  xx = vktime(vibacc,fs,rpmre,order1,bandwidth,type)
%  vibfilt=vibacc-xx;
```

```
%  y=vibfilt
%
%Performing Vold-Kalman filtering process
%
order1=1;type=0;
bandwidth1=0.66
 x1 = vktime(y,fs,RPM,order1,bandwidth1,type);
order2=2;
bandwidth2=0.66
 x2 = vktime(y,fs,RPM,order2,bandwidth2,type)
order3=3;
bandwidth3=0.66
 x3 = vktime(y,fs,RPM,order3,bandwidth3,type)
order4=4;
bandwidth4=0.66
 x4 = vktime(y,fs,RPM,order4,bandwidth4,type)
%
%Plot filtered out time domain order signal
%
figure(6)
subplot(4,1,1)
plot(t,x1(:,1));title('order 1');axis([0 5 -5 5])
subplot(4,1,2)
plot(t,x2(:,1));title('order 2');ylabel('Acceleration [m/s^2]')
axis([0 5 -5 5])
subplot(4,1,3)
plot(t,x3(:,1));title('order 3');axis([0 5 -5 5])
subplot(4,1,4)
plot(t,x4(:,1));title('order 4');xlabel('time [s]')
axis([0 5 -5 5])
%
%Frequency analysis of filtered orders
%
m=1024;
noverlap=round(m*0.9);
[yo,fo] = psde(y,m,noverlap,fs)
[yvk1,fvk1] = psde(x1,m,noverlap,fs)
[yvk2,fvk2] = psde(x2,m,noverlap,fs)
[yvk3,fvk3] = psde(x3,m,noverlap,fs)
[yvk4,fvk4] = psde(x4,m,noverlap,fs)
%
%Plot frequency analysis
%
figure(7)
plot(fo,yo,'k');xlabel('frequency [Hz]');ylabel('PSD')
axis([0 50 0 2.5]);hold on
plot(fvk1,yvk1,'b');xlabel('frequency [Hz]');ylabel('PSD')
hold on;
plot(fvk2,yvk2,'r');xlabel('frequency [Hz]');ylabel('PSD')
hold on;
plot(fvk3,yvk3,'y');xlabel('frequency [Hz]');ylabel('PSD')
hold on;
plot(fvk4,yvk4,'g');xlabel('frequency [Hz]');ylabel('PSD')
hold off;
axis([0 50 0 0.5])
%
%RPM spectrum map for filtered orders
%
figure(8)
[M1,F1,R1]=rpmmap(x1,fs,rpm,fsrpm,10,20,co*5*0.9,1024,0,80,1);
hold on;plot(F,60*F/1,'b');hold off
figure(9)
[M1,F2,R2]=rpmmap(x2,fs,rpm,fsrpm,10,20,co*5*0.9,1024,0,80,1);
hold on;plot(F,60*F/2,'r');hold off
```

```
figure(10)
[M3,F3,R3]=rpmmap(x3,fs,rpm,fsrpm,10,20,co*5*0.9,1024,0,80,1);
hold on;plot(F,60*F/3,'y');hold off
figure(11)
[M4,F4,R4]=rpmmap(x4,fs,rpm,fsrpm,10,20,co*5*0.9,1024,0,80,1);
hold on;plot(F,60*F/4,'g');hold off
%
%Sliced out orders and plot
%
ord1= ordslice(M,F,R,1);
ord2= ordslice(M,F,R,2);
ord3= ordslice(M,F,R,3);
ord4= ordslice(M,F,R,4);
figure(12)
plot(R,ord1,'b',R,ord2,'r',R,ord3,'y',R,ord4,'g')
xlabel('RPM [rpm]')
ylabel('PSD')
%
%Crest factor and kurtosis value for orders
%
c1=crest(x1);c2=crest(x2);c3=crest(x3);c4=crest(x4);
k1=kurtosis(x1);k2=kurtosis(x2);k3=kurtosis(x3);k4=kurtosis(x4);
cf=[c1 c2 c3 c4]
kf=[k1 k2 k3 k4]
%
%superimpose all the orders with original response
figure(13)
plot(t,y,'k',t,x1,'b',t,x2,'r',t,x3,'y',t,x4,'g')
ylabel('Acceleration [m/s^2]')
xlabel('time [s]')

%%%%%%%%%%%%%%%%%%%%%%%%%%%%%%%%%%%%%%%%%%%%%%%%%%%%%%%%%%%%

function xdot=vkfiltattemptmorepoints(t,x)
%
%construct stifness matrix
%
E=[0 1;-k/m -c/m];
%
%External excitation force simulation
co1=co*0.5;
co3=1.5*co;
co4=2*co;
F=1*mu*(2*pi*((co*t)/60)).^2*ru.*sin((2*pi*((co*t)/60)).*t)+...
    1*mu*(2*pi*((co*t)/60)).^2*ru.*sin((2*pi*((co1*t)/60)).*t)...
    +mu*(2*pi*((co*t)/60)).^2*ru.*sin((2*pi*((co3*t)/60)).*t)...
    +mu*(2*pi*((co*t)/60)).^2*ru.*sin((2*pi*((co4*t)/60)).*t);
xdot=E*x+[0 F/m]';

%%%%%%%%%%%%%%%%%%%%%%%%%%%%%%%%%%%%%%%%%%%%%%%%%%%%%%%%%%%%
%Sub function for simulated damaged case
function xdot=vkimpulsesub(t,x)
E=[0 1;-k/m -c/m];
F=mu*(2*pi*((co*t)/60)).^2*ru.*sin((2*pi*((0.5*co*t)/60)).*t);
impulse=10*sin((pi*2*((co*t)/60)).*t);
F=F+impulse;
xdot=E*x+[0 F/m]';
```

A3.1.2 Two-degree-of freedom system

The programme logic is shown in the Figure A3.2

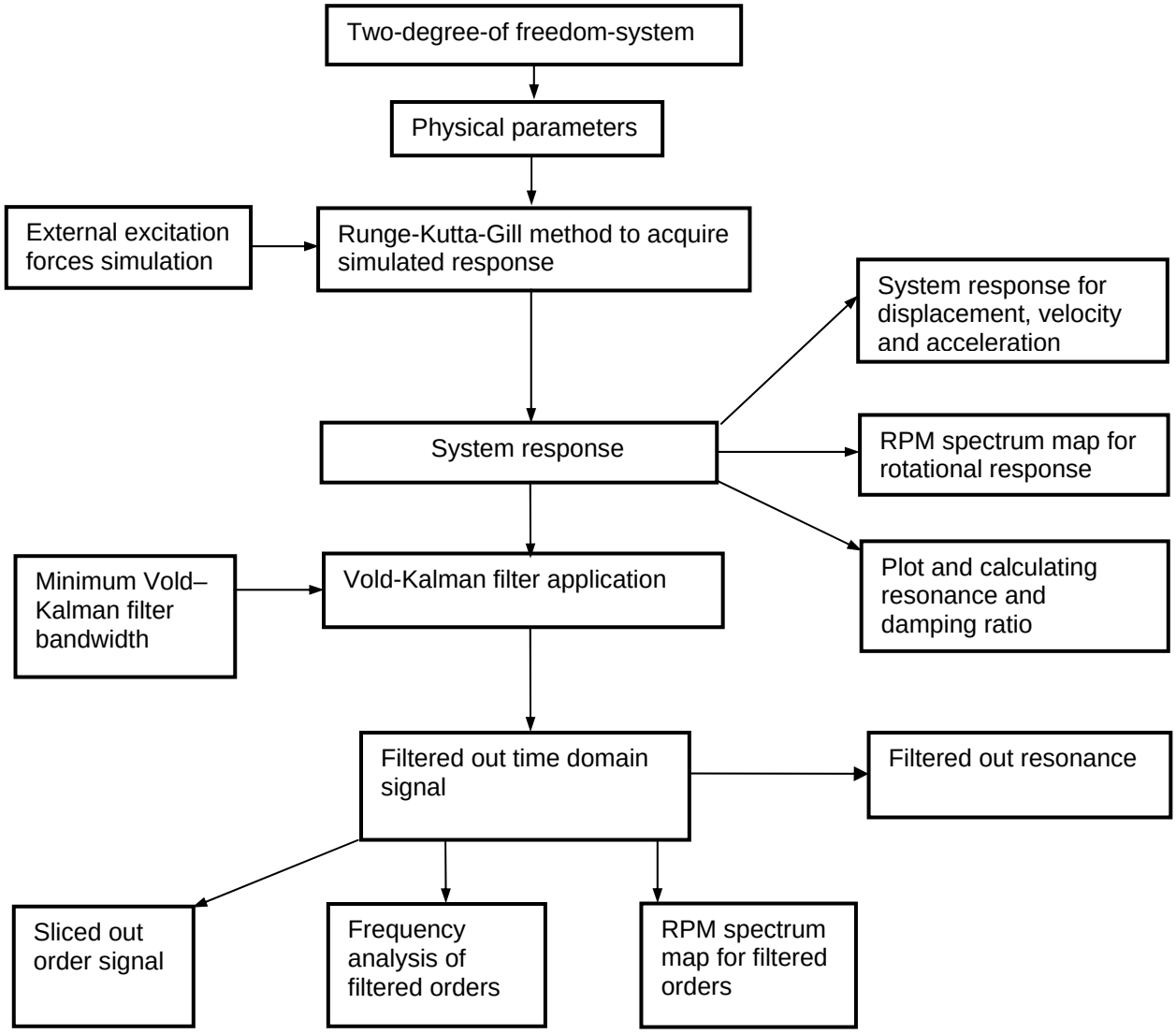

Figure A3.2 Two-degree-of-freedom MATLAB programme flow chat

```
clear all;close all;clc
% Univ. of Pretoria, Department of Mechanical and Aeronautical Engineering
% K. Wang
% Student number: 24494225
% March 2007
%**************************************************************************
%Using runge-kutta-Gill method to simulate the vibration signal under the
%known system, Vold-Kalman filter order tracking was performed for the two
%degree of freedom system
%**************************************************************************
%
%Physical parameters
%
global m k c mu ru fs
k1=100000;
k2=10000;                                %stiffness
m1=20;                                   %mass of rotor
I=0.5                                    %intertial
mu=0.05;                                 %unbalance mass
c1=35
c2=20;                                   %damping
la=0.2;                                  %center to left bearing
lb=0.3;                                  %center to right bearing
ru=0.1;                                  %normal force distance to center
t0=0;                                    %initial time
tf=5;                                    %final time
N=4096;                                  %points
g=9.81                                   %constant
co=200;                                  %RPM sweep rate
fs=N/(tf-t0);                            %sampling rate
%
%Mass, damping and stifness matrix
%
m=[m1 0
    0 I];
c=[c1+c2            -c1*la+c2*lb
   -c1*la+c2*lb     c1*la^2+c2*lb^2];
fs=N/(tf-t0);
k=[k1+k2          -k1*la+k2*lb
   -k1*la+k2*lb   k1*la^2+k2*lb^2];
nul=[0 0
     0 0];
eye=[1 0
     0 1];
%
%Runge-Kutta-Gill method to acquire simulated response
%
tspan=linspace(t0,tf,N);
x0=[0 0 0 0]';
[t,x]=ode45('vkfiltmultisub',tspan,x0);
rpm=co*t;
%
%External excitation forces simulation
co2=co*0.5;
co3=co*1.5;
co4=2*co;
rpm=co*t;
F=1*mu*(2*pi*((co*t)/60)).^2*ru.*sin((2*pi*((co*t)/60)).*t)...
    +1*mu*(2*pi*((co*t)/60)).^2*ru.*sin((2*pi*((co2*t)/60)).*t)...
    +mu*(2*pi*((co*t)/60)).^2*ru.*sin((2*pi*((co3*t)/60)).*t)...
    +mu*(2*pi*((co*t)/60)).^2*ru.*sin((2*pi*((co4*t)/60)).*t);
```

```
M=F*la;                                    %left bearing torque
%
%System response
%
%System response for vib--velocity; dip--displacement; vibacc--acceleration
%
vel=x(:,2);
dip=x(:,1);
QQ=inv(m)*[F';M'];
niu=zeros(2,4096);
eye=[1 0
     0 1];
vibacc=[nul        eye
        -inv(m)*k  -inv(m)*c]*x'+[niu
                                  QQ];
y1=vibacc(3,:);              %vertical acceleration
y2=vibacc(4,:);              %angle acceleration
fs=length(y1)/(tf-t0);       %sampling frequency
RPM=rpm;
%System response plot
figure(1)
subplot(2,1,1);plot(t,y1,'b');
xlabel('time[s]');ylabel('Acceleration [m/s^2]')
subplot(2,1,2);plot(t,y2,'r');
xlabel('time[s]');ylabel('Angular acceleration [rad/s^2]')
%
%RPM spectrum map for rotational response
%
fsrpm=fs;
figure(2)
[M,F,R] = rpmmap(y2',fs,rpm,fsrpm,10,10,co*4,1024,0,80,20);
%order line
ordline(F,1);ordline(F,2);ordline(F,3);ordline(F,4);
%
%Plot and calculating and resonances
%
%Frequency response function
for indx=1:2000
    w(indx)=0.2*(indx-1);
    f(indx)=w(indx)./(2*pi);
    a=inv(k-m.*w(indx).^2+i*w(indx).*c);
    a11(indx)=a(1,1);
    a12(indx)=a(1,2);
    a22(indx)=a(2,2);
    a21(indx)=a(2,1);
end
figure(3)
subplot(2,2,1);semilogy(f,abs(a11),'r');
title('a. alfa{a11}');xlabel('frequency[Hz]');ylabel('FRF([m/N]) in log')
subplot(2,2,2);semilogy(f,abs(a22),'b');
title('a. alfa{a22}');xlabel('frequency[Hz]');ylabel('FRF([m/N]) in log')
subplot(2,2,3);semilogy(f,abs(a12),'k');
title('c. alfa{aa12}');xlabel('frequency[Hz]');ylabel('FRF([m/N]) in log')
subplot(2,2,4);semilogy(f,abs(a21),'k');
title('d. alfa{a21}');xlabel('frequency[Hz]');ylabel('FRF([m/N]) in log')
%Calculation of resonance
nul=[0 0;0 0];
A=[c m;m nul];
B=[k nul;nul -m];
[Vv,Dv]=eig(-B,A);
dv=diag(Dv);
s=real(dv);
wd=imag(dv);
```

```
wn=sqrt(wd.^2+s.^2);
z=-s./wn;
ff=wn/(2*pi);                          %natural frequency
ff=[ff(1) ff(3)];
z=[z(1) z(3)];                         %damping ratios
%
%Vold-Kalman filter application
%
%Minimum filter bandwidth
%
%Calculating using the first natural frequency
sr=co;                                 %sweep rate
Reband1=2*z(1)*ff(1);                  %resonance 3dB bandwidth
korder=2;                              %filtered order
fh1=(korder*sr)/(30*Reband1);          %VK-filter bandwidth
bandwidth1=fh1/ff(1)
%Calculating using second natural frequency
sr=co;
Reband2=2*z(2)*ff(2);                  %resonance 3dB bandwidth
korder=2;                              %filtered order
fh2=(korder*sr)/(30*Reband2);          %VK-filter bandwidth
bandwidth2=fh2/ff(2)
%
%Notice:all use rotational response to calculate the results for demonstration
%Filter bandwidth, for convenient use 66%
%
%Filter out resonance
%
% y22=y2;
% bandwidth=0.66;
%  for i=1:N
%  rpmre(i)=ff(1)*60;
%  end
%  rpmre=rpmre'
%  order1=1;type=0;
%  xx = vktime(y2',fs,rpmre,order1,bandwidth,type)
% vibfilt=y2'-xx;
% y2=vibfilt'
% %
% bandwidth=0.66;
%  for i=1:N
%  rpmre(i)=ff(2)*60;
%  end
%  rpmre=rpmre;
%  order1=1;type=0;
%  xx2 = vktime(y2',fs,rpmre,order1,bandwidth,type)
% %
% y2=y2-xx2';
%
%Filter out time domain signal
%
bandwidth1=0.66;
type=0;
order1=1;
 x = vktime(y2',fs,RPM,order1,bandwidth1,type)
order2=2;
 x2 = vktime(y2',fs,RPM,order2,bandwidth1,type)
 order3=3;
 x3 = vktime(y2',fs,RPM,order3,bandwidth1,type)
 order4=4;
 x4 = vktime(y2',fs,RPM,order4,bandwidth1,type)
figure(4)
subplot(6,1,1);plot(t,rpm);ylabel('RPM [rpm]');xlabel('time[s]')
subplot(6,1,2);plot(t,y1,'b');xlabel('time[s]');ylabel('[m/s^2]')
```

```
subplot(6,1,3);plot(t,x,'r');xlabel('time[s]');ylabel('[m/s^2]')
subplot(6,1,4);plot(t,x2,'r');xlabel('time[s]');ylabel('[m/s^2]')
subplot(6,1,5);plot(t,x3,'r');xlabel('time[s]');ylabel('[m/s^2]')
subplot(6,1,6);plot(t,x4,'r');xlabel('time[s]');ylabel('[m/s^2]')
%
%Frequency analysis of filtered data
%
figure(5)
m=1024;
noverlap=round(m*0.9);
[yo,fo] = psde(y2,m,noverlap,fs)
[yvk1,fvk1] = psde(x,m,noverlap,fs)
[yvk2,fvk2] = psde(x2,m,noverlap,fs)
[yvk3,fvk3] = psde(x3,m,noverlap,fs)
[yvk4,fvk4] = psde(x4,m,noverlap,fs)
%
plot(fo,yo,'k');xlabel('frequency [Hz]');ylabel('PSD ')
axis([0 50 0 30]);hold on
plot(fvk1,yvk1,'b');xlabel('frequency [Hz]');ylabel('PSD ')
hold on;
plot(fvk2,yvk2,'r');xlabel('frequency [Hz]');ylabel('PSD ')
hold on;
plot(fvk3,yvk3,'y');xlabel('frequency [Hz]');ylabel('PSD ')
hold on;
plot(fvk4,yvk4,'g');xlabel('frequency [Hz]');ylabel('PSD ')
hold off;
%
%RPM spectrum map for orders
figure(6)
[M1,F1,R1] = rpmmap(x,fs,rpm,fsrpm,10,10,co*4,1024,0,80,10);
figure(7)
[M2,F2,R2]= rpmmap(x2,fs,rpm,fsrpm,10,10,co*4,1024,0,80,10);
figure(8)
[M3,F3,R3] = rpmmap(x3,fs,rpm,fsrpm,10,10,co*4,1024,0,80,10);
figure(9)
[M4,F4,R4]= rpmmap(x4,fs,rpm,fsrpm,10,10,co*4,1024,0,80,10);
%
%Sliced out order signal
%
ord1= ordslice(M,F,R,1);
ord2= ordslice(M,F,R,2);
ord3= ordslice(M,F,R,3);
ord4= ordslice(M,F,R,4);
figure(10)
plot(R,ord1,'b',R,ord2,'r',R,ord3,'y',R,ord4,'g')
xlabel('RPM[rpm]')
ylabel('rms value')
%Plot rotaional response and filtered order 1
figure(11)
plot(t,y2);hold on;plot(t,x,'r');
xlabel('time [s]')
ylabel('Angular acceleration [rad/s^2]')
%%%%%%%%%%%%%%%%%%%%%%%%%%%%%%%%%%%%%%%%%%%%%%%%%%%%%%%%%%%%
function xdot=vkfiltmultisub(t,x)
%Mass, damping and stifness matrix
m=[m1 0
    0 I];
c=[c1+c2            -c1*la+c2*lb
   -c1*la+c2*lb     c1*la^2+c2*lb^2];
fs=N/(tf-t0);
k=[k1+k2          -k1*la+k2*lb
   -k1*la+k2*lb   k1*la^2+k2*lb^2]
nul=[0 0
     0 0];
```

```
eye=[1 0
     0 1];
E=[nul eye;-inv(m)*k -inv(m)*c];
%
co2=co*0.5;
co3=co*1.5;
co4=2*co;
F=1*mu*(2*pi*((co*t)/60)).^2*ru.*sin((2*pi*((co*t)/60)).*t)+...
    1*mu*(2*pi*((co*t)/60)).^2*ru.*sin((2*pi*((co2*t)/60)).*t)...
    +mu*(2*pi*((co*t)/60)).^2*ru.*sin((2*pi*((co3*t)/60)).*t)+...
    mu*(2*pi*((co*t)/60)).^2*ru.*sin((2*pi*((co4*t)/60)).*t);
M=F*la;
Q=[F/m1 M/I]'
xdot=E*x+[0
          0
          Q];
```

A3.2 Experimental data analysis

The programme logic is shown in the Figure A3.3

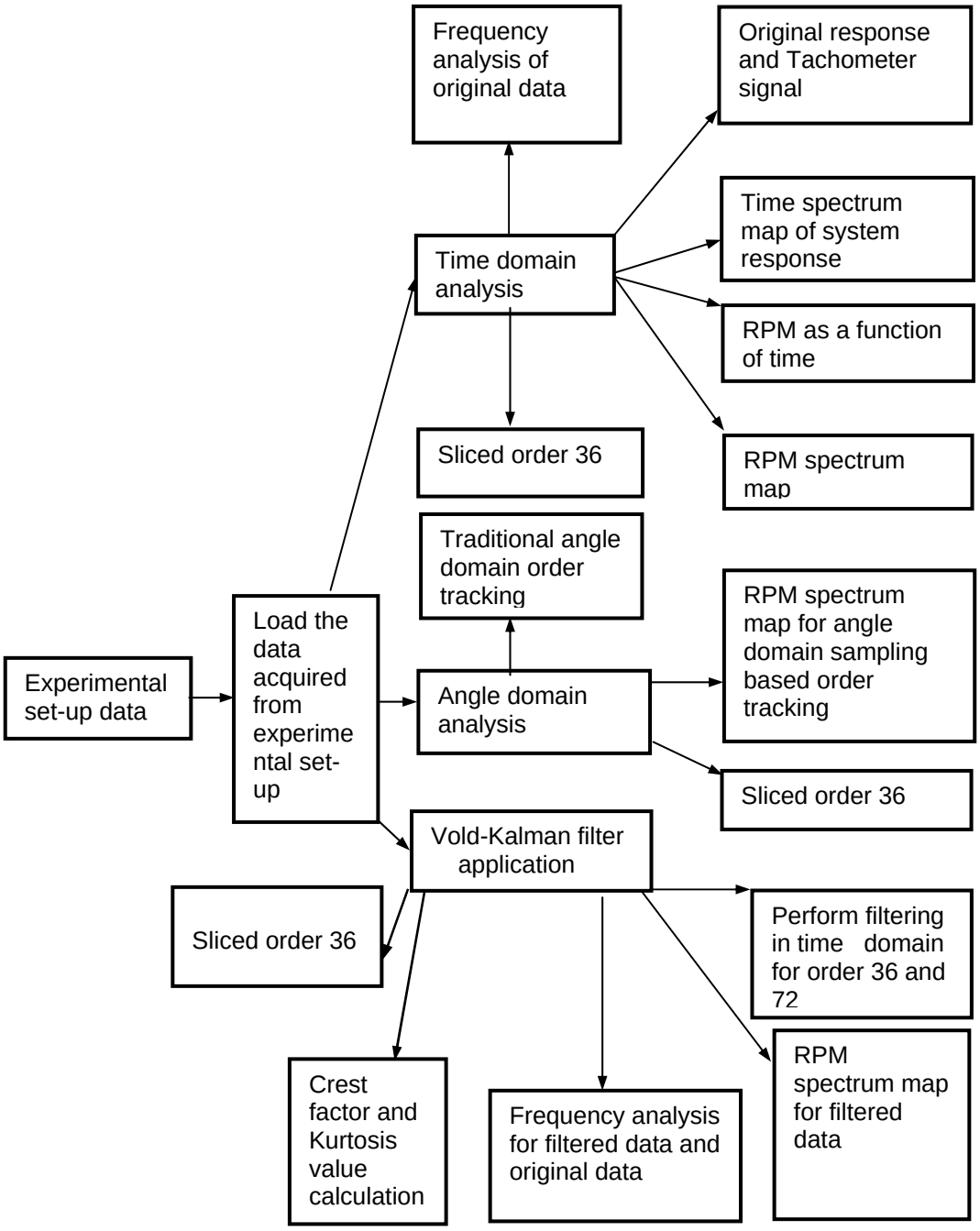

Figure A3.3 Experimental set-up data analysis

```
close all;clear all;clc
% Univ. of Pertoria
% K. Wang
% Student number: 24494225
% March 2007
%*************************************************************************
%This program is the main program for analysis the data acquired from
%experimental set-up, it includes all three order tracking analysis into
%one program, they are Fourier transform order tracking, Angle domain
%sampling based order tracking and Vold-kalman filter order tracking.
%*************************************************************************
%
%Load the data acquired from experimental set-up
%
load daright1
x = daright1(:,2);                      %the second column is the vibration
                                        %signal
xs=x;
fs = 100000;                            %accelerometer sampling frequency
tacho = daright1(:,1);                  %the first column is the tacho signal
clear daright1                          %clear the original variable
tachofs =100000;                        %tacho sampling frequency
%
%Plot original response and Tacho signal
%
t = maketime(x,fs);
figure(1)
subplot(2,1,1);plot(t,x,'b');
xlabel('time [s]')
ylabel('Acceleration [m/s^2]')
subplot(2,1,2);plot(t,tacho,'r')
xlabel('time [s]')
ylabel('voltage [mV]')
%
%Time spectrum map of the system response
%
figure(2);clf reset;fullscrn
timeh2o(x,fs,100,8192,0,5000,0.5);
set(gca,'View',[0 80]);
xlabel( 'Frequency [Hz]')
ylabel( 'Time [s]')
zlabel( 'RMS')
%
%RPM as function of time
%
fsrpm = 100000;
[rpm,trpm] = getrpm(tacho,tachofs,4,+1,1,fsrpm);
figure(3);clf;fullscrn
plot(trpm,rpm,'k')
set(gca,'FontSize',14);
title( 'RPM as function of time','FontSize',14)
xlabel( 'Time [s]','FontSize',14)
ylabel( 'RPM [rpm]','FontSize',14)
%
%RPM spectral Map
%
figure(4);clf reset;fullscrn
[M,F,R] = rpmmap(x,fs,rpm,fsrpm,700,10,1400,8192,0,3000,0.5);
%Order lines for 36,72,108 and 144 in the RPM Spectral map
```

```
ordline(F,36);ordline(F,72);
ordline(F,108);ordline(F,144);
%
%Frquency analysis of original vibration signal
%
figure(5)
[yo,fo] = fanhann(x,fs,8192,7,60);
semilogy(fo,yo,'k')
xlabel('frequency(Hz)')
ylabel('PSD')
%
%Sliced order 36
%
ord = ordslice(M,F,R,36);
figure(6);clf;fullscrn
plot(R,ord,'k')
ylabel( 'RMS')
xlabel( 'RPM [rpm]')
save R
save ord
%
%Angle domain sampling based order tracking
%
nsamp = getnsamp(tacho,tachofs,2,+1,1,760);
% Then resample data on the synchronous sampling instances
t = maketime(x,fs);
syncdata = interp1(t,x,nsamp);
%
%Traditional angle domain order tracking
%
[y,f] = fanhann(syncdata,760,4096,7,60);
figure(7);clf;fullscrn
plot(f,y,'k')
title('angle domain sampling based order tracking')
xlabel('orders')
ylabel('PSD');
%Resample rpm for angle domain rpm map
syncrpm = interp1(trpm,rpm,nsamp);
%
%RPM spectrum map for angle domain sampling based order tracking.
%
figure(8);clf;fullscrn
[Ms,Fs,Rs] = rpmmap(syncdata,760,syncrpm,760,700,10,1400,4096,0,150,.2);
title('resampling based order tracking RPM spectrum')
xlabel('orders')
%
%Sliced out order 36
%
ords = syncslice(Ms,Fs,Rs,36);
%And plot it together with the previous sliced order 36
figure(6)
hold on
plot(Rs,ords,'r')
save Rs
save ords
%
%Vold-Kalman filter application
%
y=xs;
fs=100000;
RPM=rpm
order=36;
order2=72;
bandwidth=0.1;
```

```
type=0;
%
%Perform filtering in time domain for order 36 and 72
%
x = vktime(y,fs,RPM,order,bandwidth,type)
x2= vktime(y,fs,RPM,order2,bandwidth,type)
bandwidth=0.5;
x50=vktime(y,fs,RPM,order,bandwidth,type)
bandwidth=0.1;
x10=vktime(y,fs,RPM,order,bandwidth,type)
figure(9)
plot(t,x,'b',t,x2,'r')
title('order 36 and order 72')
xlabel('time[s]')
ylabel('Acceleration [m/s^2]]')
%
%Frequency analysis for filtered data and origianal data
%
[yo,fo]=fantrans(xs,fs);
[yv,fv] = fantrans(x,fs);
[yv2,fv2] = fantrans(x50,fs)
[yw,fw] = fantrans(x10,fs)
figure(10)
plot(fo,yo,'k');hold on
plot(fv,yv);hold on;
plot(fv2,yv2,'g');hold on
plot(fw,yw,'r');hold off
axis([ 700 1000 0 0.6])
xlabel('frequency[Hz]')
ylabel('PSD')
%Plot filtered out data
figure(11)
plot(t,xs,'b',t,x,'r',t,x2,'k')
title('original signal and filtered out order 36 and 72')
xlabel('time [s]')
ylabel('amplitude [m]')
%
%RPM spectrum map for filtered out data
%
figure(12)
subplot(2,1,1);
[M,F,R] = rpmmap(x,fs,rpm,fsrpm,700,10,1400,8192,0,3000,0.1);
legend('order 36')
title('a')
axis([0 3000 700 1400 0 0.5])
M36=M;F36=F;R36=R;
subplot(2,1,2)
[M,F,R] = rpmmap(x2,fs,rpm,fsrpm,700,10,1400,8192,0,3000,0.1);
legend('order 72')
title('b')
axis([0 3000 700 1400 0 0.5])
%RPM spectrum map for the data that filtered out order 36 and 72
xw36=xs-x;xw72=xs-x2;
%plot these data into rpm spectrum map
figure(14)
subplot(2,1,1)
[M,F,R] = rpmmap(xw36,fs,rpm,fsrpm,700,10,1400,8192,0,3000,0.2);
ordline(F,36);
title('a')
subplot(2,1,2)
[M,F,Rr] = rpmmap(xw72,fs,rpm,fsrpm,700,10,1400,8192,0,3000,0.2);
title('b')
%
%Crest factor and kurtosis values calcultion
```

```
%
c0=crest(xs);c1=crest(x);c2=crest(x2);
k0=kurtosis(xs);k1=kurtosis(x);k2=kurtosis(x2);
ccc=[c0 c1 c2];kkk=[k0 k1 k2]
%
%Sliced order 36
%
ordd= ordslice(M36,F36,R36,36);
figure(6);hold on;
plot(Rr,ordd,'g');hold off;save Rr;save ordd
%
%Determine the damping ratio
%
figure(15)
plot(fo,20*log10(yo));axis([800 860 -120 0]);hold on
f1=ginput(1);x=linspace(800,860,100);y=linspace((f1(2)-3),(f1(2)-3),100);
plot(x,y);
f2=ginput(2);
zeta=(f2(2,1)-f2(1,1))/(2*f1(1))
```

Appendix 5 Angle domain sampling based order peak picking and Vold-Kalman filter order peak picking as well as crest factor and kurtosis values

Table A5.1 Angle domain peak picking results - good and fault condition (units: m^2/Hz)

(a) Good condition

Orders / Samples	36	72	108	144
1	0.0132	0.0217	0.0052	0.0026
2	0.0140	0.0243	0.0066	0.0031
3	0.0121	0.0190	0.0056	0.0027
4	0.0114	0.0231	0.0054	0.0030

(b) Fault condition

Orders / Samples	36	72	108	144
1	0.0572	0.0425	0.0263	0.0067
2	0.0344	0.0149	0.0231	0.0048
3	0.0176	0.0155	0.0212	0.0088
4	0.0098	0.0164	0.0117	0.0098

Table A5.2 Vold-Kalman filter peak picking results - good and fault condition (units: m^2/Hz)

(a) Good condition

Orders / Samples	36	72	108	144
1	0.3974	0.0202	0.0049	0.0089
2	0.4184	0.0173	0.005	0.0082
3	0.4114	0.0167	0.0049	0.0082

4	0.1605	0.0155	0.0021	0.0038

(b) Fault condition

Orders / Samples	36	72	108	144
1	0.5711	0.1705	0.0054	0.0108
2	0.4465	0.1161	0.0041	0.0088
3	0.5325	0.1424	0.0046	0.0088
4	0.2588	0.557	0.0088	0.0053

Table A5.3 Crest factors and kurtosis - good and fault condition

(a) Good condition-crest factor

Crest factor / Samples	36	72	108	144
1	5.4912	3.6155	6.9136	5.3363
2	5.9377	4.0998	4.5032	4.4104
3	6.2343	4.3219	6.6513	5.6899
4	6.9520	5.3154	6.5664	5.3230

(b) Good condition-kurtosis value

Kurtosis value / Samples	36	72	108	144
1	4.4933	4.6915	11.5191	4.1386
2	5.6581	6.1406	11.2357	5.6581
3	6.1323	6.9754	11.5398	4.0793
4	7.1822	9.7395	10.5331	3.9276

(c) Fault condition-crest factor

Crest factor / Samples	36	72	108	144
1	3.9068	2.6531	2.8331	4.9095
2	3.6710	2.7164	3.1315	4.2535
3	4.1592	2.8801	3.1324	4.4717
4	5.5409	3.8207	3.9369	5.1244

(d) Fault condition-kurtosis value

Kurtosis value / Samples	36	72	108	144
1	2.8205	2.5688	2.3679	3.0270
2	2.9826	2.6874	2.5913	3.0262
3	3.3727	3.1180	2.8848	3.1048
4	5.3247	5.2177	4.8372	3.6600